MASTER THESIS IN GEOLOGY

Hilde B. Johannessen

HOLOCENE CLIMATE VARIABILITY IN THE NORWEGIAN CURRENT AND NORTH CAPE CURRENT INFERRED FROM BENTHIC STABLE ISOTOPE RECORDS

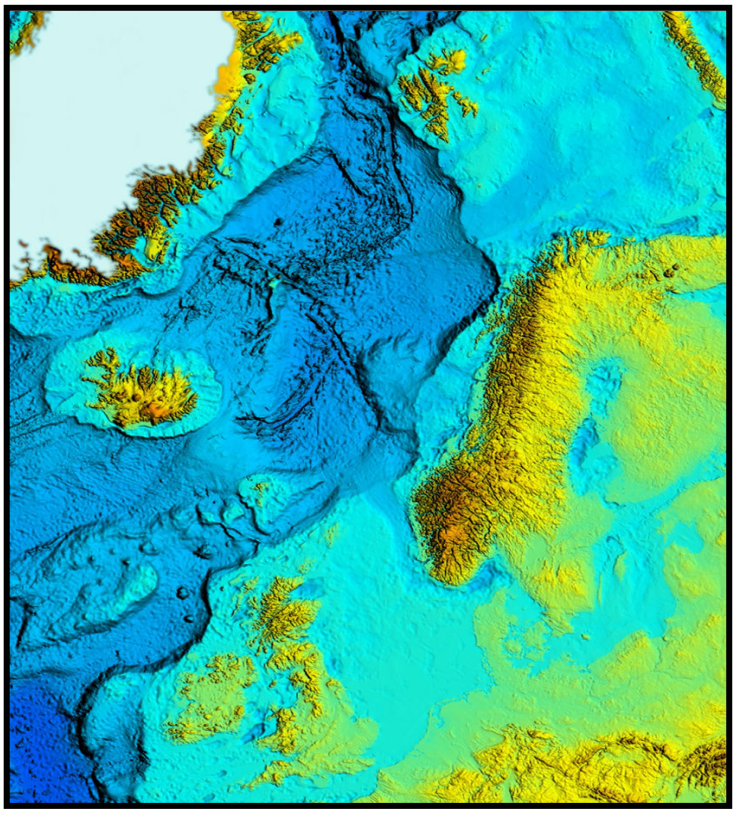

May 2006

FACULTY OF SCIENCE
Department of Geology
University of Tromsø, N-9037 Tromsø

MASTER THESIS IN GEOLOGY

Hilde B. Johannessen

HOLOCENE CLIMATE VARIABILITY IN THE NORWEGIAN CURRENT AND NORTH CAPE CURRENT INFERRED FROM BENTHIC STABLE ISOTOPE RECORDS

[1]

May 2006

FACULTY OF SCIENCE
Department of Geology
University of Tromsø, N-9037 Tromsø

[1] Front page illustration by Terje Thorsnes© NGU

Preface

This master thesis is my microscopic contribution to the geological understanding of climate changes and their causes in the marine realm of the northern North Atlantic. No attempt of surpassing all previous findings within the field of paleoclimatic reconstructions have been made, however I hope to demonstrate for the reader that I am able to look into our hypothesis and deal with it by using existing methods and research results.

A lot of people have made this possible for me, and I wish to thank you all from the bottom of my heart; Professor Morten Hald who has been my supervisor. It has been a privilege to work and learn from him during the two years of study. In addition our department is blessed with people that have been very helpful - Jan P. Holm provided maps and figures. Tove Midtun was invaluable when Morten sent me to Vienna with a huge poster under my arm. By the way; thank you Morten for this wonderful opportunity. Trine Dahl and Edel Ellingsen from our excellent geological laboratory made sure I could get all my results. Steinar Iversen, the master of all geological cruises! Gaute R. Salomonsen, Lindsay Wilson, Katrine Husum and Matthias Forwick always had time for discussions and answered numerous strange questions. Karl Heinz Valtl and Annbjørg Johansen. Thanks to all the nice people in my office and in the pavilion (Brakka) during the years, and who made the University a fun place to be. Pål J. Svanem and Steinar Gulliksen at the Radiocarbon Laboratory in Trondheim, Elsebeth Thomsen from Tromsø Museum did the species determination on my ^{14}C material and Rune Søraas at the GMS-laboratory in Bergen did all the stable isotope analyses. Thanks to the captain and crew onboard R/V Jan Mayen. An anonymous person read the corrections and improved on my English. Finally Kjell Bjørnar my beloved, grateful as I am for all your love and support. Now, let us enjoy the summer.

Hilde B. Johannessen

Tromsø 15.05.2006

Abstract

The Malangenfjord, with its deep sill and good hydrological communication with the Norwegian Sea, has been the site for a high resolution paleoclimatic investigation. By using benthic foraminifera and stable isotopes from a marine sediment core, this study will reconstruct the changes in inflow of warm Atlantic Water at a high-latitude setting. Radiocarbon dating has given ages between 8000 – 1500 cal. yrs BP. The benthic $\delta^{18}O$ values increases from 1.8‰ to 3‰ in the period from 8 to 1.5 cal. kyr yr BP. Interpretations indicate that this isotopic enrichment reflects a drop in the bottom water temperature from 10°C to 5.5°C, the latter being around 1.5°C colder than the modern temperature in the Malangenfjord. Additional data was retrieved from Ingøydjupet in the southern Barents Sea, in order to investigate the paleoclimatic changes in the North Cape Current. This record ranging from 15000 – 0 cal. yrs BP, has to tolerate a low resolution and a highly uncertain age model compared to the record from the Malangenfjord. Nevertheless it displays a deglacial unstable period, thermal optimum and a later enrichment in the benthic $\delta^{18}O$ values from 2.8‰ to 3.6‰. The preliminary interpretation suggests a late Holocene cooling with bottom water temperatures dropping from 6°C to 2.5°C, the latter being 1.5°C colder than modern temperature for the area. The study gives evidence for a long-term cooling with rapid changes superimposed on the general trend. The overall cooling trend correlates with the decreasing insolation at 70°N and isotopic data from the North GRIP ice core project. Several cold events could be interpreted as periods with reduced inflow of Atlantic Water, and vice versa for warmer events.

1 Introduction

There is a constantly ongoing debate these days among scientists, politicians and people in general regarding the climate. Is there a global warming going on or will there be a new ice age? Is the climate behaving normally? What is normal? Are the changes we are witnessing caused by human activities or are they caused by natural oscillations? Numerous theories and hypothesises have been tested throughout the years, and still many parts of the puzzle are missing in order to understand the complete picture of climate changes. A great deal of work lies ahead of us, and one way to address the problem is by looking back in time, what has happened before and how can we link this to the modern situation.

"The past is the key to the future"

The northern North Atlantic climate is warm relative to its high latitude positioning up under the North Pole. Less energy from the sun reaches these high latitude areas compared to low latitude regions. However the energy distribution is balanced with large-scale atmospheric and oceanic circulation-systems bringing heat to higher latitudes. The Norwegian climate benefits from this when heat is released to the atmosphere from the warm Atlantic Water as it cools during its journey northwards. Scientists are well aware of the changing heat budget and that it has experienced significant changes also in the past. Although it appears that the climate has been quiet and stable during the last 10 000 year, there are indications that the temperature in the Norwegian Current and the North Cape Current has varied and that the variations are amplified by increasing latitude (Kristensen et al. 2001). This high latitude northern area has a key position in the global system of both the thermohaline circulation (THC) and the important North Atlantic Deep Water (NADW) formation which takes place here (Broecker 1997). In addition, the region is also sensitive due to its proximity to the moving oceanic fronts. The unique settings from this study will hopefully contribute to the problem of linking the large-scale weather patterns, such as the North Atlantic Oscillation (NAO) and the inflow and strength of the Atlantic Water.

1.1 Presentation of the project

This study is part of the SPONCOM (Sedimentary processes and paleoenvironment on northern continental margins) project which is financed by the Research Council of Norway. It is a strategic university programme in marine geosciences at the Department of Geology, University of Tromsø.

The general goal of the programme is to assess the changes in the physical environment of the sea-floor and ambient waters and ice in selected fjords and continental margins in northern Norway and West Spitsbergen during the last glacial – interglacial cycle. This master thesis will contribute to the following subject under discussion; rapid paleoceanographic and paleoclimatic changes, particularly throughout the Holocene.

1.2 Objective

The Holocene appears to be more stable than the previous glacial – interglacial fluctuations. Glaciations and deglaciations are characterised with a high amplitude change in climate, while the Holocene shows a more uniform, low amplitude pattern of oxygen isotope values (Kristensen et al. 2001). It is normally more difficult to identify short-lived changes due to low stratigraphic resolution for the mid and late Holocene.

Hald et al. (2003) and Husum and Hald (2004) described what seems to be a long term millennial scale cooling trend throughout the Holocene by using foraminifera and stable isotopes from the Malangenfjord, northern Norway. The same site and core is the subject for a more detailed investigation by improving the stratigraphical time resolution. By this it may be possible to detect more short-lived changes. This paper intends to reconstruct the temperature in the Norwegian Current using a decadal to centennial resolution data set. In addition a new marine sediment core from the Barents Sea will reconstruct bottom temperature in the North Cape Current in the southern Barents Sea. The Barents Sea continental slope shows more variable surface temperatures than off northern Norway as a direct cause of its proximity to the Arctic oceanic front-system (Hald et al. 1996). By looking at these two different sites, it could be possible to identify the temperature

gradients that fluctuate between northern and more southern areas. Furthermore this study will look for probable causes to explain these variations. The high resolution approach makes it possible to test the influence of mechanisms with relative short cycles such as the North Atlantic Oscillation, volcanism and sunspot, but also the slow orbital changes known as the Milankovitch factors.

1.3 Background

1.3.1 Regional setting and modern environment

This study refers to two different sites and environments in northern Norway (Figure 1. 1); The Malangenfjord is located in Troms, northern Norway (69°29.9'N 18°23.6'E) and Ingøydjupet is located on the continental shelf in the southern Barents Sea outside the Coast of West Finnmark, northern Norway (71°37.3'N 22°55.5'E).

Malangen is a south-southeast oriented fjord system with several tributaries; Straumsfjorden from the east, Nordfjorden, Aursfjorden and Målselvfjorden from the south-southeast (Figure 1. 2). The total length of the fjord is 50 km and the maximum width 6 km. Syvitski et al. (1987) classified a fjord as a deep, high-latitude estuary which has been or is presently being excavated or modified by land-based ice. An estuary is a body of water where there is mixing with fresh water and sea water. Drowned river valleys formed in response to the Early Holocene postglacial sea level rise are common estuaries. The large Målselv River at the fjord head contributes with freshwater to the fjord. Both sedimentation and hydrography are controlled by the bathymetry in the fjord, which consists of several submarine thresholds and basins.

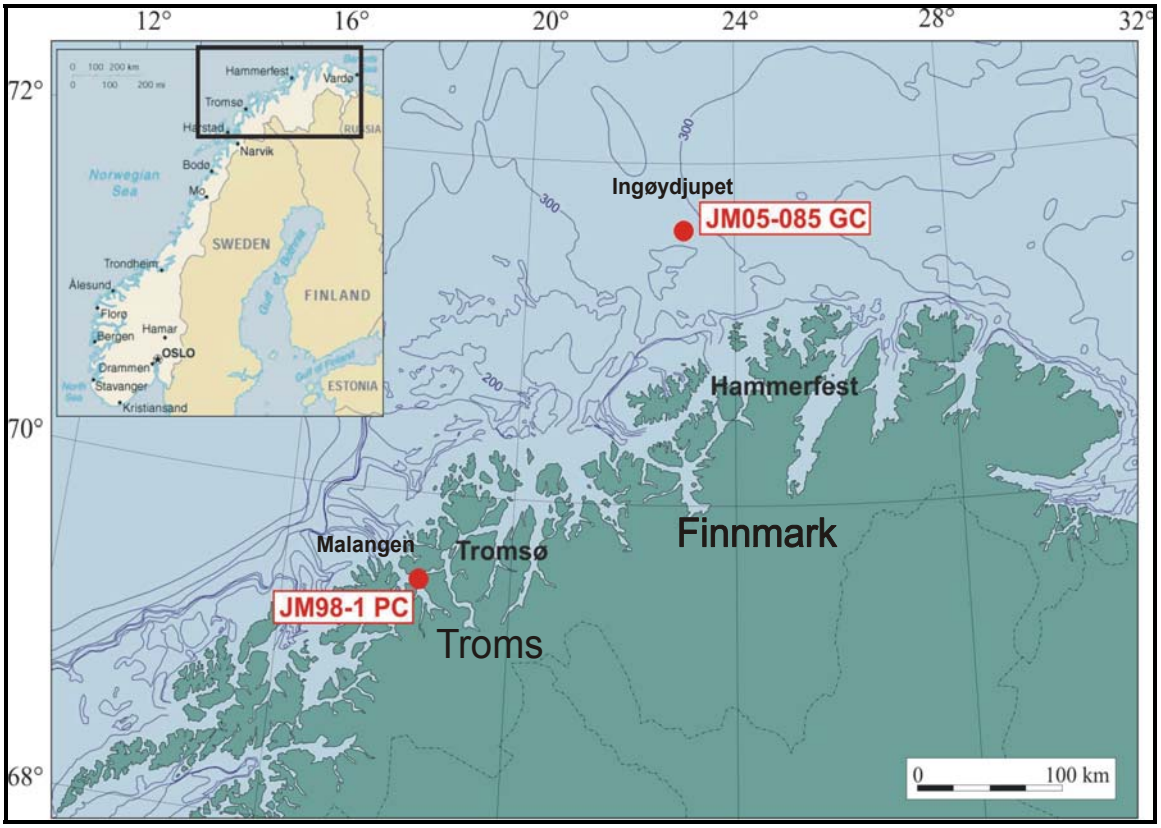

Figure 1. 1 Map showing the location for core site JM98-1 PC in the Malangenfjord and JM05-085 GC in Ingøydjupet, northern Norway.

Ingøydjupet is part of the Hammerfest Basin in the southern Barents Sea (Figure 1. 4), and also here on the continental shelf the bathymetry holds control of both sedimentation and hydrography. The Barents Sea is a shallow epicontinental ocean where most depths are less than 300 m. The core site JM05-085 GC consists of a relatively thick sedimentary sequence (Solheim et al. 1996; Faleide et al. 1993).

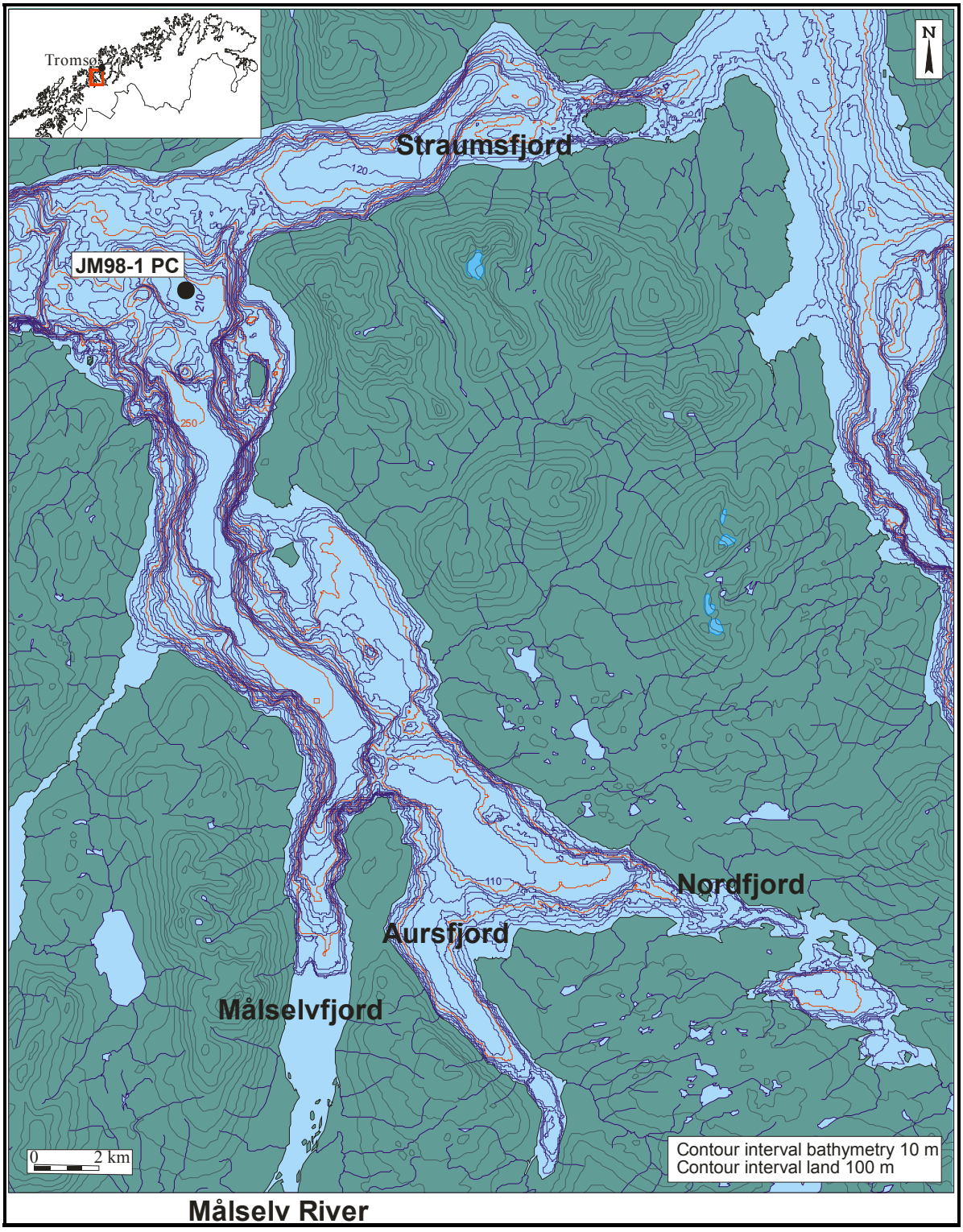

Figure 1. 2 Bathymetry of the Malangenfjord with its tributaries and topography of the surrounding mainland. Core position JM98-1 PC is marked with a black dot.

1.3.2 Bedrock and Quaternary sediments

The geology of northern Norway and western Troms is characterized by Precambrian basement (Andresen 1980; Zwaan 1995). Gneiss, supra-crustals and intrusive rocks in the Precambrian basement are draped by the Caledonian nappes of Ordovician and Silurian age. Finnmark is dominated by Caledonian nappes covering a thin sequence of autochthonous sediments, but also distinct Precambrian basement areas are present.

The Malangenfjord has several thresholds and consists of an outer and inner basin. The outer basin is mainly filled with sediments deposited before the last deglaciation, while the inner basin consists of a ~ 150 m thick Holocene sedimentary sequence. The threshold area between the basins is interpreted as end moraines deposited during the Skarpnes event (Older Dryas) and Tromsø-Lyngen event (Younger Dryas) (Lyså and Vorren 1997). The core site JM98-1 PC is situated just inside this threshold area in the small Ansnes Basin (Figure 1. 3), which is infilled with Holocene sediments (Larsen 1986). Major traverse troughs with glacial origin, such as Malangendjupet and Andfjorden, cross the shelf with depths exceeding 300 m (Holtedahl 1993). These submarine troughs are found as continuations of the fjord systems in the coastal terrain, in which large amount of glacial ice drained through during the last glacial and deglacial period (Jørgensen et al. 1997).

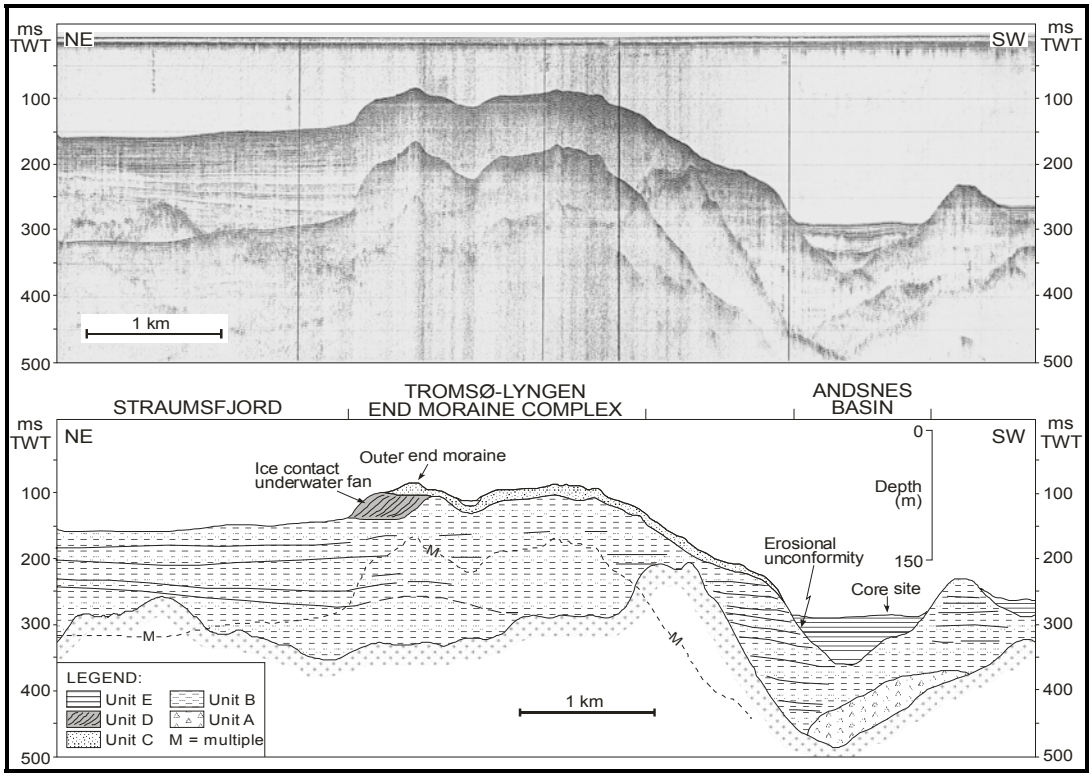

Figure 1. 3 A seismic profile and interpretation from the Malangenfjord. Upper panel: high resolution profile across the Ansnes basin and the Tromsø-Lyngen (Younger Dryas) moraine complex into Straumsfjorden. Lower panel: Interpretation of the profile shown in upper panel. The core site JM98-1 PC is indicated (From Hald et al. 2003).

The development of the Barents Sea during Quaternary is influenced by the opening of the Norwegian-Greenland Sea during the Tertiary. This rifting led to uplifting of land areas, which were exposed to erosion and large amounts of sediments were transported and deposited in the western Barents Sea. Later erosion by both fluvial and glacial activity has again removed vast amounts of sediments. The bathymetry is generally dominated by shallow banks less than 150 m in the south and deeper banks in the north such as Tromsø basin, Nordkapp basin and Bjørnøya basin with depths of 150 - 300 m (Figure 1. 4).

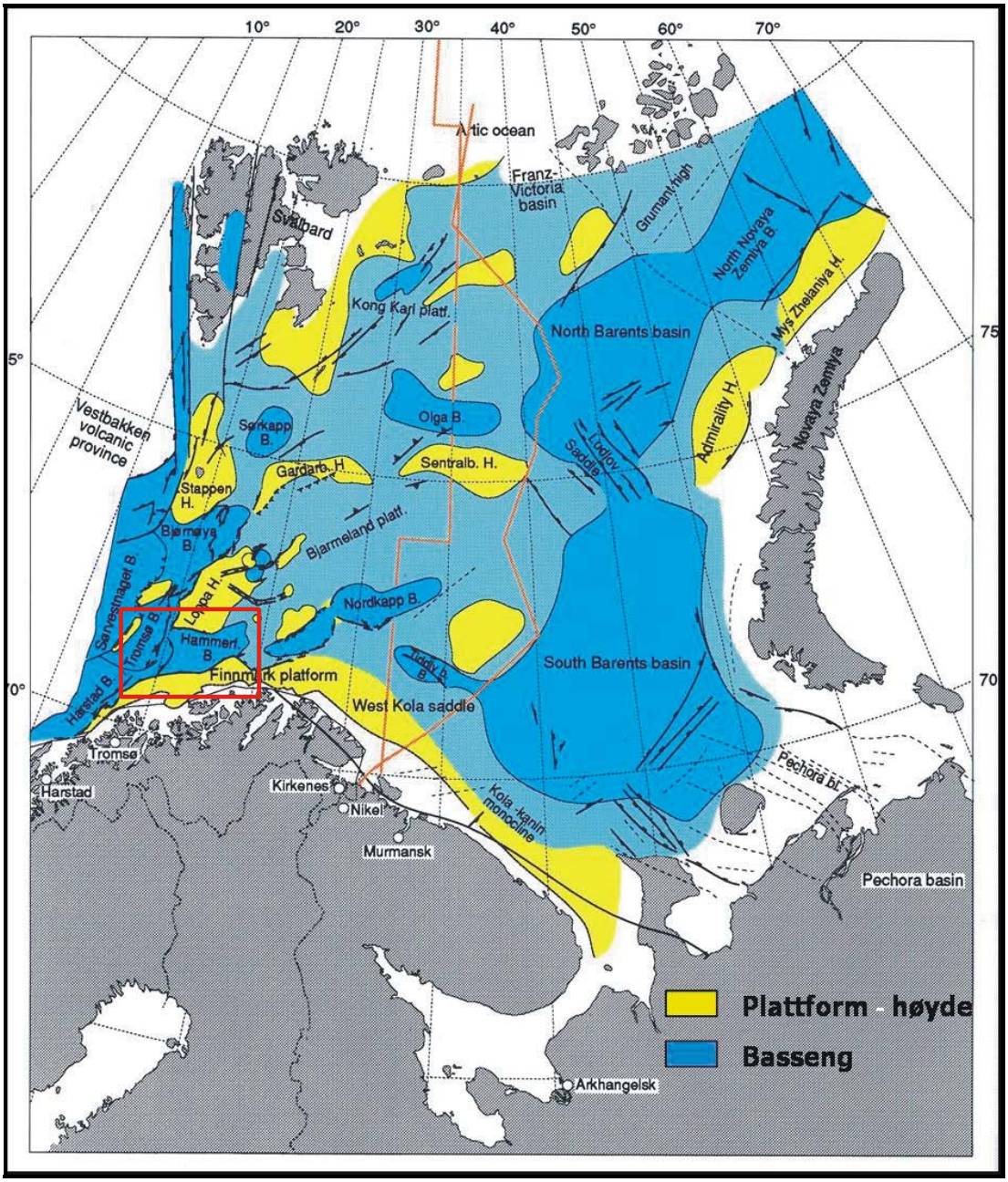

Figure 1. 4 Main elements from the Barents Sea. Study area and core site JM05-085 GC is indicated with the red box. Yellow colour: platform, heights. Blue colour: basins.

1.3.3 Oceanography, sea-ice and climate

The great ocean conveyor belt is the main feature in the North Atlantic oceanic circulation system (Figure 1. 5). This global circulation pattern is sensitive to temperature and salinity

changes and is also called the thermohaline circulation (THC) (Broecker 1997Broecker 1997). Of importance for this conveyor belt is the generated downward flowing deep water along the Antarctic continent which drains into all three major oceans (Figure 1. 5). Of importance for our latitudes are the warm, saline wind driven surface currents originated in the Gulf of Mexico, which moves up north as the North Atlantic Current (NAC). The warm Atlantic surface water releases heat to the atmosphere as it cools. The cooling affects the density which results in a downward convection at high latitudes. This cold sinking bottom water current flows south along the East Greenland margin and continues all the way into the northeast Pacific where it reappears at the surface approximately 1200 years later[1]. This turnover is a vital part of the THC and North Atlantic Deep Water production (Broecker 1997).

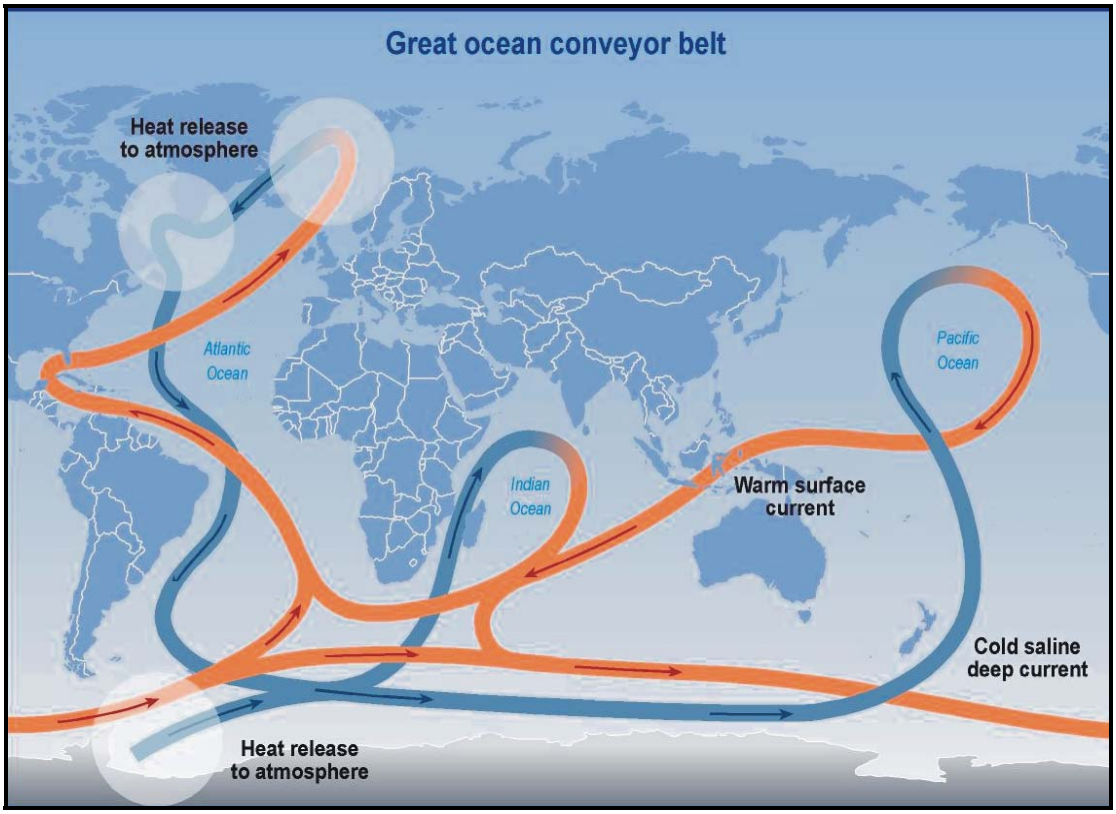

Figure 1. 5 Principle sketch showing the main features of the thermohaline circulation. Red colour indicates warm surface water currents, and blue colour indicates cold deep water currents (Figure from IPCC 2001).

[1] http://en.wikipedia.org/wiki/Thermohaline_circulation

A fjord is semi-enclosed coastal body of water which has a free connection with the open sea and within which sea water is measurably diluted with fresh water derived from land drainage (Syvitski et al. 1987). Malangen has its submarine sills well below sea level and therefore allows a relatively good hydrological communication with the NAC and the open ocean. The surface water properties in a typical Norwegian fjord are low and variable saline water masses which flow out of the fjord system (Kristensen et al. 2004). Replacing this is the intermediate water mass which lies between the upper brackish water and down to the depth of the sills. During summer season the heavy, saline Atlantic Water flows in over the outer sill in Malangen and continues as a bottom current further in fjord. This process will renew and supply oxygenated deep water for the fjord basins.

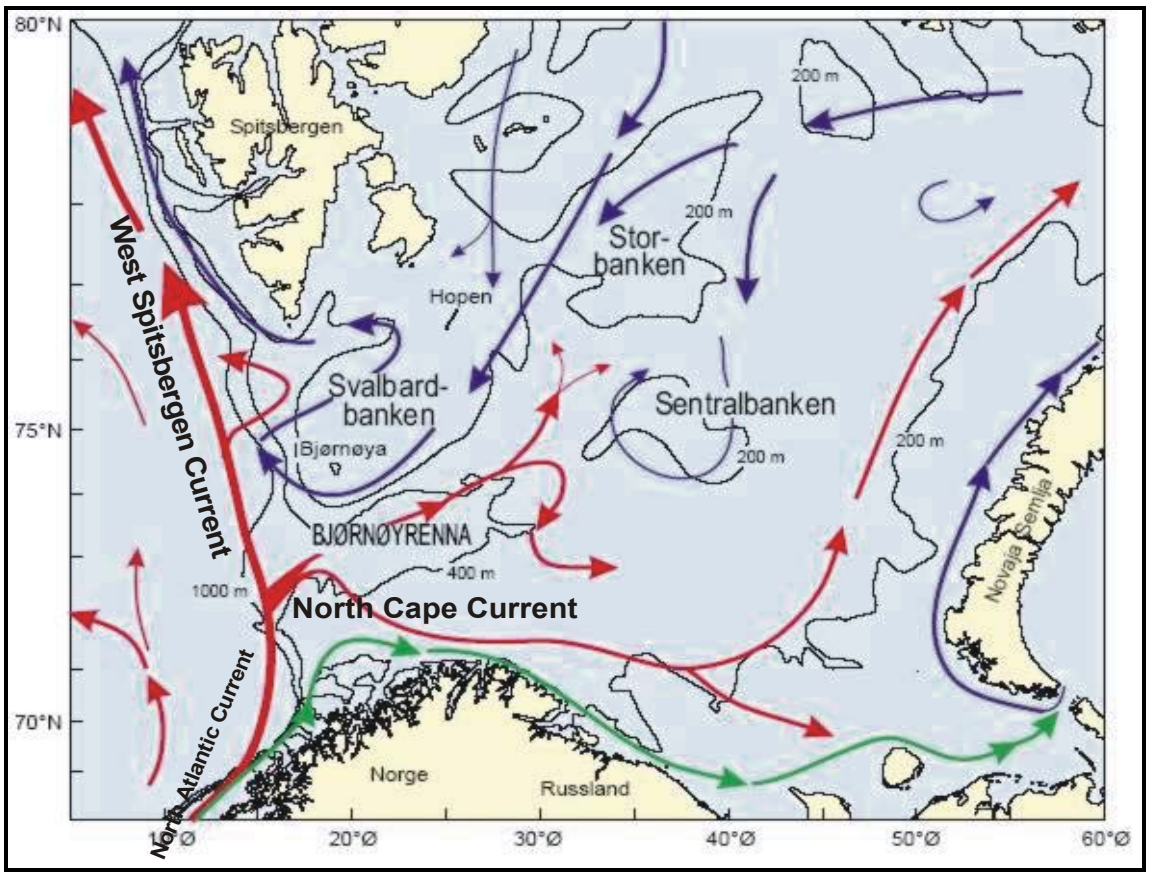

Figure 1. 6 The main features of the surface water circulation and bathymetry in the Barents Sea. Red arrows: North Atlantic Water. Blue arrows: Arctic Water. Green arrows: Coastal Water (Figure from Ingvaldsen et al. 2005b).

There are three different surface water masses in the study area in northern Norway and the Barents Sea (Ingvaldsen et al. 2005b); (1) warm saline *Atlantic Water* from the NAC with a temperature > 3°C and salinity > 35‰ (2) cold *Arctic Water* from the north with a temperature < 0°C and salinity < 35‰ and (3) the warm but not very salty Norwegian *Coastal Water* with temperature > 3°C and salinity < 34.7‰) (Figure 1. 6).

The boundary between the Atlantic Water and Arctic Water is called the Polar oceanic front. The Norwegian Coastal Current overlies the NAC as a westward thinning wedge[2], and it is originating from the Baltic Sea. The Norwegian Coastal Current mixes with water masses from Skagerrak and low saline water from the Norwegian fjords as it flows northwards along the Norwegian coast. Outside the coast of Troms the NAC divides into two branches; one branch follows the continental shelf edge north towards West Spitsbergen while the other branch flows along the edge of Tromsøflaket and into the Barents Sea (Figure 1. 6). The branch which flows into the Barents Sea is called the North Cape Current, and is divided into two new branches; (1) southerly branch along the coast towards Novaya Zemlya and (2) northerly branch flowing into Bjørnøyrenna and Hopendjupet (Figure 1. 6). In addition there is other locally formed water masses present in the Barents Sea; Freshwater supply from melting of ice and formation of dense bottom water through rejection of brine during freezing (Midttun 1985). Modern bottom water temperature is around 4°C all through the year, while the surface waters experience some warming during the summer months (Figure 1. 7). The salinity for the bottom waters in the Barents Sea is around 35‰ all through the year, while the surface waters experience some freshening during summer months from melting and enhanced river input (Figure 1. 8).

[2] http://oceancurrents.rsmas.miami.edu/atlantic/norwegian.html

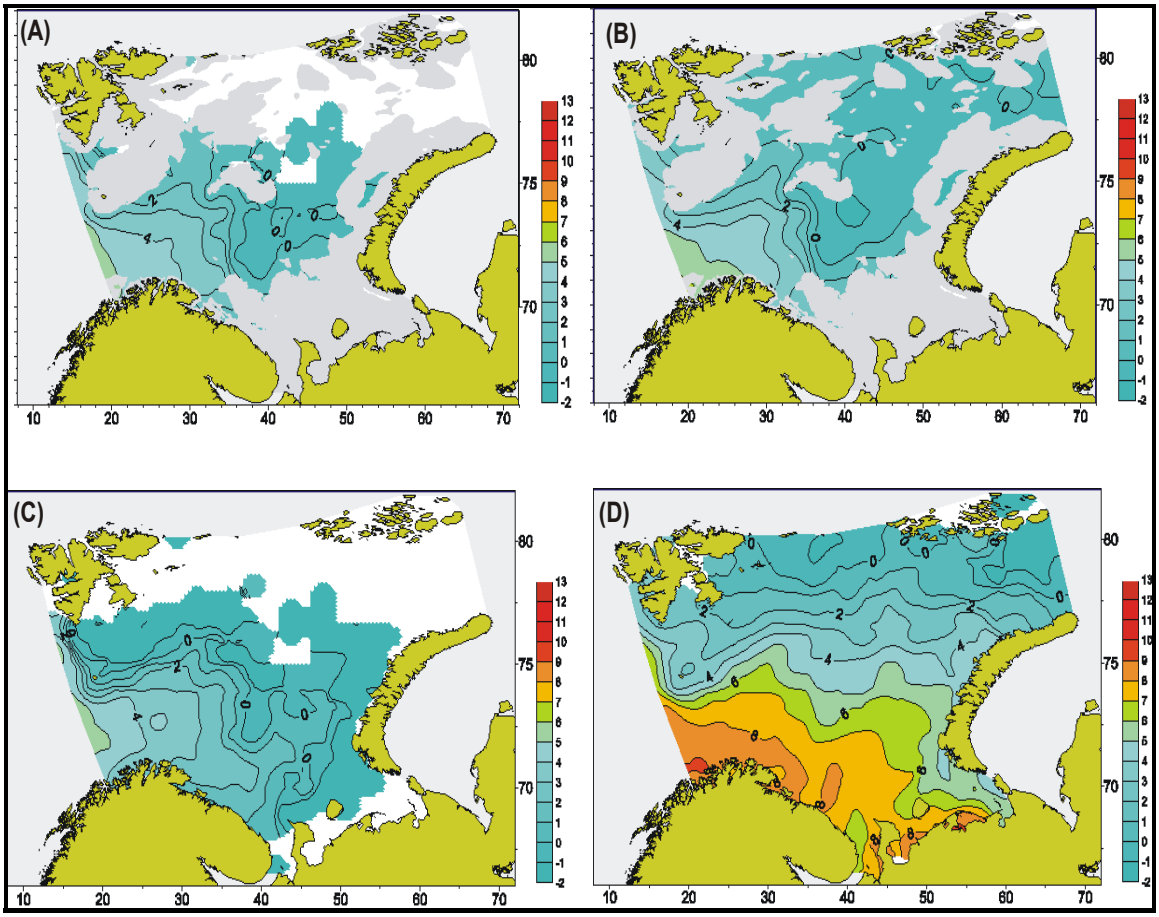

Figure 1. 7 Modern temperature conditions in the Barents Sea. (A) Bottom water temperature, March. (B) Bottom water temperature, September. (C) Surface water temperature, March. (D) Surface water temperature, September (Graphics from National Oceanographic Data Center, http://www.nodc.noaa.gov.

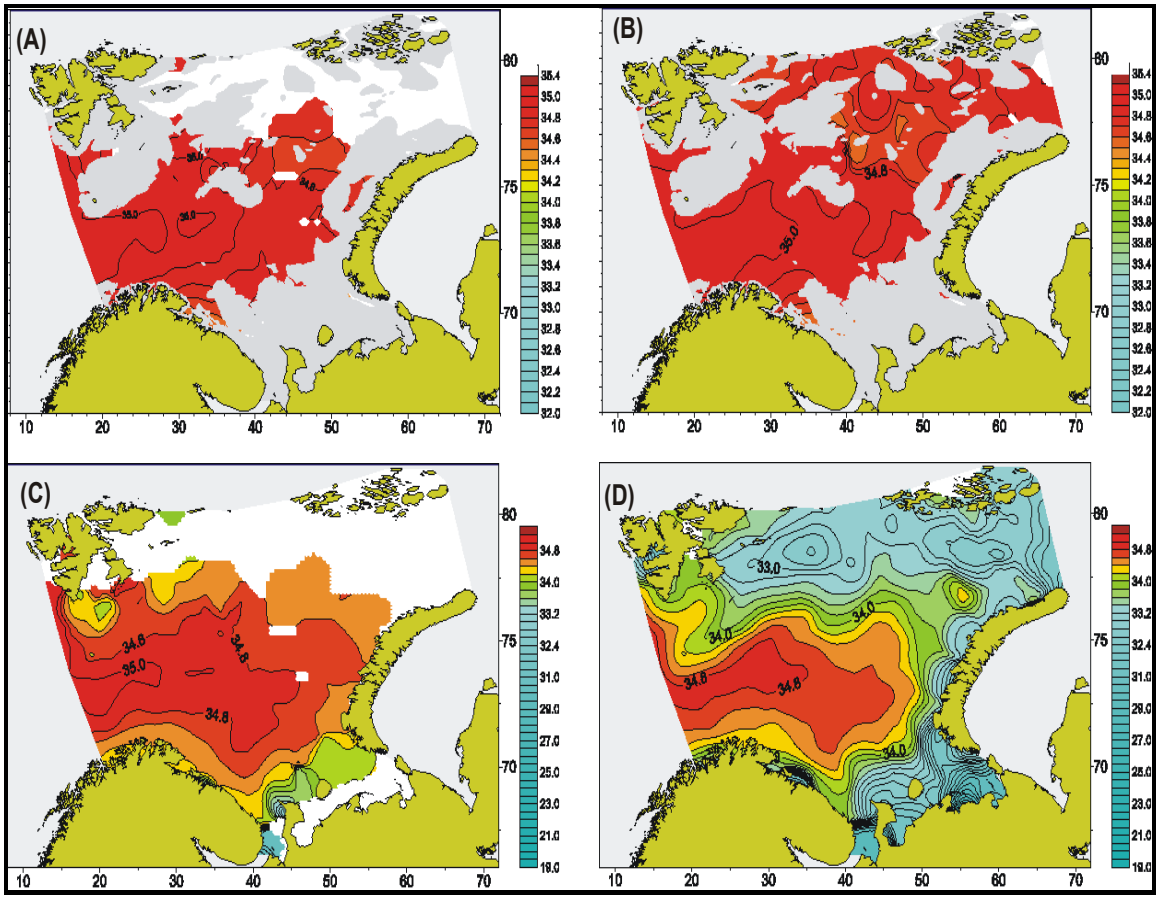

Figure 1. 8 Modern salinity in the Barents Sea. (A) Bottom water salinity, March. (B) Bottom water salinity, September. (C) Surface water salinity, March. (D) Surface water salinity, September (Graphics from National Oceanographic Data Center, http://www.nodc.noaa.gov).

The Barents Sea is characterized by large, annual variations with respect to temperature and salinity, sea-ice cover and volume flux of Atlantic Water into the Barents Sea (Figure 1. 9). Maximum extent of the ice cover is often controlled by the oceanic polar front system, which due to weak Atlantic inflow sometimes can migrate southward (Ingvaldsen et al. 2005b). Sea ice is formed in the northern and eastern part of the Barents Sea and normally reaches its maximum position at 74°N. This means sea ice usually never covers the core site JM05-085 GC at present time.

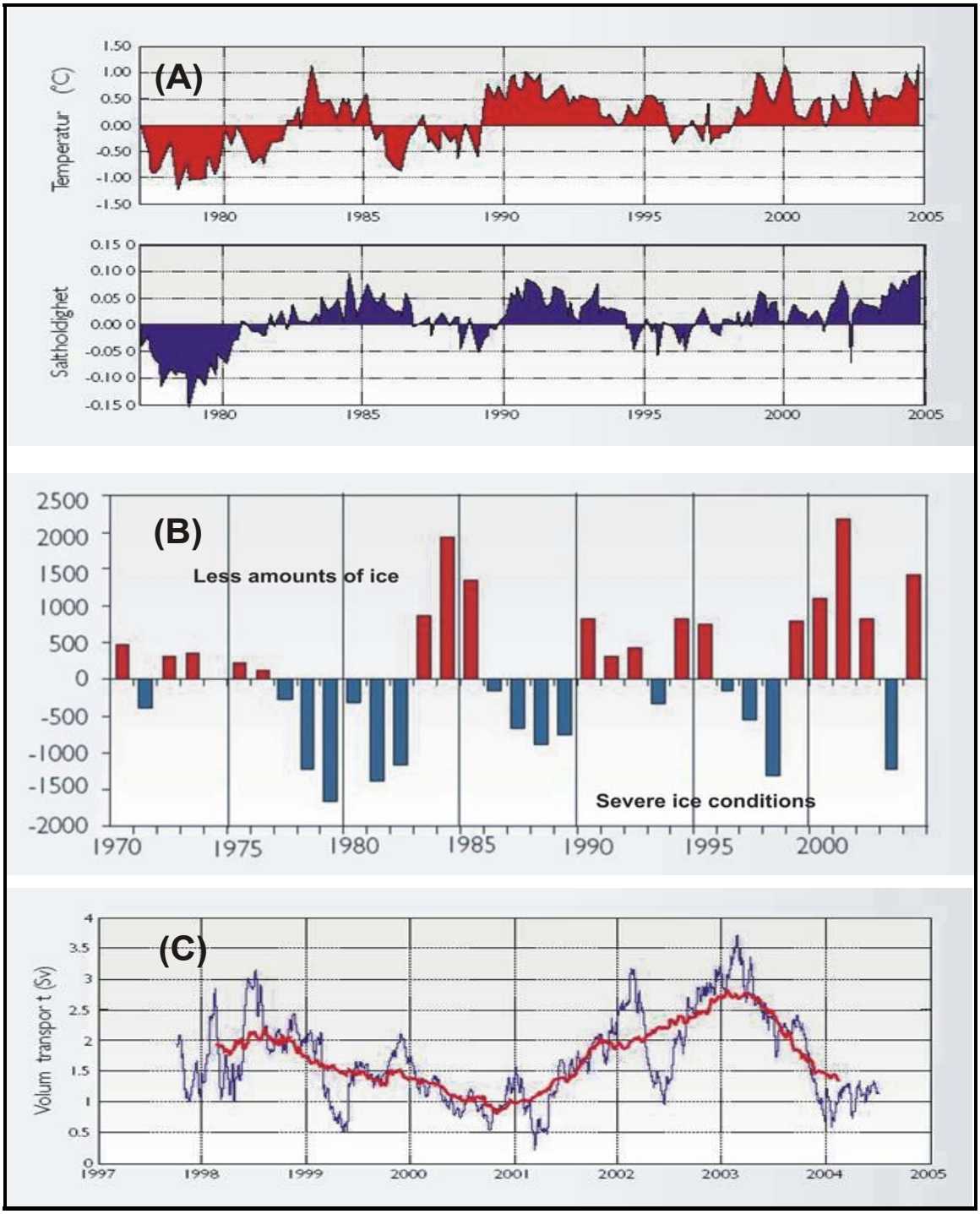

Figure 1. 9 Physical properties from the Barents Sea. (A) Temperature and salinity anomalies between 50 and 200 m depth, from the Fugløya-Bjørnøya transect period 1977 – 2004. (B) Ice index for the period 1970 – 2004. Positive values indicate small amounts of ice, while negative values indicate more severe ice conditions. (C) Atlantic water volume flux into the Barents Sea in the period 1997 – 2004 (figures from Ingvaldsen et al. 2005b)

Ingvaldsen et al. (2005a) proposed that local wind conditions controls the influx and strength of the Atlantic Water. They did not find any correlation between temperature and volume influx of Atlantic Water (Figure 1. 9). The Atlantic Water inflow is also connected to the Atlantic Subpolar Gyre (Hátún et al. 2005). The cold East Greenland Current continues south into the Labrador Sea and further southeast to form the subpolar gyre in an anticlockwise current system (Figure 1. 10). The gyre is driven by the global wind system, but the mechanisms behind the changes in the subpolar gyre are at this time not fully understood. When the subpolar gyre has a strong index the salinity of the Atlantic inflow is reduced by mixing of less saline water masses, while a weak gyre will ensure free passage and formation of dense saline water in the North Atlantic. Hátún et al. 2005 concluded by modelling that the position and strength of the subpolar gyre controls the intensity and salinity of the Atlantic inflow and thus the deep water formation. This is in agreement with results from the Fugløya-Bjørnøya transect (Figure 1. 9) which also pointed out the connection between high temperature and high salinity in the Barents Sea (Ingvaldsen et al. 2005b).

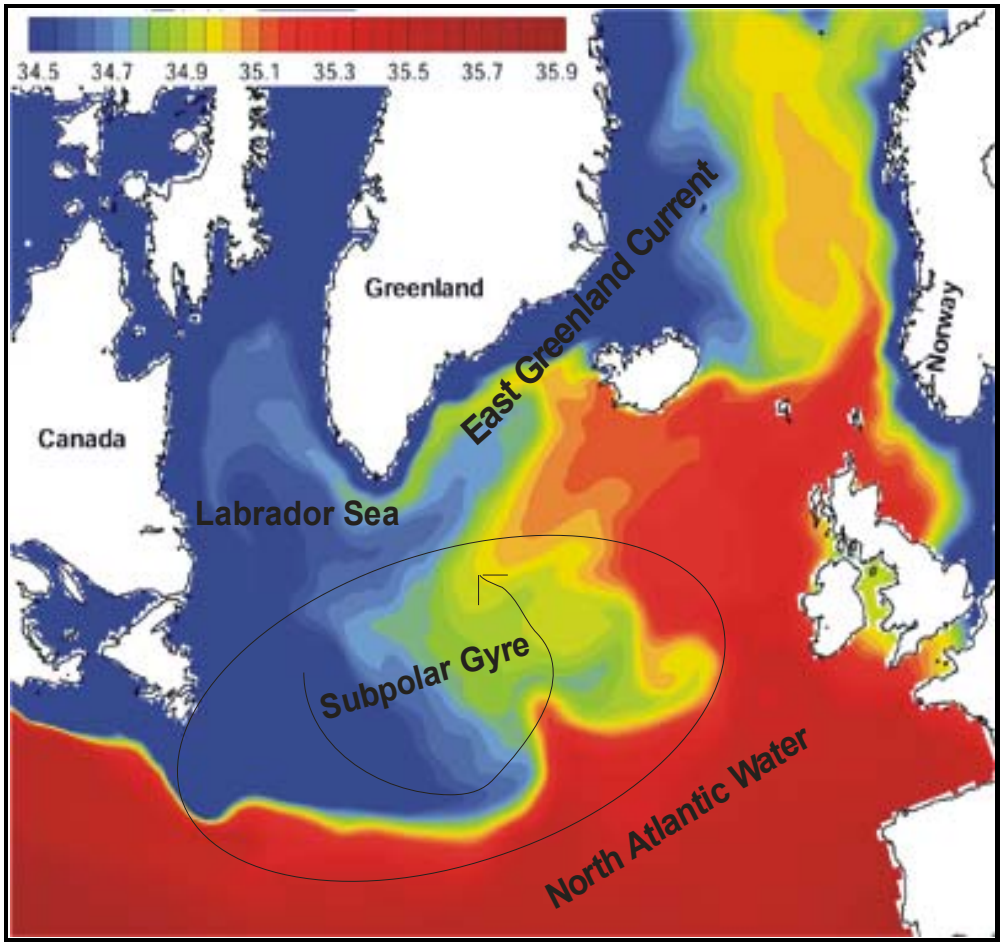

Figure 1. 10 The Atlantic Subpolar Gyre. The strength and distribution of the Subpolar Gyre controls the intensity and salinity of the inflowing North Atlantic Water (red colour). Blue colour indicate cold and less saline water (Modified after Hátún et al. 2005).

1.4 Climate forcing mechanisms

Scientists from all over the world try to solve the puzzle of climate changes, and our area holds a key position when seeking to understand the changing climate and oceanography. The debate regarding the forcing mechanisms of our unstable climate has, in addition to anthropogenic factors, evolved around orbital forcing, atmospheric forcing, solar activity and volcanism (IPCC 2001).

1.4.1 Orbital forcing

The climate on Earth is controlled by various internal and external factors such as the amount of ice in the system, ocean variability, solar and orbital variations, volcanism, and lately also anthropogenic factors[3]. A relationship between the orbital factors and global climate changes was suggested in the 1976 Science paper "Variations in the Earths orbit: Pacemaker of the ice ages" by Hayes, Imbrie and Shackleton. These factors also known as the Milankovitch Theory vary in several patterns and influences on the amount of solar insolation reaching our atmosphere; (1) the eccentricity fluctuating on a 100,000 year scale, changing the earth's orbit from circular to elliptic and back again, (2) the earth's axial tilt which varies between 21.5° and 24.5° with a 41,000 year periodicity is responsible for seasonal changes and (3) the precession of the equinoxes which operates on cycles of 23,000 years. All these factors in combination give different scenarios on how and when the sun is closest to the Earth, and thus affects the climate more[4].

1.4.2 North Atlantic Oscillation

The NAO is in charge for affecting the wind-driven surface water circulation on an interannual and decadal scale in the North Atlantic Ocean (Hurrell 1995), and it is a measure for the variability in the atmospheric circulation by looking at the differences between the Iceland low pressure system and the Azores high pressure system (Figure 1. 11). This north-south pressure system is especially prevailing during winter with enhanced

[3] Reference - http://en.wikipedia.org/wiki/Climate_change
[4] Reference - http://en.wikipedia.org/wiki/Milankovitch_cycle

pressure systems operating. When the winter-index is in a positive mode, the pressure difference is large and produces westerly winds stronger than normal across the North Atlantic towards Europe and Scandinavia. Hot and humid air masses give mild winters in northern Europe, holding the cold polar air masses back. A negative index is caused by small pressure differences and weaker westerly winds towards northern Europe. This allows for the cold polar air masses to flow southwards, giving cold winters in our region (Hurrell 1995; Visbeck et al. 2001).

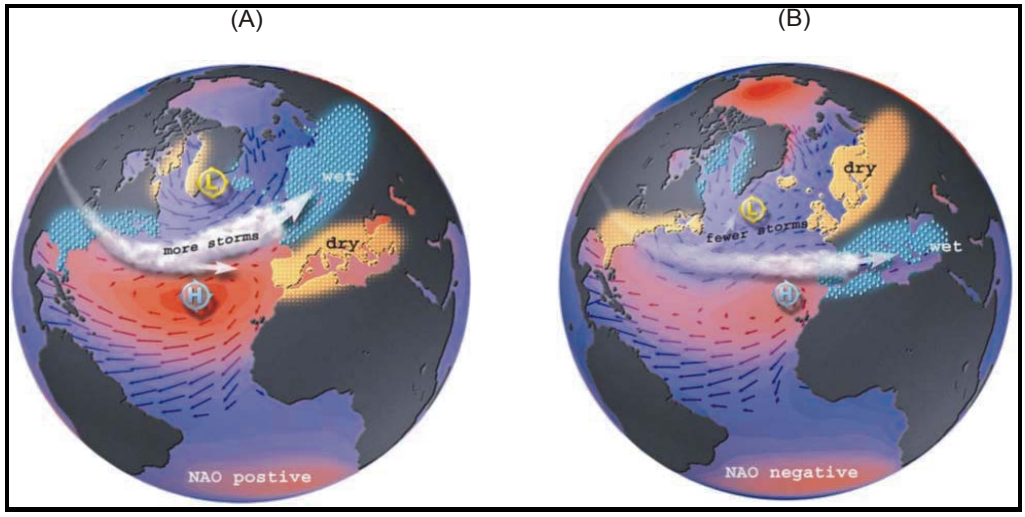

Figure 1. 11 An illustration of the NAO-index. (a) Positive index with enhanced low pressure and enhanced high pressure gives stronger westerly winds over the European continent. (b) Negative index with a smaller pressure gradient gives a weaker west-wind belt over the European continent (Graphics from Martin Visbeck, Lamont-doherty Earth Observatory, USA).

1.4.3 Volcanism

The Earth is a constantly active planet, with erupting volcanoes being one of the evidences for the internal processes going on. Normally lower global temperatures are linked with eruptions, when large amounts of aerosols (particles) are injected into the atmosphere, increasing the reflectivity and cooling the climate (Jørgensen et al. 1997).

1.4.4 Solar activity

The sun is the most important contributor of energy to the Earth's climate system. The activity of the sun varies, and different cycles have been identified; 11 yrs "Schwabe cycle", 22 yrs "Hale cycle", 70-90 yrs "Gleissberg cycle", 210 yrs "Suess cycle and 2300 yrs "Hallstatt cycle[5]. These variations alter the amount of energy emitted from the sun, and the output energy seems to correlate with the number of sunspots on the surface of the sun (Friis-Christensen and Lassen 1991). Sunspots are large dark areas on the sun's surface which are colder than the normal surface temperature, and they appear when the sun is in its most active mode. The areas surrounding these spots are brighter and hence warmer, so more energy is emitted during intervals with high sunspot numbers.

[5] http://en.wikipedia.org/wiki/Solar_variation

2 Material and methods

2.1 Cruise

The collection of data for this study was carried out using R/V "Jan Mayen" (JM). The R/V "Jan Mayen" is a multi-use vessel, designed for fishery and marine biological, geological and oceanographic surveys in open and ice covered waters. The range of geological surveys includes geological bottom sediment sampling and acoustic registrations of the sediment layers below the sea-bed. The ship is equipped with up to date instruments and has special designed features for improved acoustic surveying and bottom sediment sampling.

2.1.1 Seismic lines and 3.5 kHz system profiling

A sedimentary sequence has less density and thus lower seismic velocity compared to continental or basaltic crust. Seismic profiling is a method of acquiring information of the structures below the earth's surface or in this case, the sea floor (Kearey et al. 2002).

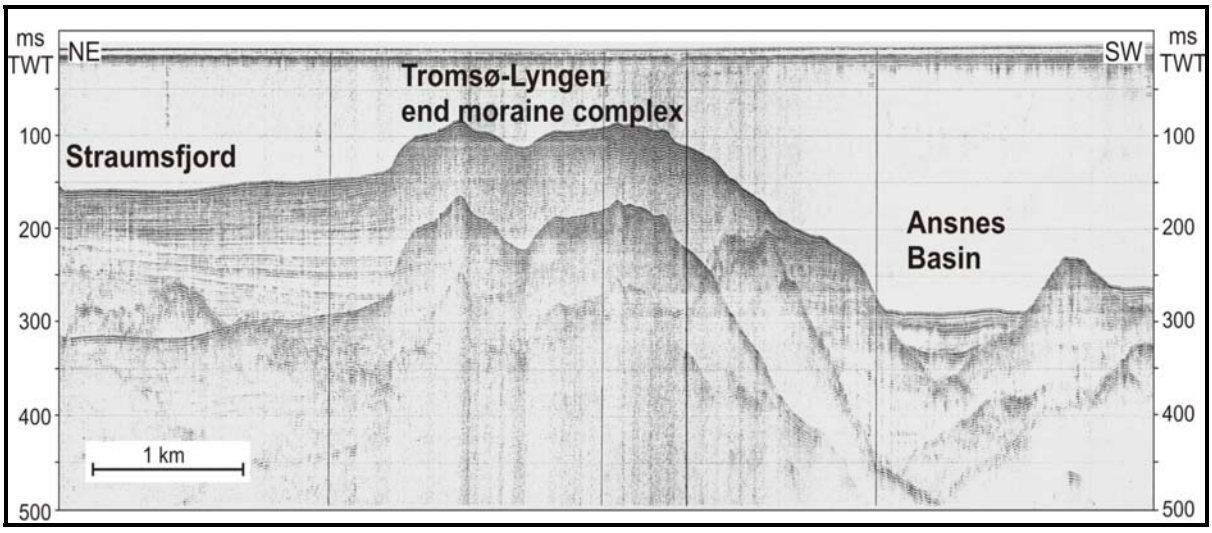

Figure 2. 1 A high resolution seismic profile across the Ansnes basin (core site for JM98-1 PC) and the Tromsø-Lyngen (Younger Dryas) moraine complex into Straumsfjorden. For location see fig. 1.3. (Modified after Hald et al. 2003).

As it is of interest for us finding high accumulation area, the core sites were based on several high resolution surveys using the 3.5 kHz seismic profiler and airgun array with streamer. Profiling is done by producing repeated seismic signals and continuously measuring the backscatter from underground reflecting surfaces. These reflecting surfaces are the interfaces between layers with different acoustic impedance, which is a product of P-wave velocity and density (Kearey et al. 2002). Whenever either one of these seismic properties changes, we get a seismic signal reflected back. Seismic profiling is done by an air gun array which is towed behind the vessel together with an array of hydrophones for recording, or alternatively a boomer/sparker array. The principle for both methods is to create a sharp sonic pulse in the water. A 3.5 kHz bottom penetrating echo sounder (Geopulse transmitter ORE 137) is mounted in the hull of R/V "Jan Mayen". An echo sounder is principally the same as a seismic profiling system. Only difference is that the echo sounder has less energy compared to the air gun, and therefore can not penetrate as deep into the sediments. Normally this would be ~ 20 meters deep, while profiles acquired with the seismic system can reach 450 – 500 meters deep. The advantage with the high frequency echo sounder is higher resolution for the data acquired.

2.1.2 Sediment coring

Two different marine sediment cores are subject for analysis in this study. Piston core (PC) JM98-1 from the Malangenfjord is 7.6 m long and was sampled during a cruise in 1998 from a water depth of 213 m in the Ansnes Basin (Figure 1.2). Gravity core (GC) JM05-085 from the Barents Sea is 4.87 m long and was retrieved in 2005 at a water depth of 408 m from the Ingøydjupet Basin (Figure 1.2). Cranes and trawl winches onboard the ship operated the different types of coring equipment (Figure 2. 2).

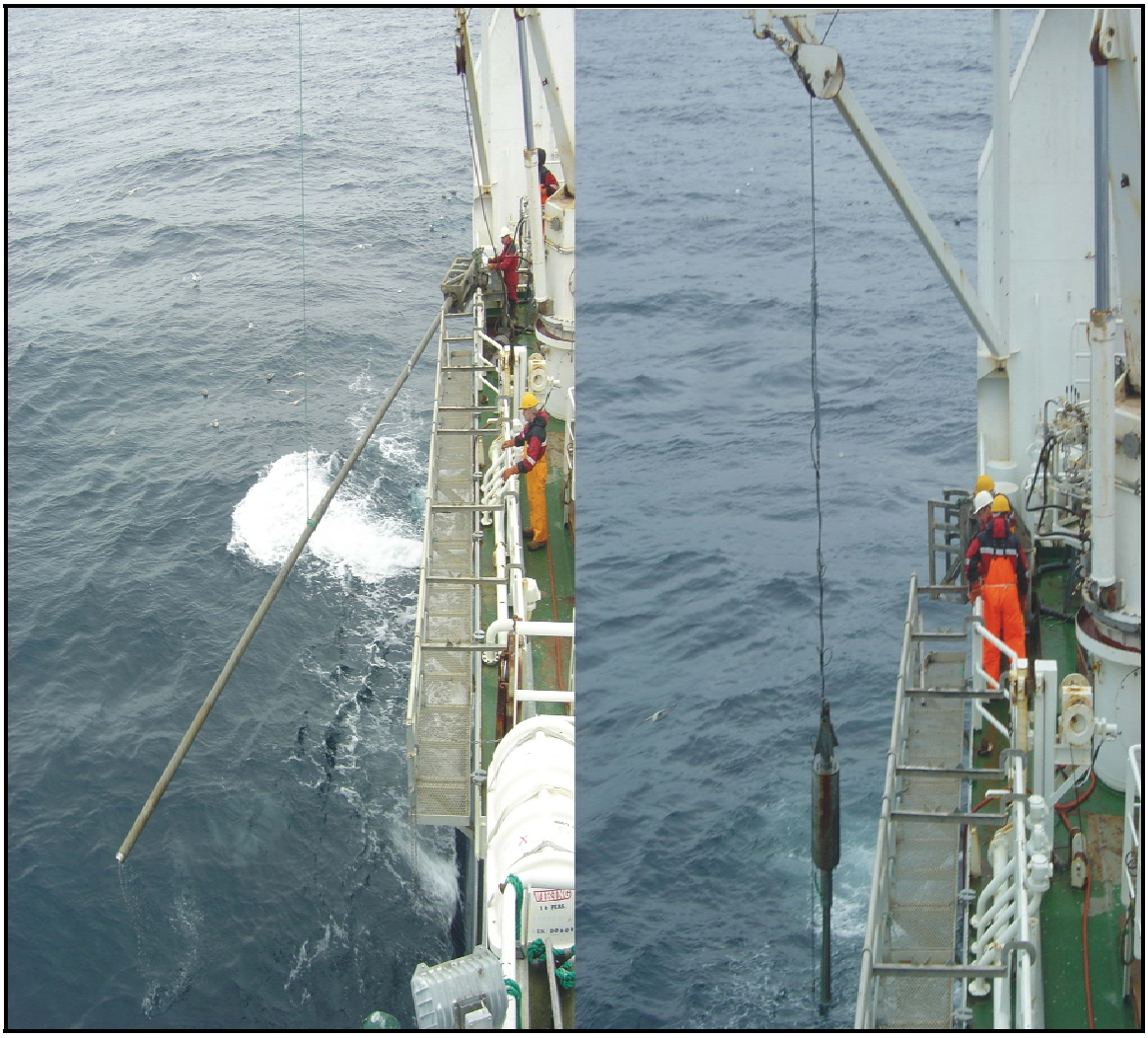

Figure 2. 2 The crew onboard R/V "Jan Mayen" handling the piston corer.

A gravity corer consists of a steel barrel with a plastic liner inside. The assembly is fitted with both a core cutter and core catcher at the end. The steel pipe is driven into soft sediment by a heavy weight as it drops a given distance to the sea bottom. Once it stops cutting down through the sediments, it is gently raised with the winch. The metal core catcher at the bottom holds the sediment inside the plastic liner, as does the partial vacuum created by a valve that closes at the top. The core cutter helps the steel pipe penetrate the sediment. The core liner onboard R/V "Jan Mayen" is 6 m long. In best cases 6 m of sediments are collected inside the core liner, but often the recovery is less. Sediment from

both the core cutter and core catcher is sampled in plastic bags; this is to get an idea of the properties for the lower most sediment at the core site. Next the core liner is being marked in detail, cut into sections and brought to storage for further laboratory analysis. The principle of piston coring is the same as gravity, but the steel pipe is triggered to fall down freely for the last few meters before it hits the sea bottom. It is possible to retrieve cores 12 meters long with the piston core equipment, but this requires relatively good weather conditions with calm sea as the equipment is launched outside the ships side. The gravity coring is more stable and easy handled as it is being lowered through a moonpool on deck.

2.1.3 CTD

R/V "Jan Mayen" is also equipped with a Sea-Bird 911 and this was used to measure conductivity, temperature and pressure vertically in the water column at the core sites. Conductivity and pressure were recalculated into salinity and depth respectively. The Sea-Bird 911 can obtain up to 12 in-situ water samples from the profile. The data are processed using a software package from the Sea-Bird Electronics Inc. that comes along with the CTD.

2.2 Laboratory analysis

The 1 m long core sections from both JM98-1 PC and JM05-085 GC were opened and described visually with respect to colour, structures, grain size composition, clasts and fossils.

2.2.1 Multi-Sensor Core Logging

Before the core sections from JM05-085 GC were opened, they were examined by using a Multi-Sensor Core Logger (MSCL) (Figure 2. 3). This is a GEOTEK-system for logging physical properties in sediment cores at small sampling intervals (Weber et al. 1997; Gunn and Best 1998). A conveyor system pushes each core section through sensors, which scan the core as it passes. The sediment core was analysed every 5 millimetre. The computer controlling the conveyor also controls the sensors, and all the data are automatically correlated and generated as a graphic display where the sampling points are plotted with

depth. Sediment core JM98-1 PC was not analysed using a MSCL, but instead magnetic susceptibility was measured manually each cm using a Bartington MS2E magnetometer.

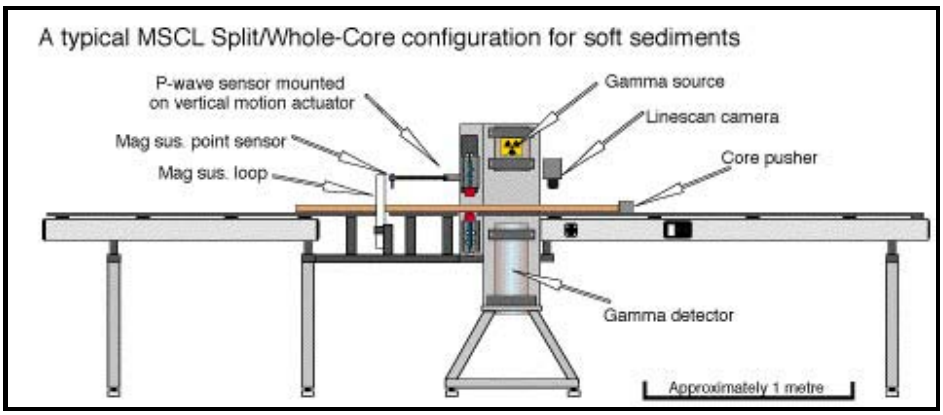

Figure 2. 3 A principle sketch showing the different properties for a multi sensor core logger (from Geotek Ltd).

The main properties measured with the MSCL are density, P-wave velocity and magnetic susceptibility. Magnetic susceptibility quantifies the magnetic behaviour of a material in an external magnetic field, and it is often used to correlate and log major stratigraphic changes in sediment cores. Mineral material derived from the continents will show higher magnetic susceptibility than for instance carbonate derived from biological production. Such records may give information about ice-rafting and changing sediment sources through the glacial and interglacials (Robinson 1986). P-wave velocity and density are related to acoustic impedance and seismograms which can be used to compare sediment records with high resolution seismic records. It is important to make sure that the core sections have reached room temperature before measurements are carried out because different temperature for core section and laboratory environment will cause large variations in the P-wave velocity (Weber et al. 1997). When the sampled core is cut into 1 m sections onboard the ship, it is not always possible to make sure the core liner is completely filled with sediments (Figure 2. 4). This will give an incorrect, reduced or no signal at all from the current core section when run through the MSCL.

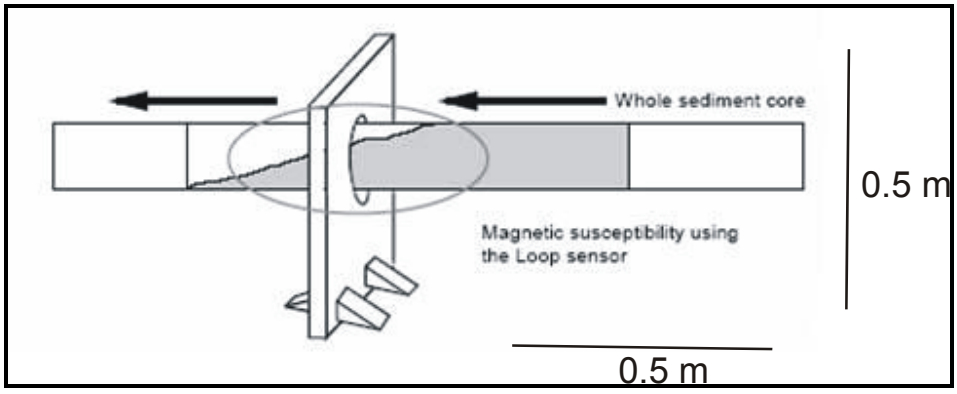

Figure 2. 4 Core liner which is not completely filled with sediments in the top.

2.2.2 Lithological analysis

Grain size analysis may give information of transport, sorting and hence genesis for the sediment. The Wentworth-Udden scale was used for classification of the grain sizes (Table 2. 1). Bulk density samples were taken every cm for the high resolution core from Malangen (JM98-1 PC), while the core from Ingøydjupet (JM05-085 GC) was sampled less frequently every 10 cm. In order to ease the sieving process with regard to the material's cohesiveness, all samples were freeze-dried prior to the sieving. The following fractions were determined by dry-sieving: 1 mm, 100 µm and 63µm, while smaller fractions (<63µm) was analysed by using the sedigraph technique (Coakley and Syvitski 1991). This technique is based on measuring the time of settling for the material in suspension. The time used is simplified a measure for the grain size. Standard procedures on a Micromeritics Sedigraph were followed.

Grain size fraction	Diameter
clay	less than 0.004 mm
silt	0.004 mm to 0.0625 mm
fine sand	0.0625 mm to 0.2 mm
medium sand	0.2 mm to 0.6 mm
coarse sand	0.6 mm to 1 mm
very coarse sand	1 mm to 2 mm
pebble (or gravel)	2 mm to 64 mm
cobble	64 mm to 256 mm
boulder	more than 256 mm

Table 2. 1 Wentworth-Udden scale for grain size classification

The core sections were also analysed with respect to colour differences, and a helping tool in so regard is the Munsell Soil Colour Chart (Munsell 1973) which helps us determine colours objectively rather than subjectively. It was Professor Albert H. Munsell who in 1905 created a rational way to describe colours. The Munsell colour chart is still the most widely accepted system of colour identification and continues being used today.

By using x-radiography it is possible to identify structures, clasts and fossils which are not easy detectable at the core surface. The core halves were photographed at the Geological Laboratory at University in Tromsø using a Phillips K 140 Be X-ray unit.

To describe the compressive strength of the core sediment, the undrained shear strength was investigated by means of the fall-cone test. A cone with known weight and angle was placed vertically over and barely touching the materials surface. Next the cone was released, and by its own weight penetrated the sediment. This was done every 10 cm for both core JM98-1 PC and JM05-085 GC. The penetration given in millimetre is then recalculated according to calibrated dataset from Hansbo (1957) and this gives a direct measure of the undrained shear strength.

2.2.3 Total carbon and total organic carbon

Measuring the total carbon (TC) and total organic carbon (TOC) will reflect the amount of biogenic production in the water. This was measured every 5 cm in the core JM05-085 GC and every 10 cm in the core JM98-1 PC. TOC was obtained by room temperate HCl (10%) extraction of crushed sample material, assuming that the dissolved material was carbonate carbon ($CaCO_3$), and next combusted in the Leco at 1350°C. Standard procedures for Leco IR 212 were followed for JM98-1 PC samples, while standard international procedures for Leco CS 200 were followed for JM05-085 GC samples. The $CaCO_3$ was calculated from the equation: TC – TOC * 8.3333 (Stein et al. 1994).

2.2.4 Stable oxygen and carbon isotope analysis

All stable oxygen and carbon isotope measurements were carried out at the Geological Mass Spectrometer (GMS) laboratory at the University in Bergen. This was done using a Finnigan MAT 251. Results are reported with respect to VPDB standard through calibration against CM03 standards. The reproducibility of the system is ± 0.06 for $\delta^{13}C$ and ± 0.07 for $\delta^{18}O$, based on replicate measurements of an internal carbonate standard. All isotope values are presented per mil (‰). The grain size fraction 1 mm – 100 μm from both cores was used for benthic foraminiferal stable isotope analysis, and each sample contained carbonate tests from the benthic, infaunal foraminifera *Cassidulina neoteretis*. This proxy is suitable for reconstructing bottom water conditions. Sediment core JM98-1 PC was sampled more or less every cm to provide a high resolution record, while core JM05-085 GC was sampled approximately every 10 cm. The samples were prepared according to Shackleton and Opdyke (1973); Shackleton et al. (1983).

This method measures the ratio of $^{18}O/^{16}O$ as a deviation from a PDB belemnite standard or SMOW (Standard mean ocean water). This ratio can however show variations due to changes in ocean temperature, ice volume, salinity or/and vital effect. In general when the foraminifer produces its carbonate test, it will reflect the isotopic composition of the ambient water in which it develops. Urey (1947) was the first to discover the relationship between temperature dependent fractionation of oxygen and precipitation of carbonate.

Simplified we can say that the light ^{16}O isotope is enriched in warm waters, giving low $\delta^{18}O$ values. During colder periods the fractionation increases and producing high $\delta^{18}O$ values. Later work done by O'Neil and Adami (1969) and Shackleton (1974) has confirmed his theories and the use of stable oxygen isotopes. Not all species secrete their carbonate test in equilibrium with the sea water. This equilibrium is called the vital effect, and the probable cause is incorporation of isotopically-light metabolic CO_2 into the carbonate test (Grossman 1987). *Cassidulina neoteretis* is in equilibrium with the ambient water, and no correction for vital effect was done (Duplessy et al. 1980; Poole 1994). Grossman (1987) suggested that calcareous tests of *Cassidulina sp.* which are sampled at depths less than 500 m tend to be enriched by as much as 1‰ relative to equilibrium. It is therefore worth mentioning that both cores from our study have been retrieved from water depths less than 500 m. However his studies did not specify the Cassidulina on species level. The presence of ice in the system will affect the oxygen isotope record by showing heavier values in the worlds oceans. The ice volume effect is adjusted for by subtracting the following equation of Fairbanks (1989) from the isotopic values: 0.08842651163 * ^{14}C age * 0.001 – 0.2195683836. This is based on the results where a sea level change of 10 m represents 0.11‰ change in the $\delta^{18}O$ signal. It is possible to convert the isotope values into paleotemperatures, and it is calculated for the bottom water by using the following equation of Shackleton (1974): $T\ (°C) = 16.9 - 4 * (\delta^{18}_{foraminifer} - \delta^{18}_{water})$, where the "$\delta^{18}$ water" is standard mean ocean water composition (SMOW). This has a value of 0.2 in the Malangenfjord (Mikalsen et al. 2001a). This value considers the possible freshwater input from rivers in the fjord. For the southern Barents Sea, it is assumed less influence by river input and the $\delta^{18}O$ for water is set to 0‰ reflecting the North Atlantic mixing line (Risebrobakken 2003).

The biogenic calcite ratio $^{13}C/^{12}C$ is primarily a function of dissolved inorganic carbon (DIC), which is affected by the water mixing on the continental shelves. A carbon isotope record can be used to monitor variations in productivity, deep water formation and ventilation (Berger and Vincent 1986). Simplified we can say that carbon is part of the photosynthesis ($^{12}CO_2 + H_2O \rightarrow {}^{12}CH_2O + O_2$) and all organic matter in the photic zone is enriched in ^{12}C isotope through fractionation. This process leaves the surface waters

enriched in ^{13}C relative to deep waters. The organic matter ($^{12}CH_2O$) will as time goes by settles into the deeper waters, where decomposition leads to depletion of ^{13}C. This downward transfer of carbon is referred to as the "pumping action", and it is also controlling the distribution of oxygen in the oceans. Reduced ventilation gives less oxygen and less decay of organic matter, which in turn gives less release of nutrients and reduced productivity, and this will be reflected in the $\delta^{13}C$ record. When it comes to vital effect, it turns out that almost all biogenic carbonates are influenced by disequilibrium relative to the ambient water. Species which are in $\delta^{18}O$ equilibrium with the water are more likely to present an accurate record of $\delta^{13}C$ than those which are not in equilibrium. Another factor is the microhabitat effect. Oxidation of organic matter and the release of isotopically light CO_2 in the sediments lead to depletion of $\delta^{13}C$ in the pore water relative to the ambient water. Infaunal species such as the *Cassidulina neoteretis* are under influence of the pore water in which it lives (Grossman 1987). By this one could assume that epifaunal species in reality are preferable for stable carbon isotope measurements. For this study *C. neoteretis* was used because of its abundance throughout the record, and it is a problem for epifaunal species that they more easily can be exposed to resedimentation.

2.2.5 AMS radiocarbon dating

^{14}C radiocarbon dating is widely used to determine the ages of samples younger than ~ 55'000 years. The radioactive isotope ^{14}C is produced in the earth's stratosphere through interaction with neutrons from cosmic rays and ^{14}N. The ^{14}C isotope rapidly oxidizes to form CO_2, which trough photosynthesis is absorbed by all living organisms. Following death and burial of an organism, the material looses ^{14}C as it converts to ^{14}N by radioactive decay. The radioactive clock has been set by the known interval of time (half life), which reflects the time it takes for a radioactive material to decay to half its original amount (Bowman 1990). We are operating with the Libby-half life of 5570 ± 30 years. This method assume that (1) the ^{14}C production in the atmosphere have been constant through time, (2) the concentration of ^{14}C is equal for all parts of the system, (3) the half life is known and (4) there is only decay of ^{14}C after the organisms death (Bowman 1990). All of these

assumptions are in fact sources of error which we have to adjust for, or have in mind when interpreting the ^{14}C ages.

Accelerator mass spectrometry (AMS) radiocarbon dating was performed on bivalves and molluscs. The samples were prepared at the Radiocarbon Laboratory in Trondheim and measured at the Svedberg Laboratory in Uppsala, Sweden. All dates are converted into calendar years using the new calibration curve and data set in CALIB.html version 5.0.2 marine04 (Reimer et al. 2004; Hughen et al. 2004), meaning all ages are reported as calendar years unless indicated otherwise. This new calibration curve replaces the dataset of IntCal98 which was previously used for the 8 samples from sediment core JM98-1 PC (Hald et al. 2003). In addition 2 samples with bivalve fragments from sediment core JM05-085 GC were dated. Corrections were done for the marine reservoir effect, to adjust for the differences between ^{14}C-dated terrestrial material and marine material. While the global mean reservoir correction is about 440 years, the complexity of ocean circulation creates local variations of several hundred years or more. The average reservoir age for northern Norway is 465 ± 35 (Reimer and Reimer 2001; Reimer et al. 2001).

3 Results

The two sediment cores which are subject for description, different analysis and methods as described in chapter 2, are in this chapter presented with their results. Calibrated ^{14}C dates give basis for the age model and chronology, laboratory work provides different lithological data and last but not least the measurements of stable isotopes are presented. All datasets are enclosed in the appendix (enclosed CD) for further reading.

3.1 Core JM98-1 PC - The Malangenfjord

3.1.1 Lithological description

Hald et al. (2003) described core JM98-1 PC based on visual inspection, grain-size distribution, measuring the total carbon / total organic carbon and magnetic susceptibility (Figure 3. 1). Two facies (Unit I and II) were identified in the core and only the upper unit is investigated further in this study. Unit I covers the upper most 460 cm of the core, and it consists of soft, bioturbated and olive grey (5y 4/2) mud. As previously stated, a hiatus divides the units. Otherwise the unit is relatively uniform downcore. Hald et al. (2003) interpreted the unit as interglacial marine mud.

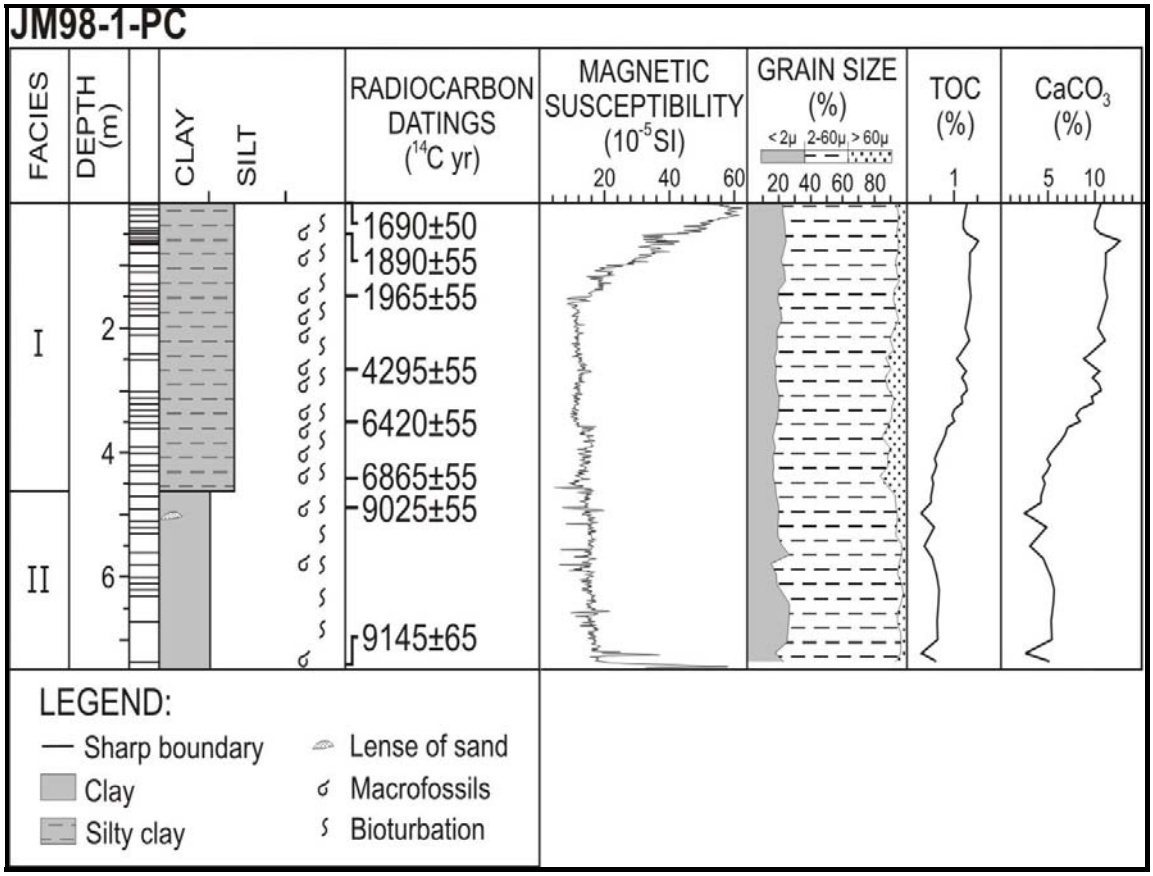

Figure 3. 1 Lithostratigraphy of core JM98-1 PC as described by Hald et al. (2003).

3.1.2 Chronology and sedimentation rate

Hald et al. (2003) published eight ages covering a period from 1650 ± 50 ^{14}C yr BP to 9145 ± 65 ^{14}C yr BP from core JM98-1 PC. Radiocarbon ages were dated from bivalves (*Bathyarca pectunculoides*, *Nuculana pernula*, *Pecten* sp., *Astarte elliptica)* and mollusks (*Siphonodentalium lobatum* & *Scaphander punctostriatus*). *Nuculana pernula* and *Siphonodentalium lobatum* is classified as a deposit feeder (E. Thomsen 2006, pers. comm.) and we should be aware of the uncertainties related to deposit feeders when incorporating old organic matter from the sediments in which they live (Forman and Polyak 1997). For this high resolution study all ^{14}C ages which previously have been used by Hald et al. (2003), were calibrated to calendar years all over again with the latest calibration curve and data set - CALIB version 5.0.2 marine04 (Hughen et al. 2004). The calibration

programme designs a curve for the probability of the calibrated ages (Appendix 7.1.2). Each curve were studied closely to make sure the best interval was chosen, and it was decided to use the arithmetic mean for the 2σ age interval of highest probability (95.4%) in all cases. The average marine reservoir effect of 465 ± 35 from northern Norway where used (Reimer and Reimer 2001; Reimer et al. 2001). All dates were in sequence and a stratigraphic chronology could be established (Table 3. 1).

Lab Code	Core id.	Depth (cm)	^{14}C age	Calibrated age BP	2σ maximum cal. age (arithmetic middle) minimum cal. age	Material	Weight (mg)	Relative area under probability distr.
TUa2432	JM98-1 PC	1	1650 ± 50	1580	cal. BP 1748 (1583) 1418	Mollusc, *Siphonodentalium lobatium*	13,3	1.000
TUa2433	JM98-1 PC	48	1890 ± 50	1870	cal. BP 2028 (1870) 1712	Fragments of 1 bivalveshell, *Nuculana pernula*	290	1.000
TUa2110	JM98-1 PC	148	1965 ± 55	1970	cal. BP 2131 (1969) 1806	2 bivalve shells (paired), *Pecten sp.*	1383,9	1.000
TUa2434	JM98-1 PC	267,5	4295 ± 55	4950	cal. BP 5129 (4948) 4767	2 bivalve shells (paired), *Astarte elliptica*	205	0.988
TUa2435	JM98-1 PC	350	6420 ± 55	7430	cal. BP 7430 (7307) 7183	Mollusc, *Scaphander punctostriatus*	124,8	1.000
TUa2113	JM98-1 PC	441	6865 ± 55	7700	cal. BP 7842 (7708) 7574	Shell fragment, *Pecten sp.*	120	1.000

Table 3. 1 Radiocarbon ages from core JM98-1 PC. The dates have been calibrated with the CALIB version 5.0.2 marine04 (Hughen et al. 2004) using a ΔR of 65 years ± 35.

A hiatus was identified in the core at 460 cm by Hald et al. (2003), and this transition represents the boundary between Unit I and Unit II. This hiatus was linked to a tsunami resulting from the Storegga slide on the continental margin of the Norwegian coast (Bondevik et al. 2003). The Storegga Tsunami is dated to c. 7312 ± 35 ^{14}C yr (S. Bondevik, pers. comm., 2006; Bondevik et al. 2003), and this has been used as a relative time marker and maximum age at the boundary between Unit I and Unit II in core JM98-1 PC. The age model has consequently been adjusted according to this interpretation (Figure 3. 2).

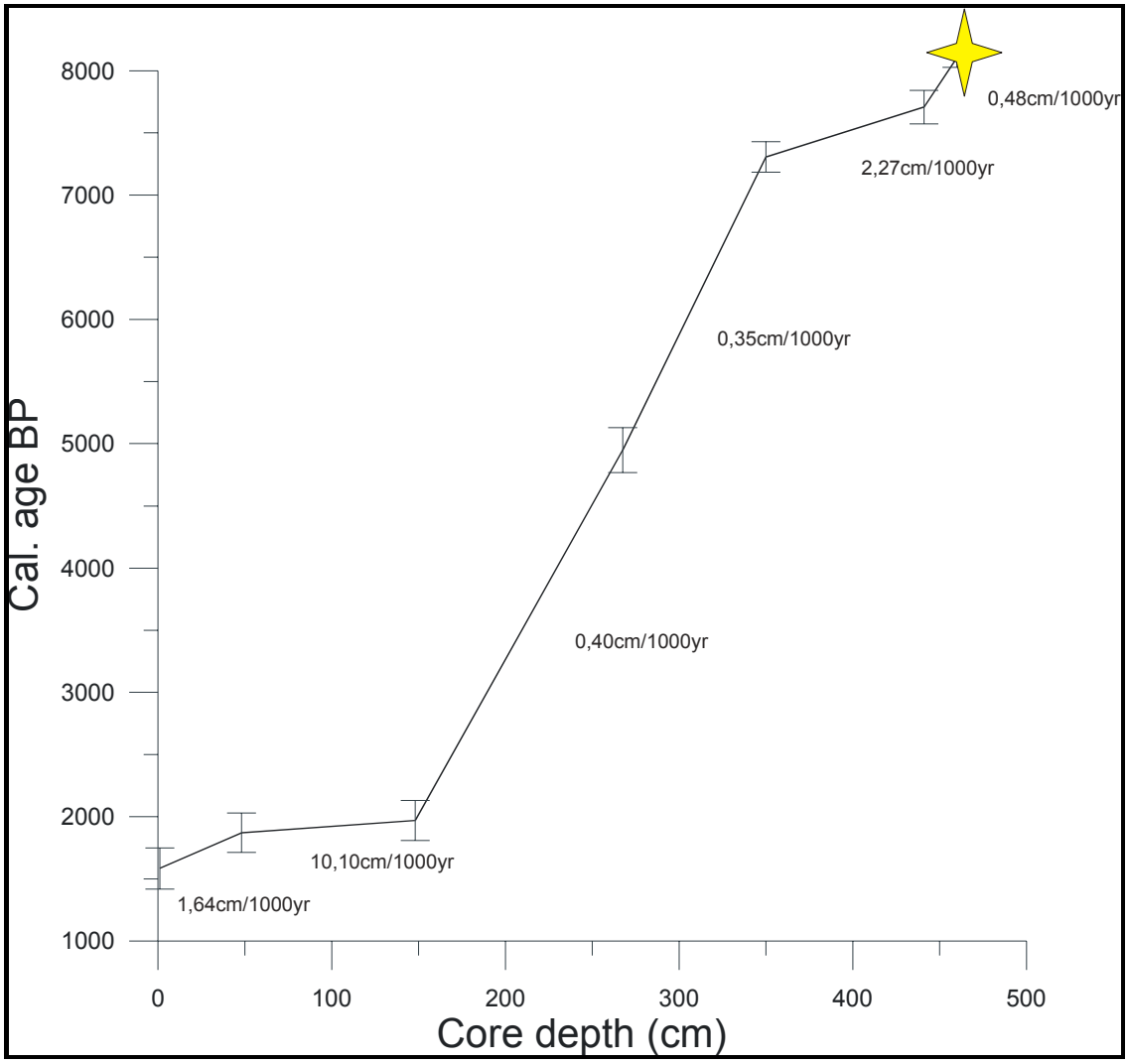

Figure 3. 2 The age model with sedimentation rates from core JM98-1 PC. Linear interpolation was made between the calibrated ages and vertical error bars on the curve indicate 2σ standard deviation for the calibrated ages. The yellow star indicates the Storegga Tsunami-age which has been used as a fixed point and maximum age in the age model.

Linear interpolation was used between the calibrated ages to estimate the sedimentation rate, meaning that we assume the sedimentation rate has been constant between the intervals. The sedimentation rate per 1000 year varies from 10 meters to 0.33 meters (Table 3. 2). The high sedimentation rate at ~10 meters per 1000 years occurs for the period between 1969 – 1870 cal. yrs BP, and this is relatively high compared to the other intervals.

Depth interval (cm)	Cal. age BP interval	Sedimentation rate cm/year	sedimentation rate m/1000 years
1 - 48	1583 - 1870	0,16	1,64
48 - 148	1870 - 1969	1,01	10,10
148 - 267,5	1969 - 4948	0,04	0,40
267,5 - 350	4948 - 7307	0,03	0,35
350 - 441	7307 - 7708	0,23	2,27
441 - 460	7708 - 8105	0,05	0,48

Table 3. 2 Sedimentation rate for core JM98-1 PC calculated per year and per 1000 year by using linear interpolation.

3.1.3 Grain-size distribution

The grain-size distribution shows a large dominance of the fraction < 63 μm (Figure 3. 3). It represents well over 90% of the sediments, with only a few intervals at the lower most part of the unit showing decreasing content. Otherwise, the fraction display an increasingly trend toward present time. The fine sand fraction, 0.063 – 0.1 mm, makes up between 2 – 6% and shows an overall decreasing trend towards present time. The medium sand fraction, 0.1 – 1 mm, also has a decreasing trend upwards in the unit with small fluctuations around 2%. An all time high peak is identified at 430 cm core depth. The coarser fraction > 1 mm fluctuates between 0 – 2% all through the record.

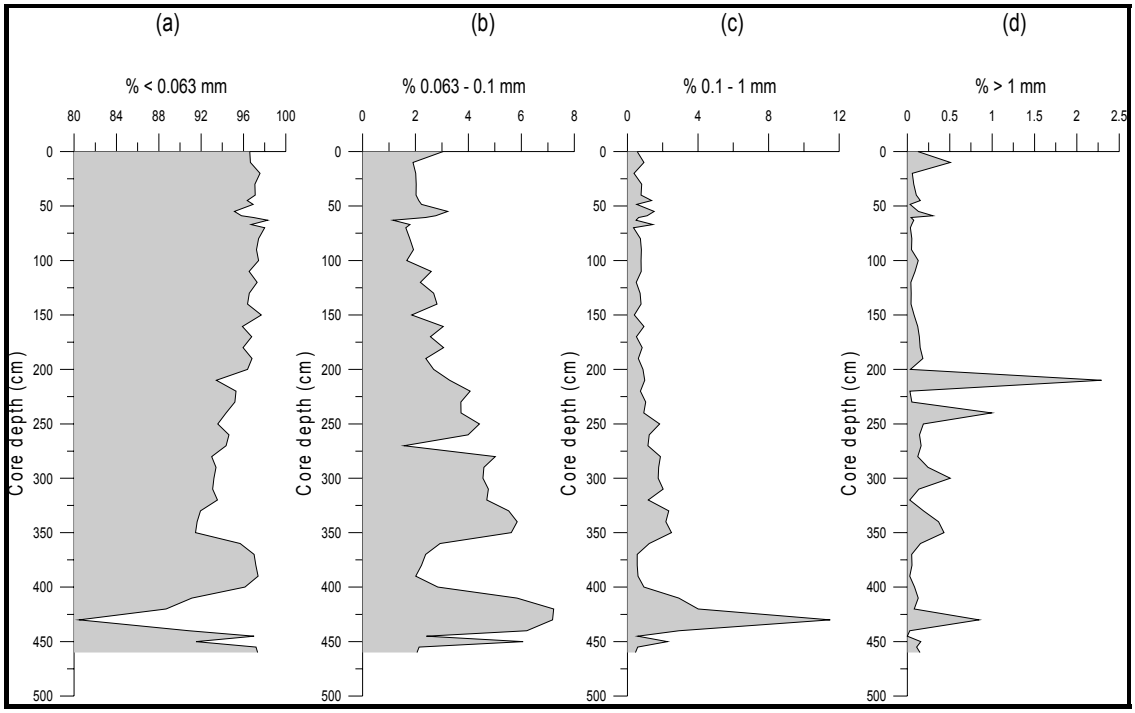

Figure 3. 3 Grain-size distribution for core JM98-1 PC plotted against core depth (cm). (a) % < 0.063 mm. (b) % 0.063 – 0.1 mm. (c) % 0.1 – 1 mm. (d) % > 1 mm.

As the grain-size fraction < 63 μm constitutes over 90% of the sediments in the unit, this fraction was more carefully examined by using the sedigraph. The sedigraph result is presented in Figure 3. 1. From the figure we can read that the grain-size fraction < 63 μm mainly consists of silt (63 μm – 2 μm), while the clay fraction (<2 μm) represent approximately 20%.

3.1.4 Total organic carbon and $CaCO_3$

The curves for the total organic carbon (TOC) and $CaCO_3$ show a parallel trend upwards in the unit (Figure 3. 1). The values are increasing in the lower 150 cm of unit I and appear relatively stable in the upper 300 cm of this unit.

3.1.5 Magnetic susceptibility

The magnetic susceptibility shows a stable signal in the lower 250 cm of unit I, while the upper most 200 cm shows an increasing magnetic signal (Figure 3. 1).

3.1.6 Stable oxygen and carbon isotopes

To allow for a high resolution investigation of the sediment core JM98-1 PC, a number of 178 samples were analyzed with respect to stable isotopes in addition to the samples previously done by Hald et al. (2003); Husum and Hald (2004). Taking the sedimentation rate into account, samples were prepared at an interval of 30-100 years (Figure 3. 4). The lower most part of the unit (430 – 460 cm) had a low number of foraminifera. Some of the intervals in this part of the core had to be combined using the average cm depth and cal. age (Table 3. 3).

depth, cm		average depth, cm	average age, cal. BP
427,25			
428,25		428,25	7545
429,25			
430,25			
431,25		431,25	7554
432,25			
434,25			
436,25		437,00	7573
438,25			
439,25			
442,25			
444,25		444,25	7771
445,25			
446,25			
447,25			
448,25		449	7875
449,25			
450,5			
451,25			

Table 3. 3 Samples with low numbers of the specie *C. neoteretis* had to be combined to give a sufficient amount of foraminifera for the analysis. A new average core depth and calibrated age was calculated from the combined intervals.

This study has provided additional data and higher resolution for sediment core JM98-1 PC, which previously was investigated by Hald et al. (2003). The new record shows an average time resolution of 39 years.

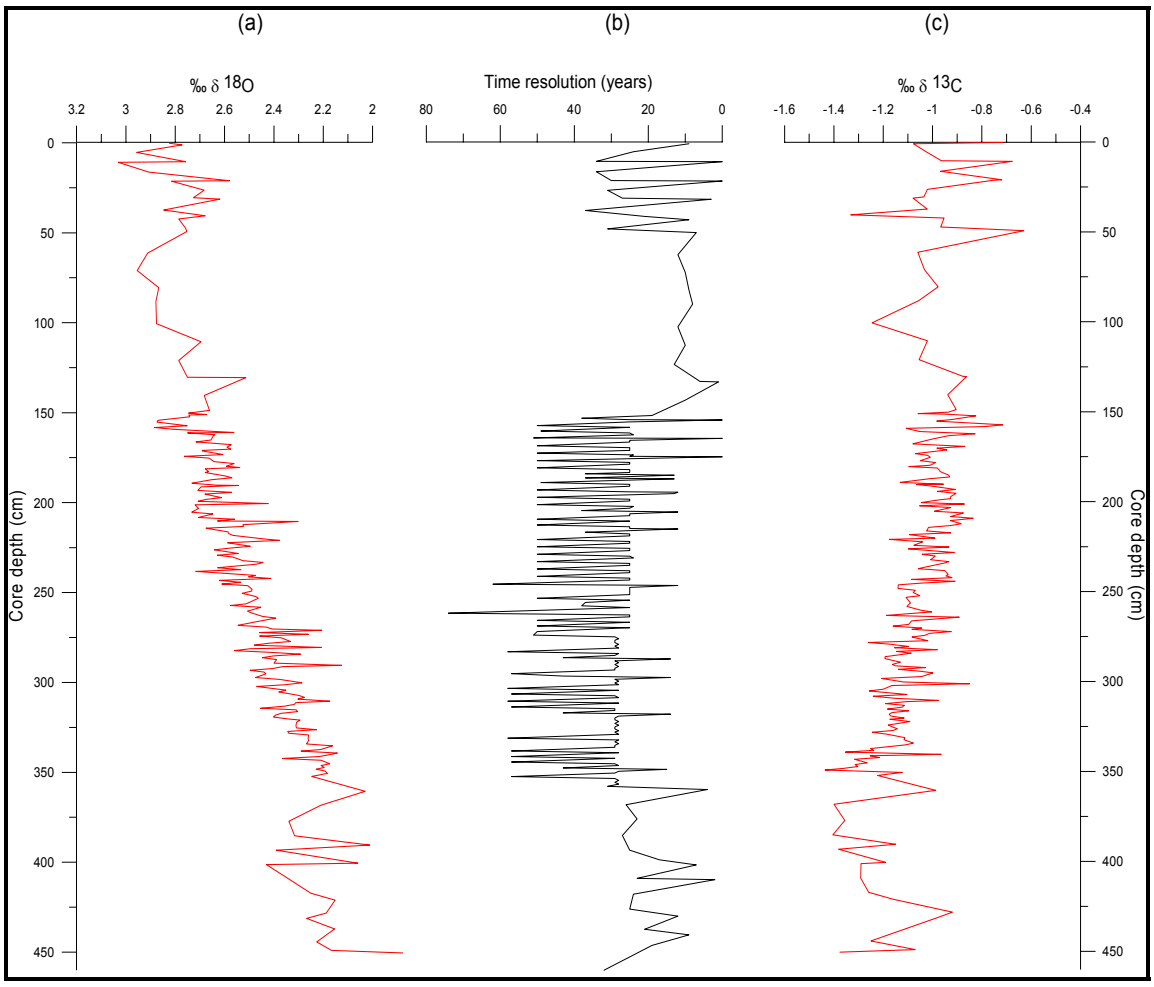

Figure 3. 4 Stable isotope values of the benthic foraminifer *Cassidulina neoteretis* from core JM98-1 PC. (a) ‰ $\delta^{18}O$ isotope values plotted against core depth (cm). All values have been corrected for ice volume effect (Fairbanks 1989). (b) Time resolution plot for the isotope records. Average resolution is 39 years. (c) ‰ $\delta^{13}C$ isotope values plotted against core depth (cm).

The $\delta^{18}O$ values have been corrected for the ice volume effect (Fairbanks 1989), and vary between 1.8 ‰ and 3 ‰ (Figure 3. 4). The result shows a quite clear increasing trend towards the core top. The relatively high resolution for the dataset, which also is indicated in the figure, makes it possible to identify rather rapid, short lasting events in the record.

All the $\delta^{13}C$ results are negative and show an overall trend toward higher values upwards in the core (Figure 3. 4). They vary from -1.44 ‰ to -0.63 ‰, with the higher values in the core top. In particular in the upper part of the core the variations seem to be somewhat larger of amplitude than the oxygen isotopic variations. Low values are seen in the core top and they are comparable with the equally low values at the lower most part of the record.

3.1.7 Compilation of results JM98-1 PC

All datasets from the Malangenfjord record JM98-1 PC are here compiled and plotted against calibrated age BP. For the grain-size distribution it can be recognized some kind of transition at 7 cal. kyr BP (Figure 3. 5), where heavily fluctuated records seem to stabilize. Another thing worth mentioning is the IRD signal which reaches maxima at 3.5 cal. kyr BP. The silt content rises steadily, while the clay fraction seems to have some increasing trend in the upper most part of the record from ~2 cal. kyr BP. This signal is also seen in the water content (Figure 3. 6) which displays increasing level at the same interval as the clay fraction, and subsequently the shear strength decreases (Figure 3. 6). The magnetic susceptibility has after being stable throughout the entire record, an increasing signal at this same transition at 2 cal. kyr BP (Figure 3. 6). The carbonate content has increased gradually upwards in the record, with a slightly decreasing signal at the shift around 2 cal. kyr BP (Figure 3. 6). The stable isotopes from the Malangenfjord record display the long term trend of enrichment, with low amplitude, high frequency, short term changes superimposed on the general trend (Figure 3. 7). Minima levels in the $\delta^{13}C$ record can be identified around 7 and 2 cal. kyr BP.

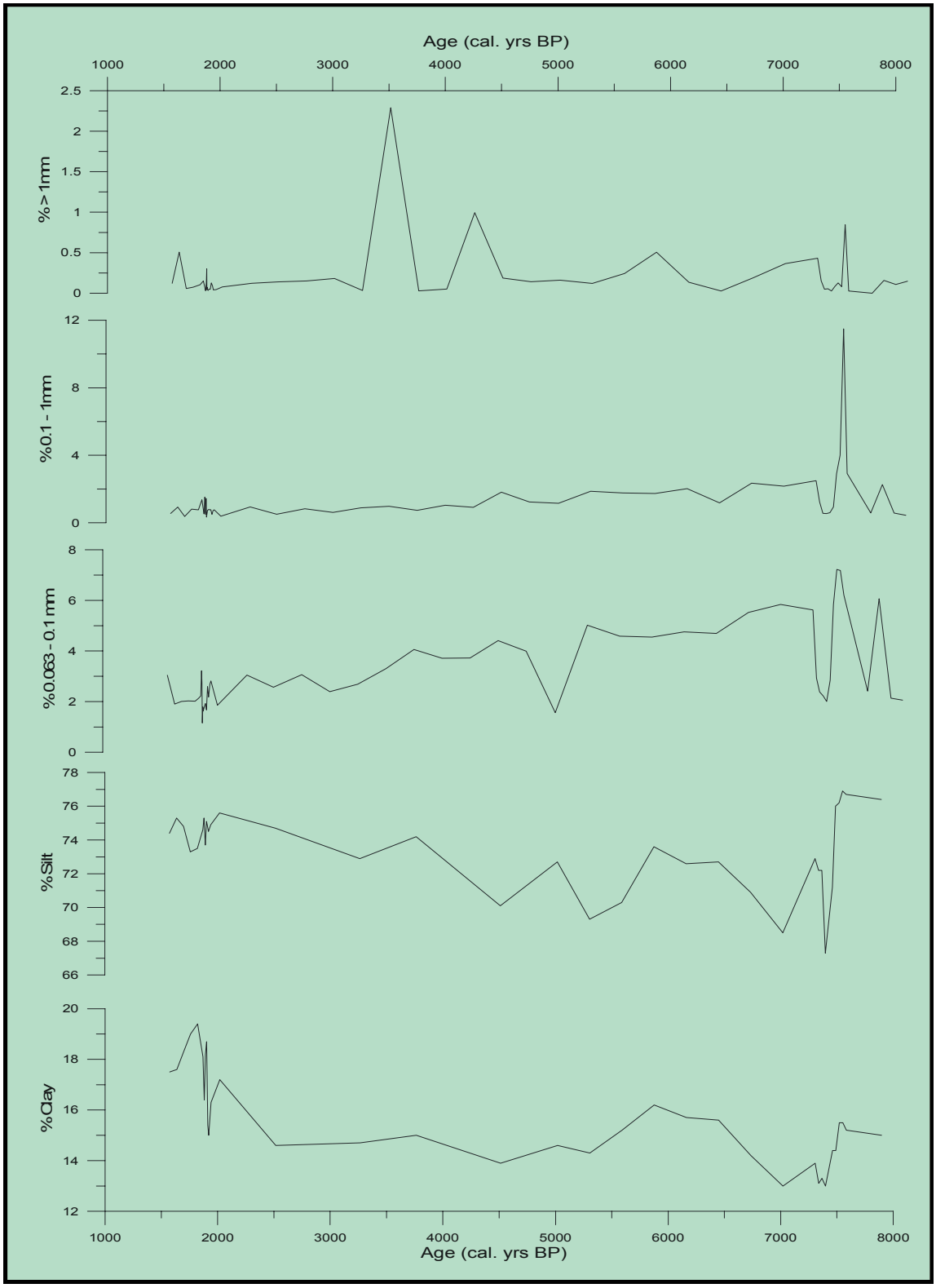

Figure 3. 5 Grain-size distribution for core JM98-1 PC plotted against age (cal. yrs BP).

Figure 3. 6 TC, TOC, $CaCO_3$ and physical properties for core JM98-1 PC plotted against age (cal. yrs BP).

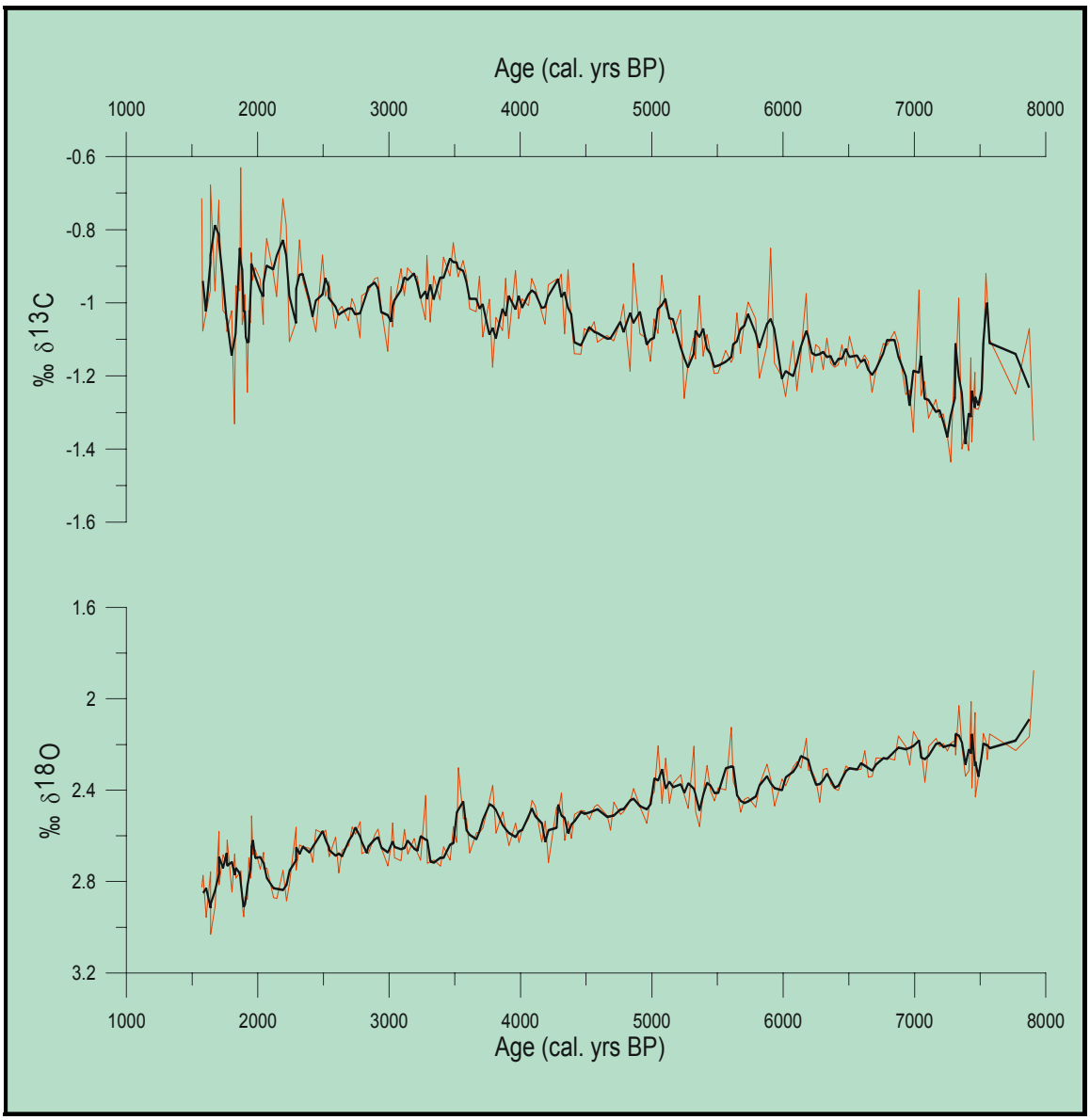

Figure 3. 7 Stable isotopes smoothed with a running average of 3 from core JM98-1 PC plotted against age (cal. yrs BP).

3.2 Core JM05-085 GC – The southern Barents Sea

3.2.1 Lithological description

Only the upper 292.5 cm of the total core length of 487 cm are subject for detailed investigation in this study. This represents the three upper sections made from cutting the core in ~1 meter segments. The visual description of core JM05-085 GC revealed a relatively uniform stratigraphy (Figure 3. 8). Just briefly mentioning section IV and V (292.5 - 487 cm); they are both coarser than the upper three sections, experiencing more pebbles and sand lenses. The units are massive and it is difficult to recognise boundaries. The colour is grey (4/1 2.5y) all through the two last meter sections. Section III (192.5 – 292.5 cm) is containing sandier material compared to the upper two sections and has visible pebbles and sand lenses. The colour is greenish grey (4/2 5y) throughout the whole section. Section II (92.5 – 192.5 cm) and section I (0 – 92.5 cm) changes into a massive clay rich material. The colour is dark grey (3/2 5y) and changes gradually to a brownish grey colour (4/2 2.5y) in the upper 130 cm of the core.

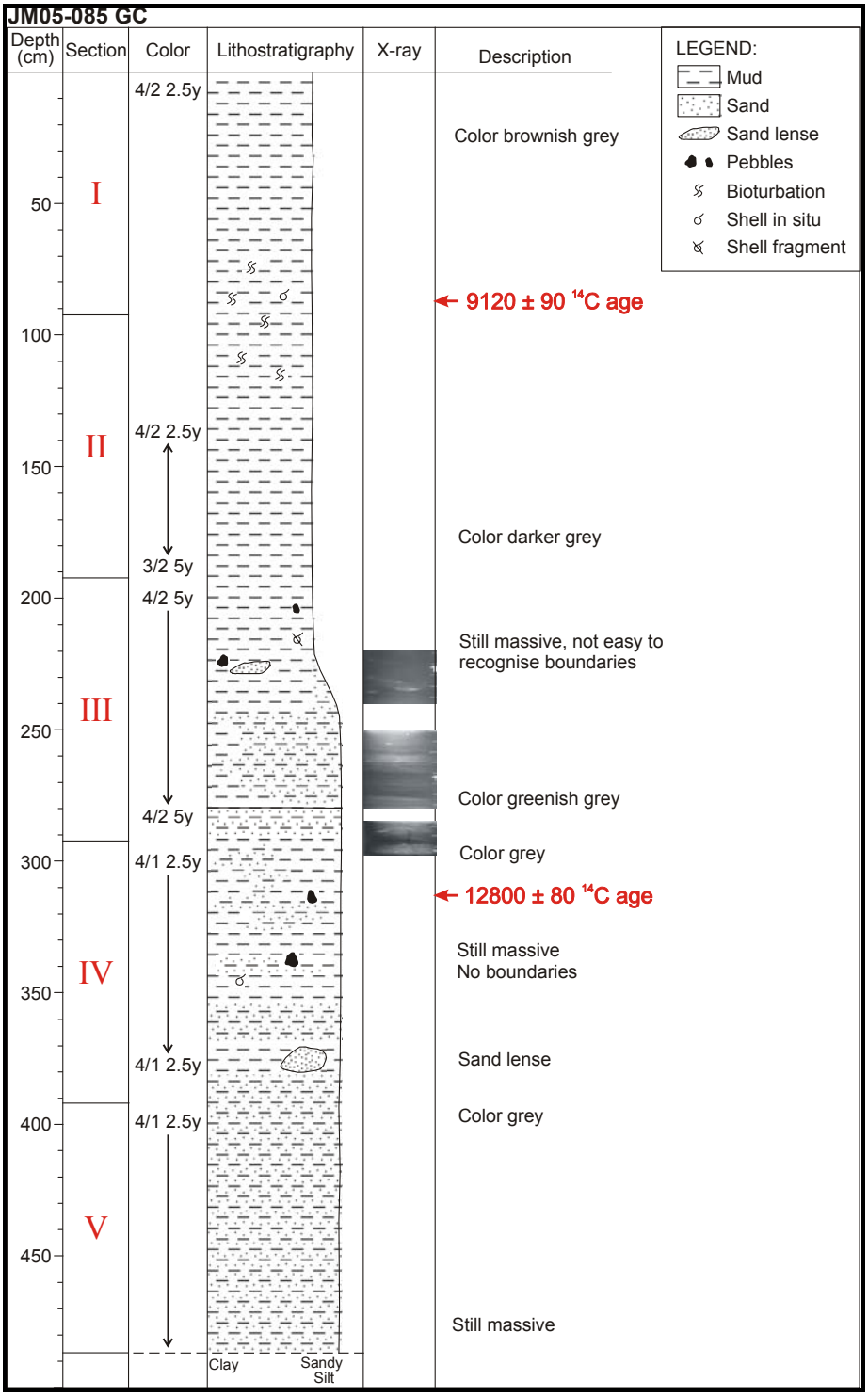

Figure 3. 8 Lithological log with descriptions for core JM05-085 GC. All five sections are included with the total core length of 487 cm. ^{14}C ages derived from shell material at 87 cm and 312 cm are also pointed out.

3.2.2 Chronology and sedimentation rate

Two ages of 9120 ± 90 ^{14}C yr BP and 12800 ± 80 ^{14}C yr BP were dated from the bivalve shells *Bathyarca pectunculoides* and *Bathyarca sp*. (family: *Arcidae*) respectively. This bivalve is widely distributed over the North Atlantic (Tebble 1966), and lives attached to rocks in sandy deep water benthic habitats (Abbot 1996). This reduces the chances for resedimentation and influence of old organic mater from the sediments. The latter is known to be an uncertainty related to deposit feeders in the sense of yielding too old radiocarbon ages (Forman and Polyak, 1997). Both ^{14}C ages were calibrated to calendar years using the latest calibration curve and dataset CALIB version 5.0.2 marine04 (Hughen et al. 2004). The calibration programme designs a curve for the probability of the calibrated ages (Appendix 7.2.2). Each curve were studied closely to make sure the best interval was chosen, and it was decided to use the arithmetic mean for the 2σ age interval of highest probability (95.4%) in all cases. This gave calibrated ages of 10360 and 15070 (rounded up to nearest 10 yr) (Table 3. 4).

Lab code	Core id.	Depth (cm)	^{14}C age	Calibrated age BP	2σ maximum cal. age (cal. age intercepts) minimum cal. age	Material	Weight (mg)	Relative area under probability distr.
TUa5657	JM05-085 GC	87	9120 ± 90	10360	10543 (10358) 10172	Bathyarca pectunculoides	0,0431	1.000
TUa5658	JM05-085 GC	312	12800 ± 80	15070	15408 (15074) 14740	Bathyarca sp.	0,0138	1.000

Table 3. 4 Radiocarbon ages from core JM05-085 GC. The dates have been calibrated with the CALIB version 5.0.2 marine04 (Hughen et al. 2004) using a ΔR of 65 years ± 35.

The age model and sedimentation rate (Figure 3. 9) for core JM05-085 GC is based only on the two ^{14}C dates obtained at 87 cm and 312 cm core depth. An assumption that the core top represents present day time was made when reconstructing ages with linear interpolation. By this assumption one should keep in mind that the core top could actually be missing or disturbed. There was however no signs of disturbance in the core top when visually inspecting the core. With only two dating points in the sediment core, the age model is considered to be preliminary and subject to large uncertainties compared to the

Malangenfjord record. The sedimentation rate is somewhat modest throughout the core, varying only from 0.08m – 0.4m / 1000yrs (Table 3. 5).

Depth interval (cm)	Cal. age BP interval	Sedimentation rate cm/year	sedimentation rate m/1000 years
0 - 87	0 - 10358	0,008	0,084
87 - 312	10358 - 15070	0,048	0,477

Table 3. 5 Sedimentation rate for core JM05-085 GC calculated per year and per 1000 year.

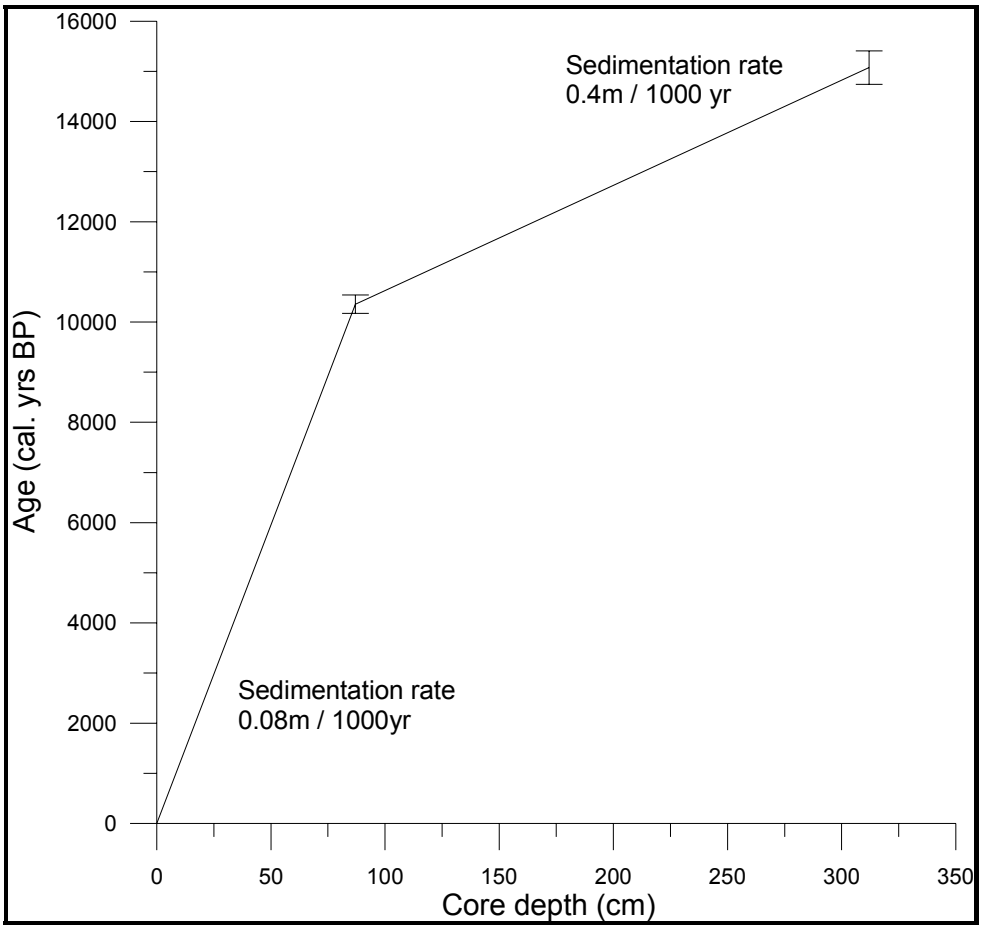

Figure 3. 9 The age model with linear interpolation for core JM05-085 GC. Sedimentation rates are also specified. Vertical error bars on the curve indicate the 2σ standard deviation for the calibration of ^{14}C ages.

3.2.3 Grain-size distribution

The grain-size distribution in core JM05-085 GC is illustrated by Figure 3. 10, and it shows that the sediment mostly consists of the fine fraction < 0.063 mm. The level seems to be fairly constant throughout the record, with a small decreasing interval around 150 cm core depth. For the upper part of the core this fine fraction stabilizes and accounts for as much as 96%. The fraction 0.063 mm shows fluctuations throughout the entire record and steadily increases towards upper parts of the core. The 0.1 mm fraction fluctuates in the lower parts and displays a maximum content around 150 cm core depth and then decreases upwards. The coarser fraction > 1 mm is present with some small maxima in the lower parts of the core, and decreases almost completely upwards with only some scattered existences (Figure 3. 10).

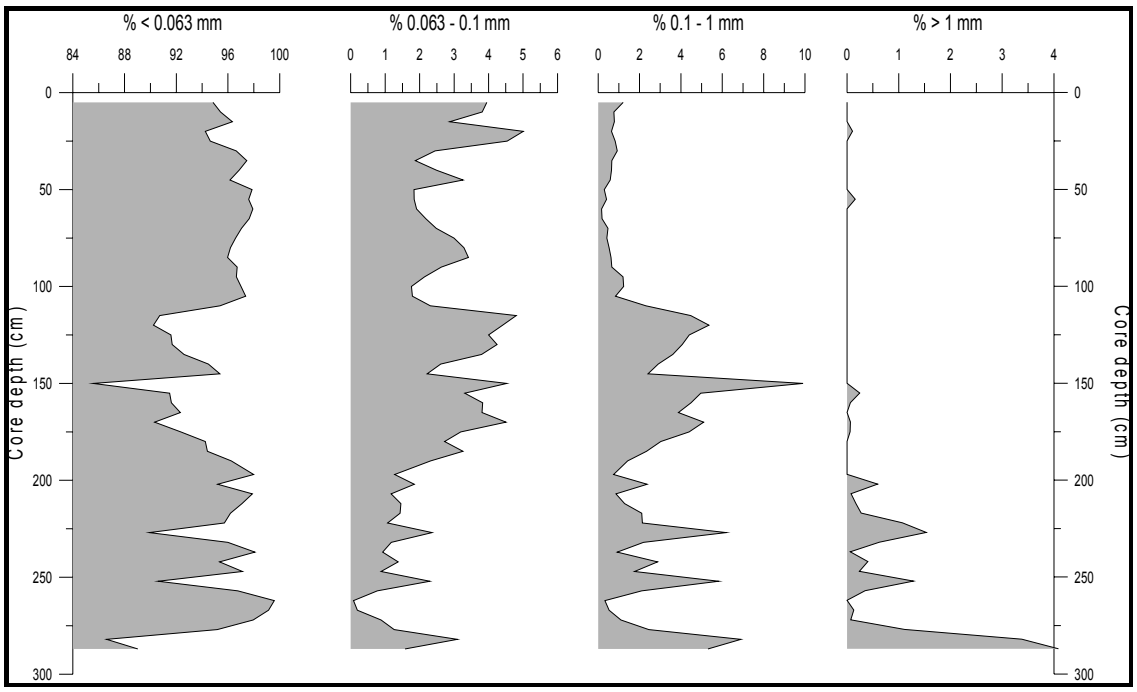

Figure 3. 10 Grain-size distribution for core JM05-085 GC plotted against core depth (cm).

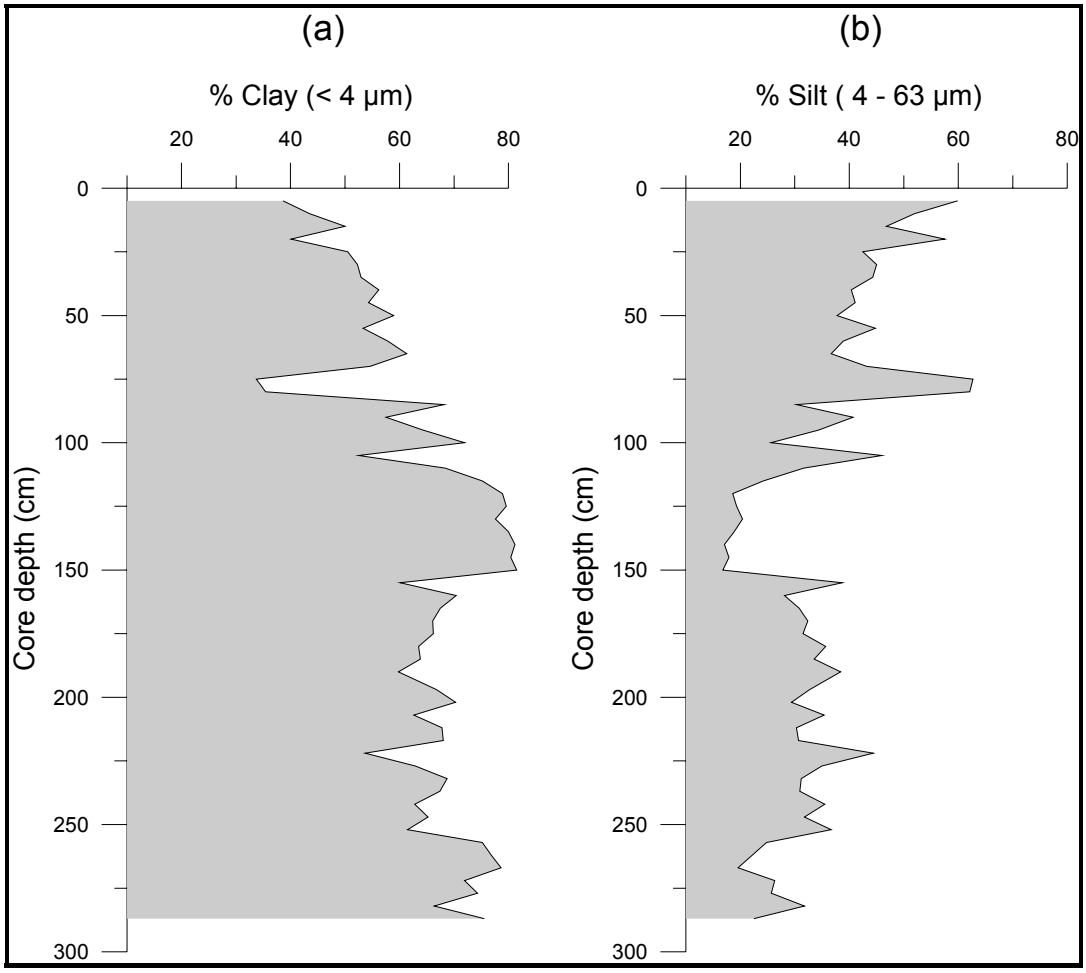

Figure 3. 11 Sedigraph results for core JM05-085 GC plotted against core depth (cm). (a) % clay. (b) % silt.

As the fine fraction forms such a large part of the sediments, it was further analysed using the sedigraph in order to differentiate between the silt (63 – 4 µm) and clay (< 4 µm). The clay content fluctuates around 60% in the lower parts of the core, and representing almost 80% in the interval between 150 – 110 cm core depth (Figure 3. 11). After this clay maximum-interval, the content decreases to 40 – 50% in the upper 100 cm of the core. The silt fraction is fluctuating around 40% in the lower part of the core, and representing only 20% in the interval between 150 – 110 cm core depth. The silt content increases to c. 60% in the upper 100 cm of the core. There seems to be a transition in the distribution of clay and silt at approximately 100 cm core depth.

3.2.4 Undrained shear strength

The fall-cone test was done every 10 cm in the sediment core JM05-085 GC, and the undrained shear strength was calculated from existing tables (Hansbo 1957). The shear strength varies from 1.8 – 5.9 t/m^2 and do not seem to be stable at any part in the record (Figure 3. 12).

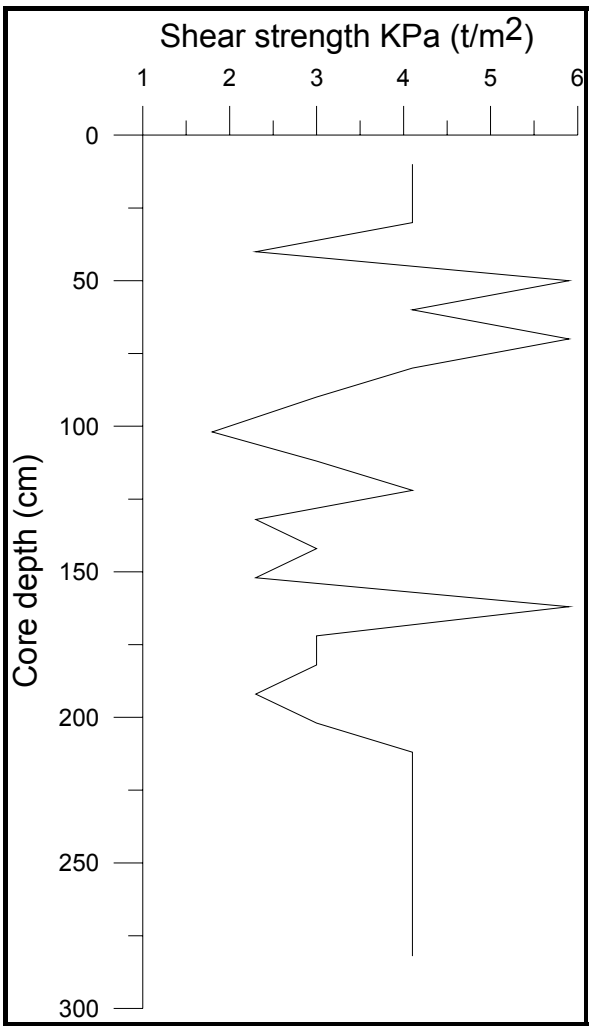

Figure 3. 12 Undrained shear strength calculated from fall-cone test and conversion tables (Hansbo 1957).

3.2.5 Radiography

From the radiography of core JM05-085 GC it was possible to detect subsurface features as bioturbation and clasts. Only selected examples of the most interesting photos are presented here (Figure 3. 13). Nothing much could be identified in the upper 170 cm. The first clasts / IRD-event is between 220 - 230 cm core depth (Figure 3. 13a). From this interval and downcore, more is happening in terms of clasts, IRD and sub horizontal lamination as interpreted in Figure 3. 13.

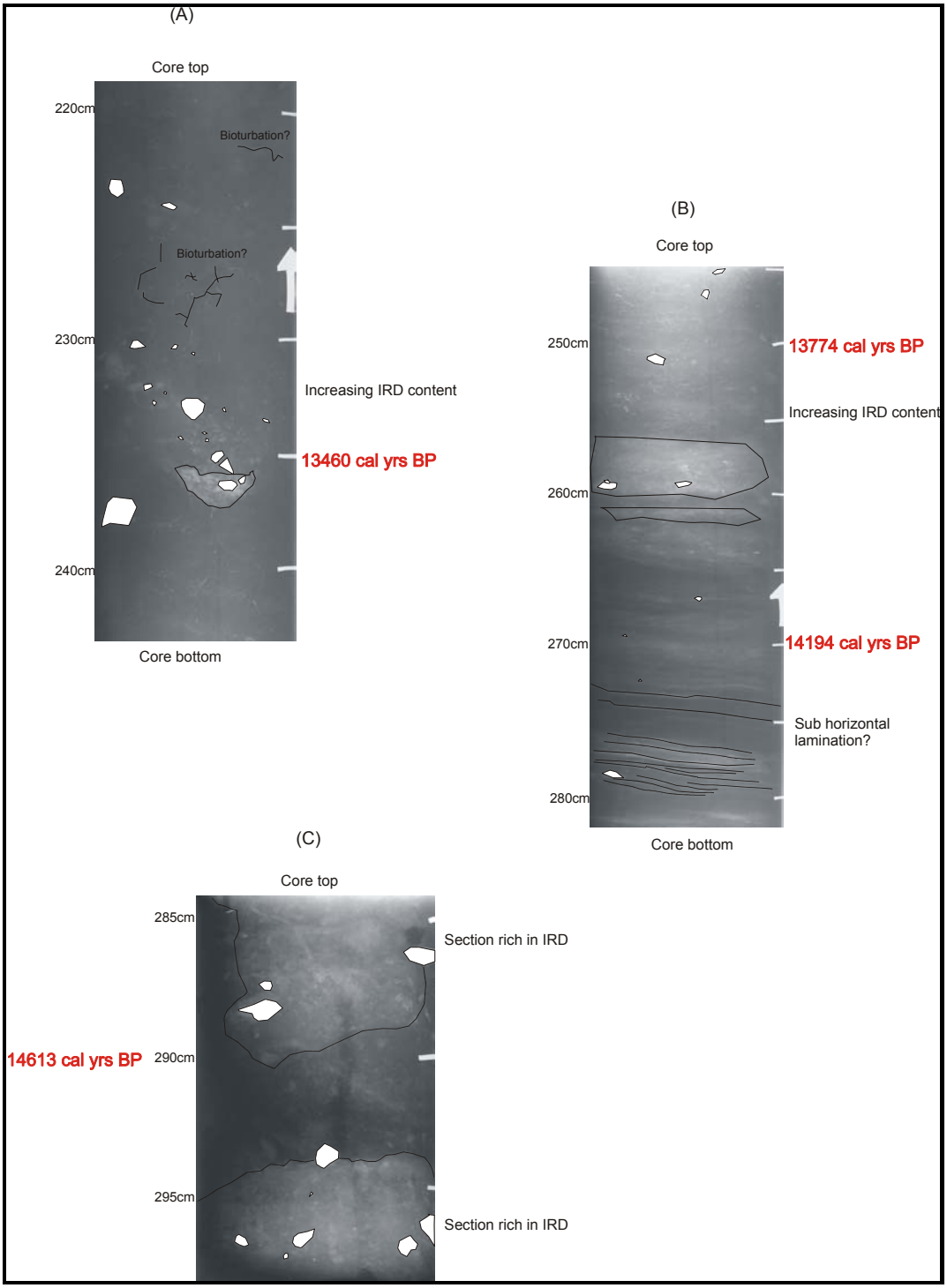

Figure 3. 13 Radiography photos from selected intervals in core JM05-085 GC. (a) Core depth 220 – 240 cm, IRD event. (b) Core depth 245 – 280 cm, IRD events and sub horizontal lamination. (c) Core depth 285 – 295 cm, sections rich in IRD. Age (cal. yrs BP) is also indicated. The lithological log in figure 3.5 shows intervals for the photos.

3.2.6 Total carbon and total organic carbon

The total carbon (TC) and total organic carbon (TOC) was measured every 5 cm in core JM05-085 GC. From the assumption that the inorganic carbon represents calcium carbonate, the ‰ $CaCO_3$ was calculated (Figure 3. 14).

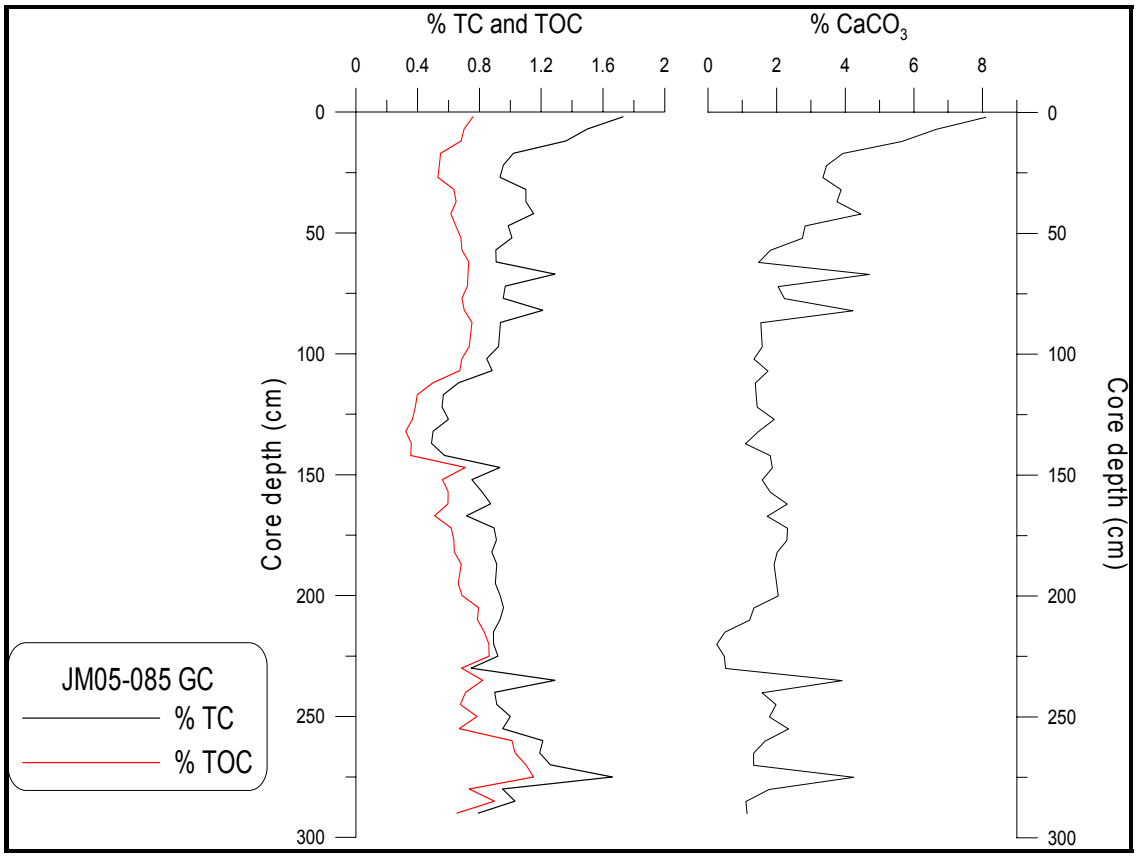

Figure 3. 14 Left side: Total carbon and total organic carbon for core JM05-085 GC plotted against depth in core (cm). Right side: % $CaCO_3$ for core JM05-085 GC plotted against core depth (cm).

The total carbon content constitutes less than 2 %, and the total organic carbon amount to less than 1 % in the sediment (Figure 3. 14). The two curves fluctuate and run parallel throughout the core. Both records seem to decrease in the lower parts of the core until approximately 110 cm, where the TOC curve flattens and the TC curve increases slightly toward the core top. The $CaCO_3$ curve fluctuates around 2% in the lower 200 cm of the core, while the upper 100 cm show an increase in the record (Figure 3. 14).

3.2.7 Multi sensor core logging

From the MSCL the following results are presented; P-wave velocity, sediment density, magnetic susceptibility and impedance. All records seem to be relatively stable with only small fluctuations (Figure 3. 15). The anomalies in the P-wave velocity are most probably related to the cutting of the core sections at 92.5 cm and 192.5 cm depth. The density record decreases in the core top, and this could be due to the fact that the upper core section was not completely filled with sediments in the top. The magnetic susceptibility fluctuates somewhat in the lower parts, and shows a decreasing trend upwards from approximately 225 cm. The impedance record follows the density curve quite well.

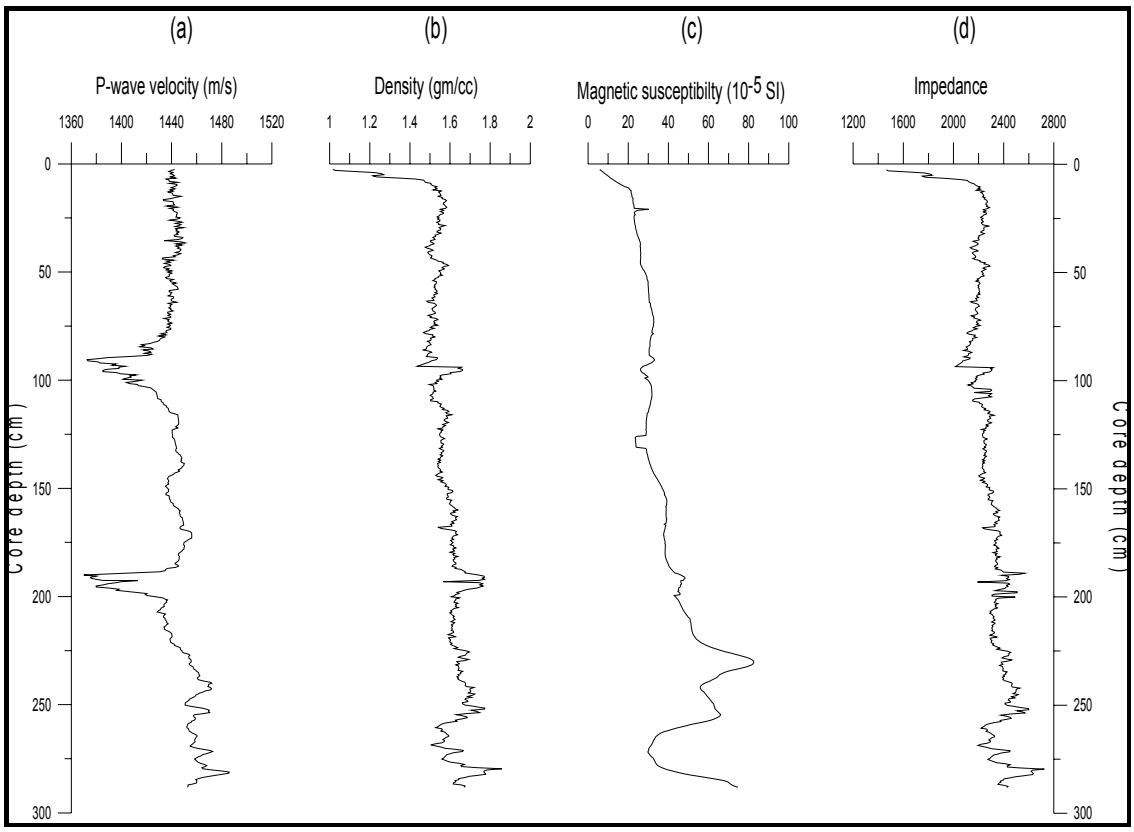

Figure 3. 15 A compilation of the MSCL-results for core JM05-085 GC plotted against core depth (cm). (a) P-wave velocity (m/s^2). (b) Density (gm/cc). (c) Magnetic susceptibility (10^{-5} SI). (d) Impedance (ρ*v)

3.2.8 Stable oxygen and carbon isotopes

A number of 46 samples were analysed from the sediment core JM05-085 GC, and this represent approximately every 5 cm through the upper 3 meters of the core. The upper most meter of the core (section I) had an abundant number of *Cassidulina neoteretis*, while section II and section III contained less amount. The depth intervals between 125 cm – 150 cm (section II) and 252 cm – 277 cm (section III) had little or no foraminifera for isotope analysis, and thus measurements are lacking for these barren zones.

The $\delta^{18}O$ values have been corrected for the ice volume effect (Fairbanks 1989), and vary between 3.87 ‰ and 2.69 ‰ (Figure 3. 16). At the lower most part of the core the values are relatively heavy and fluctuating rather much. Well-defined lighter peaks are found at 212 cm, 165 cm, 125 cm and 110 cm core depth, whereas one prominent heavier peak is identified at 100 cm depth. After the heavy peak at 100 cm depth the degree of fluctuations and values decrease, with its minimum value at 60 cm before increasing again towards the core top.

The $\delta^{13}C$ values vary between -1.0 ‰ and 0.02 ‰ (Figure 3. 16). Also the carbon isotope record show higher amplitude fluctuations in the lower most part of the core. It seems like the amplitude of the fluctuations are decreasing upwards after 100 cm core depth. The general trend for the carbon values is toward smaller values upwards in the core until 50 cm depth, where the curve show increasing values towards the core top.

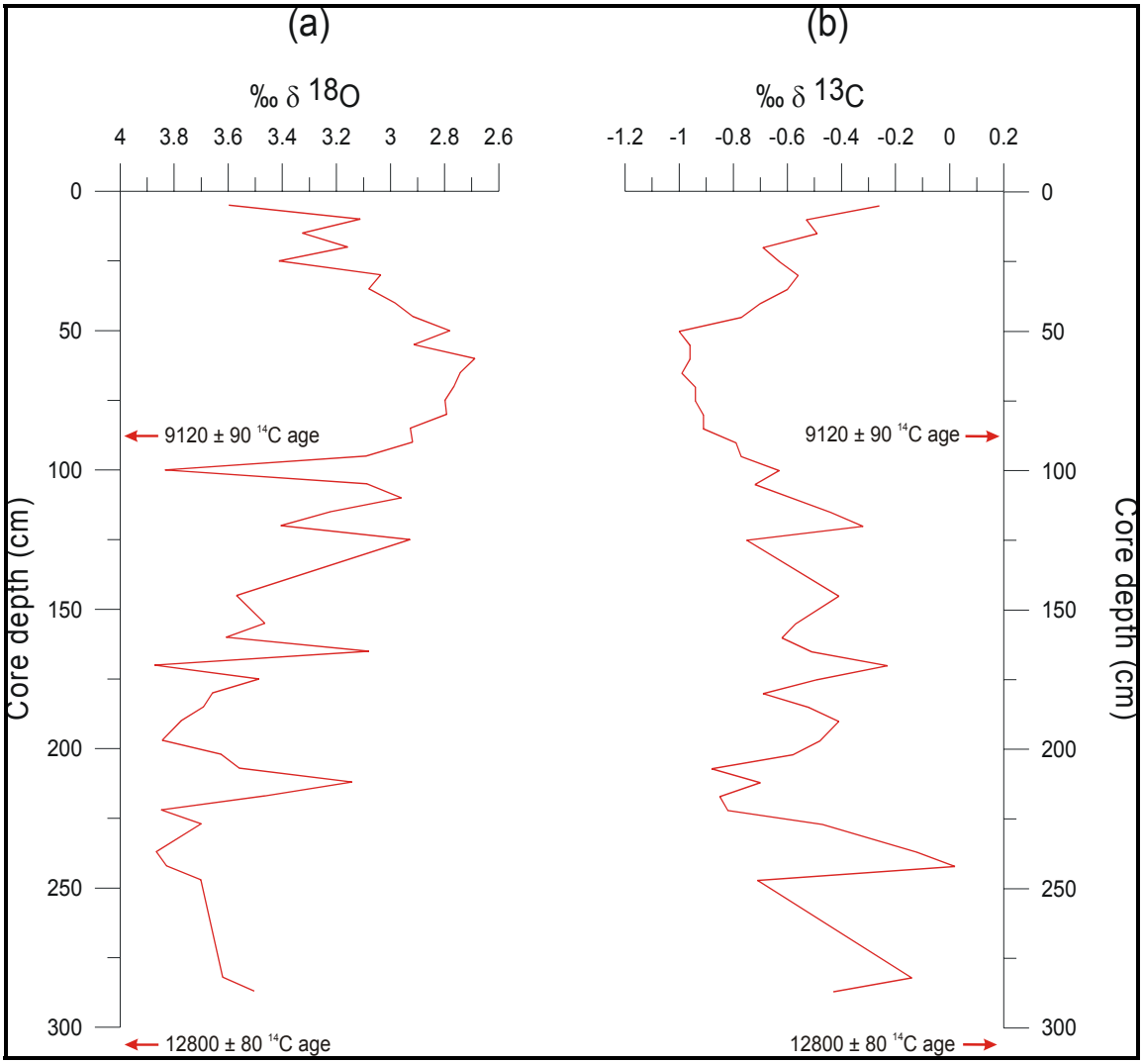

Figure 3. 16 Stable isotope values from core JM05-085 GC measured on the benthic foraminifer *Cassidulina neoteretis* plotted against core depth (cm). The two ^{14}C ages from 87 cm and 312 cm in the core are also indicated. (a) ‰ $^{18}O/^{16}O$ isotope values. All values have been corrected for ice volume effect (Fairbanks 1989). (b) ‰ $^{13}C/^{12}C$ isotope values.

3.2.9 Compilation of results JM05-085 GC

All datasets from the Ingøydjupet record JM05-085 GC are here compiled and plotted against calibrated age BP. For the grain-size distribution it can be seen that all fractions have relatively many fluctuations in the lower parts from 15 – 10.5 cal. kyr BP (Figure 3.

17). There seems to be some kind of shift in the records between 11 – 10 cal. kyr BP, where the coarser fractions get less dominant and the silt fraction increases. The multi sensor core logger-results are plotted against calibrated age in Figure 3. 18 and all records have fluctuations in the lower parts from 15 – 10.5 cal. kyr BP. Also here it seems to be a transition at around 11 – 10 cal. kyr BP. After this period the records are fairly stable with only small excursion in the upper parts. In Figure 3. 19 the stable isotopes are plotted against calibrated age together with TC, TOC, $CaCO_3$ and one of the physical properties, undrained shear strength. The $\delta^{18}O$ record is unstable and fluctuating with heavy values in the lower parts from 15 – 10.5 cal. kyr BP (Figure 3. 19). From 10.5 cal. kyr BP the $\delta^{18}O$ record become depleted and it is relatively stable until the shift between 7 - 6 cal. kyr BP. After this the $\delta^{18}O$ signal is getting gradually enriched towards present day time. The $\delta^{13}C$ record also shows fluctuations in the lower parts from 15 – 10.5 cal. kyr BP with high values (Figure 3. 19). After the transition at 10.5 cal. kyr BP, the values are relatively low but stable until ~ 6 cal. kyr BP. The upper and youngest part of the $\delta^{13}C$ record show increasing values. The carbonate content undulated around 3% in the lower parts from 15 – 6 cal. kyr BP (Figure 3. 19). After the transition at 6 cal. kyr, the CaCO3 content is increasing gradually, reaching its maximum of 8% in the core top.

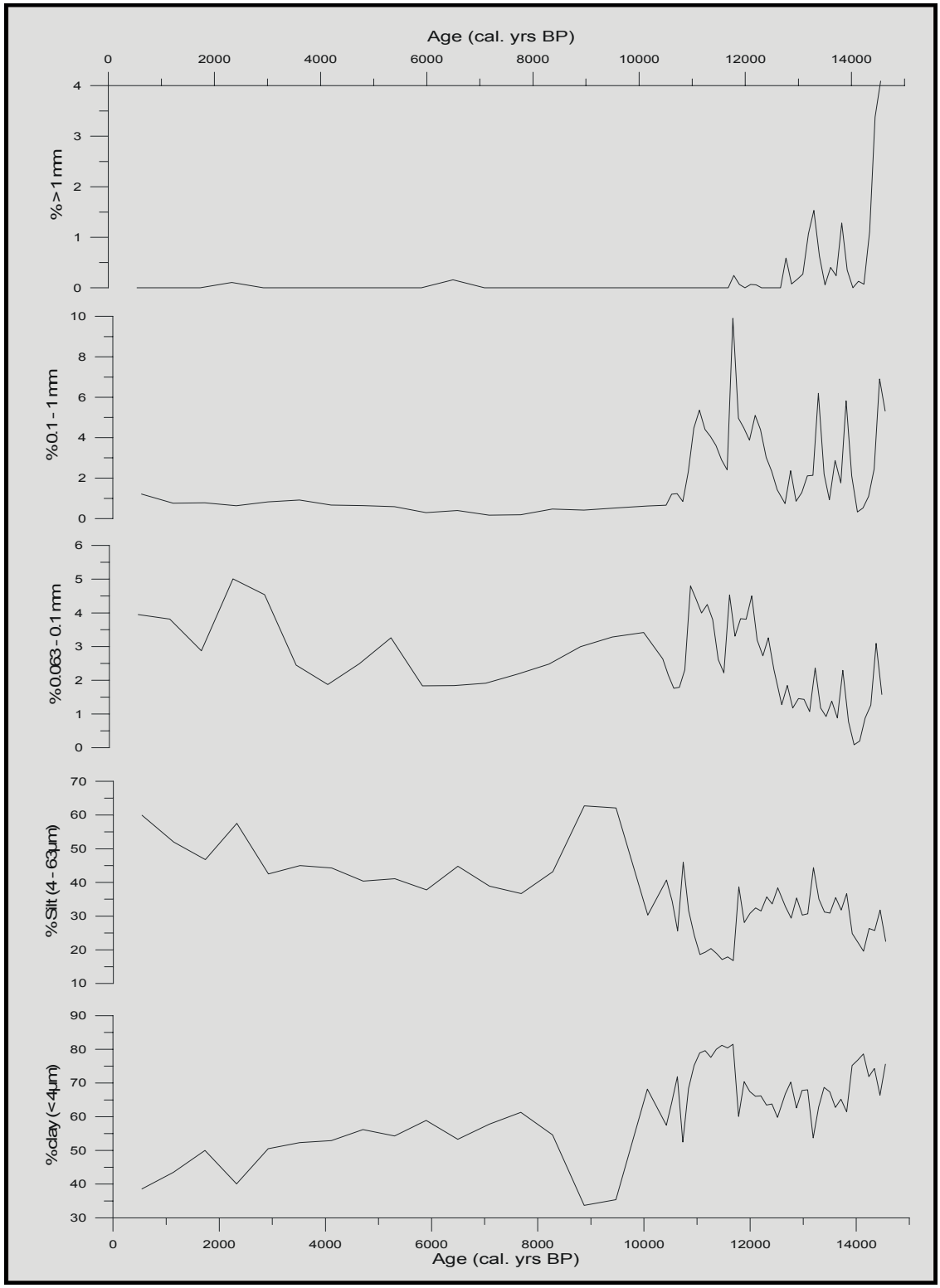

Figure 3. 17 Compilation of grain-size distribution for core JM05-085 GC plotted against age (cal. yrs BP).

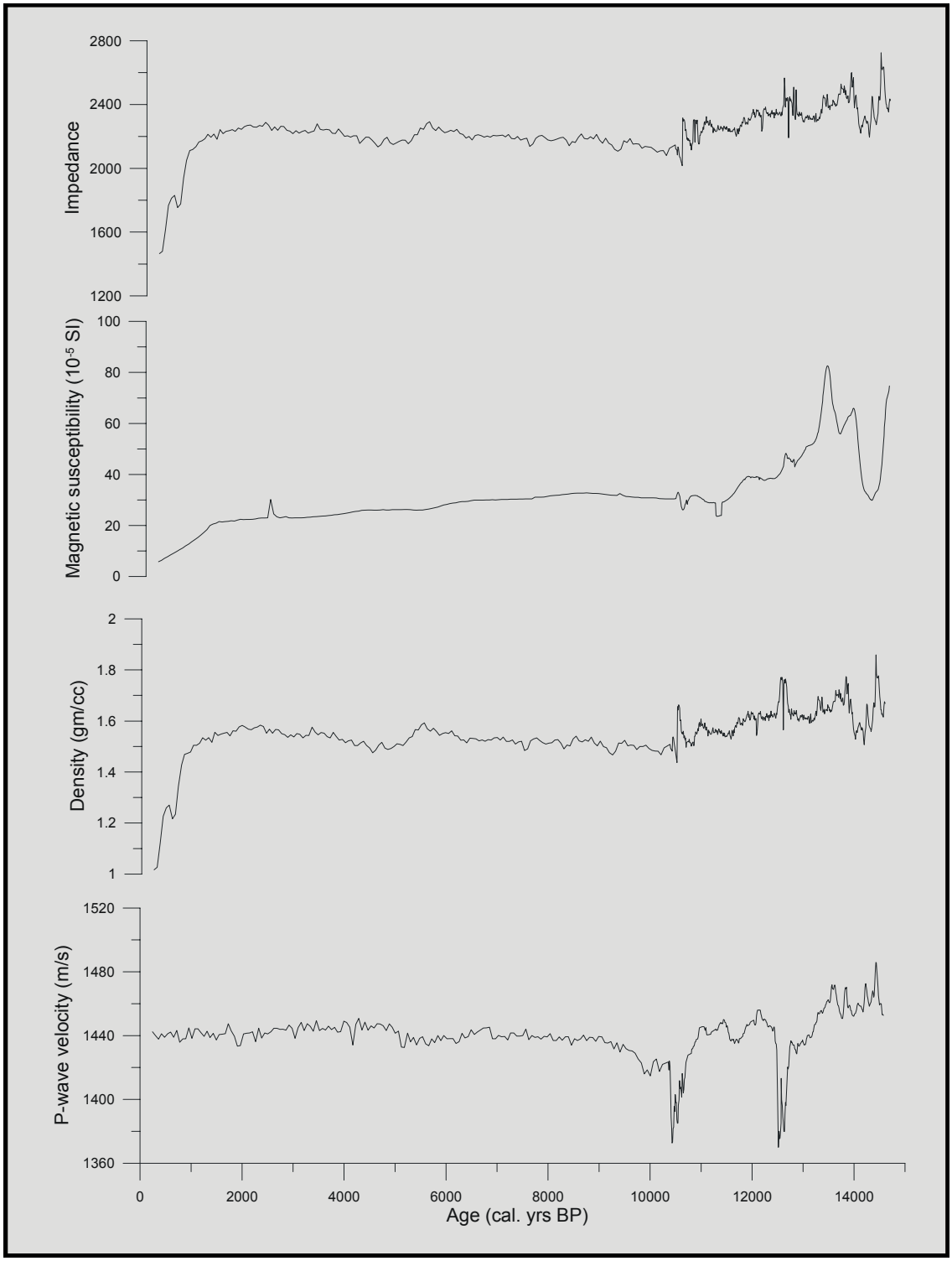

Figure 3. 18 Multi sensor core logger-results for core JM05-085 GC plotted against age.

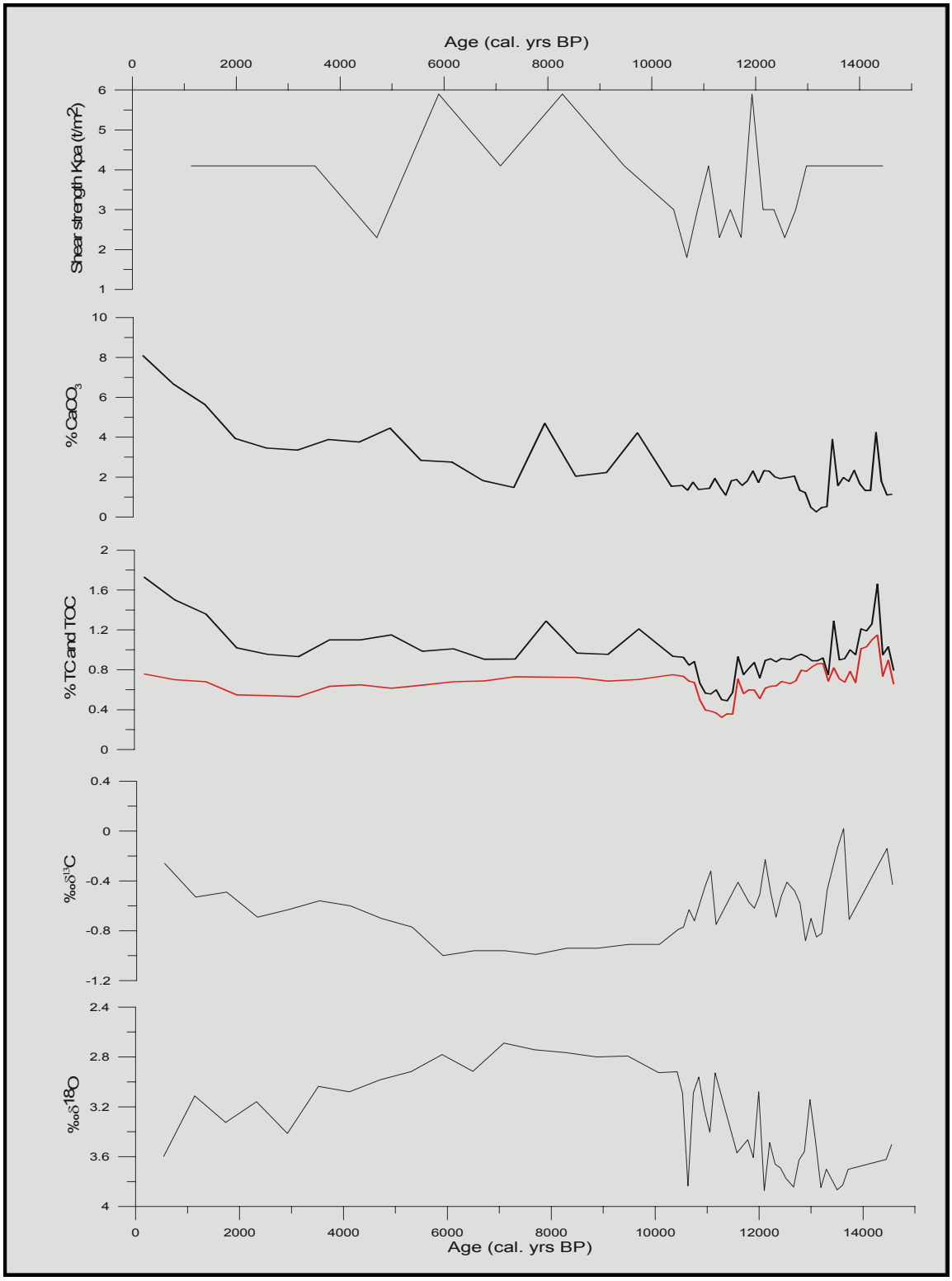

Figure 3. 19 Stable isotopes, TC, TOC and $CaCO_3$ from core JM05-085 GC plotted against age (cal. yrs BP).

4 Discussion and interpretations

The aim of this chapter is to look into the results and reconstruct the bottom water temperatures and paleoceanography in the Malangenfjord and southern Barents Sea. This has been done by using the stable oxygen and carbon isotopes as proxies. The oxygen isotopes reflect as we know the temperature and the isotopic composition of the water (i.e. salinity and global ice volume). After correcting the $\delta^{18}O$ signal for the ice volume effect (Fairbanks 1989) (Figure 4. 1), the remaining signal is mainly related to changes in temperature and salinity. We are using the relationship that 0.2‰ change in the $\delta^{18}O$ corresponds to 1°C temperature change (Shackleton 1974) and based on the North Atlantic mixing line that 0.6‰ change in the $\delta^{18}O$ might represent 1‰ salinity change (Andersson et al. 2003). When it comes to factors controlling salinity changes we should consider precipitation, river runoff, melting of local glaciers or a change in the rate of water mixing (Duplessy et al. 2005). For the Malangen-record which spans 8000 – 1600 cal. yrs BP it is assumed that little ice is present in the system, but for the Barents Sea-record which covers a period over the last 15000 cal. yrs BP, one has to consider the final phase of the deglaciation (15 – 11.5 cal. kyr BP) and possible meltwater events resulting from it.

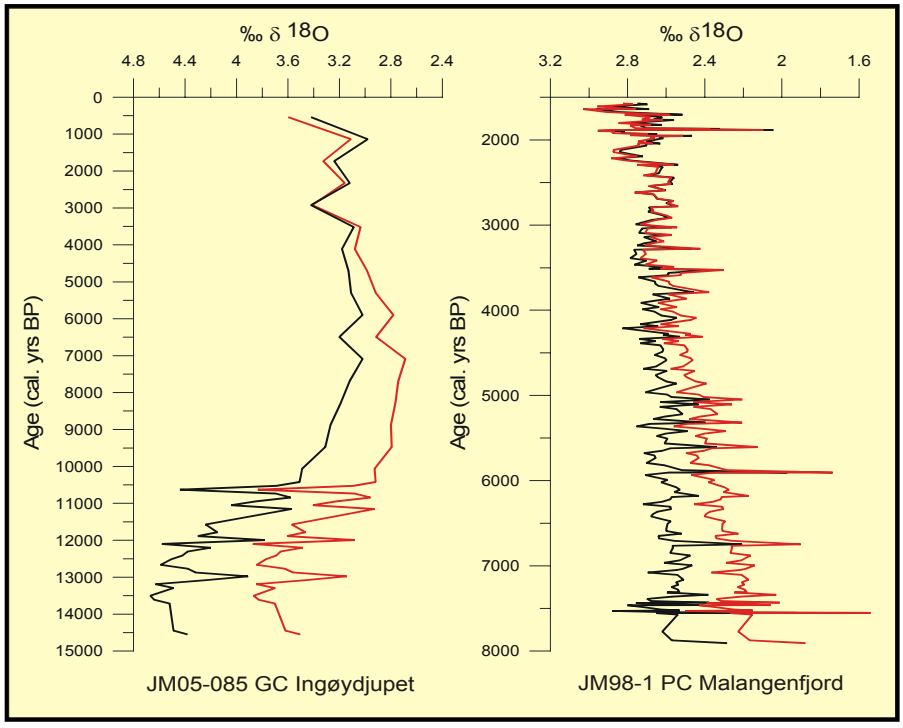

Figure 4. 1 Plot showing the ice volume effect for both records. Black curves illustrate oxygen isotopes affected by the ice volume. Red curves show oxygen isotope values corrected for the ice volume.

4.1 The final phase of the deglaciation 15 – 10.5 cal. kyr BP

This period is only represented by sediment core JM05-085 GC from Ingøydjupet in the southern Barents Sea. The stable oxygen isotope record show minimum values of 2.9‰ and maximum values of 3.8‰ with the general trend toward lighter values in this interval (Figure 4. 2). If we were not to correct for the global ice volume, the oxygen isotope values would be enriched with 0.6 – 0.8‰ for this period (Figure 4. 1). From the study of Fairbanks et al. (1989) we know that 10m sea level change equals 0.11‰ $\delta^{18}O$. With the assumption that the isotopic signal reflects temperature changes, the record show a variation between 1.5°C and 5°C (Figure 4. 2). The record starts out with a bottom temperature of 2.8°C in what has been interpreted as part of the Bølling interstadial, and following this is a 1.5°C decrease in temperature in a stadial most likely the Older Dryas (Figure 4. 2). Allerød interstadial is entered at ~13 cal. kyr BP with virtually a 3°C warming, giving temperatures similar as present in the southern Barents Sea. An almost 3°C drop in temperature indicates the onset of Younger Dryas at 12.8 cal. kyr BP. The initiation of the Holocene interglacial is seen with a 2.5°C warming in Preboreal at 11.5 cal. kyr BP, a period characterized by several fluctuations which is a widespread signal in the North Atlantic (Husum and Hald 2002). The pronounced peak at ~10.6 cal. kyr BP indicating a severe temperature drop of 3°C prior to the thermal optimum has been measured twice by the GMS-laboratory in Bergen, and thus should reflect a trustworthy value (Figure 4. 2).

The 0.9‰ change in the oxygen isotope signal is equivalent to a 1.5‰ change in the bottom water salinity, and this is relative large numbers realistically speaking. As long as this study do not provide any independent proxy record for temperature, it is difficult to distinguish whether the oxygen isotope signal reflects temperature or salinity, ideally it will probably reflect a bit of both. Risebrobakken et al. (2003) concluded that both the North Atlantic and Nordic Sea mixing lines only gave insignificant small changes in the salinity for their study area in the Nordic Seas, and related the $\delta^{18}O$ signal to temperature changes only. Most of the deglaciation had already taken place outside the coast of Finnmark in the southern Barents Sea, and the Younger Dryas moraine is situated well inland (Jørgensen et al. 1997), but IRD signals provide evidence of glacial influence in this final phase of the

deglaciation. Freshwater input from decaying ice sheets, ice bergs or sea ice has a very low $\delta^{18}O_{water}$ signal compared to the saline member of ocean water, and the rejection of brine during sea ice formation will also affect the bottom water salinity. Sea level changes could also alter the influence of river runoff. The IRD peaks seem to correlate with the light isotope intervals / warm periods at 14.5 and 13 cal. kyr BP, and especially the peak at 13 cal. kyr BP can be taken for a meltwater event with light $\delta^{18}O$ and $\delta^{13}C$ values in combination with IRD (Figure 4. 2). The Bølling/Allerød period is not well defined in this record which is not of very high resolution, but there are lighter peaks in the $\delta^{18}O$ signal which can be interpreted as these warm periods. The carbon isotopes also fluctuate significantly, with the general trend towards smaller values. The only positive value in the $\delta^{13}C$ record is at 13.6 cal. kyr BP with a maximum value of 0.02‰. This coincides with a relatively enriched $\delta^{18}O$ signal which could be interpreted as the Older Dryas period.

4.2 The Postglacial Optimum *10.5 – 6 cal. kyr BP*

The transition between 11 – 10 cal. kyr BP which is identified in all records from core JM05-085 GC (figures 3.17, 3.18 and 3.19), reveal a shift towards more stable and depleted $\delta^{18}O$ and $\delta^{13}C$ levels during the onset of what is known as the thermal optimum. The $\delta^{18}O$ values display a shift from 3.8‰ to 2.9‰, while the $\delta^{13}C$ values show smaller depletions from -0.3‰ to – 0.8‰ (Figure 4. 2). The oxygen isotope values continue with a small gradually depletion reaching a minimum around 7 cal. kyr BP and some instability in the signal is seen at the transition to the Neoglacial time at 6.5 – 6 cal. kyr BP (Figure 4. 2). The tentative bottom water temperatures calculated show maximum values of 6°C and it is fairly stable throughout this interval. This temperature is in the order of 2°C warmer than the modern bottom water temperature at the core site in Ingøydjupet. The carbon isotopes display a depleted stable interval between 10.5 and 6 cal. kyr BP. IRD has ceased at this transition (Figure 4. 2) and the grain-size distribution show dominance of silt and clay (Figure 3.17). The disappearance of IRD compare well to the end of the deglaciation phase (Ebbesen et al. 2006). The maximum temperature for the Ingøydjupet record ends with an enrichment of both the oxygen isotope values and carbon isotope values and a gradual cooling from around 6 cal. kyr BP (Figure 4. 2).

The high resolution oxygen isotope record from the Malangenfjord starts at 8 cal. kyr BP with relatively low values of 1.8‰ which gradually are enriched towards heavier values (Figure 4. 3). In this interval between 8 and 6 cal. kyr BP, the total shift is from 1.8‰ to 2.3‰ and may represent a 2°C cooling if the $\delta^{18}O$ signal is attributed to temperature only. This shift could represent the transition from a hydrological setting with high bottom water temperatures around 10°C to an unstable colder scenario with slowly decreasing bottom water temperatures. The overall trend in the carbon isotope curve from the Malangenfjord is long term enrichment with short-lived changes superimposed on the general trend. A $\delta^{13}C$ minimum is seen around 7.5 – 7 cal. kyr BP. With the assumption that the lower most part of the Malangenfjord-record displays the climate optimum at around 8 cal. kyr BP with high stable bottom water temperatures, this period seems to be of shorter duration than the southern Barents Sea record. This could also be a question of low resolution for the Ingøydjupet record, not catching up on the actual existing trend. There is a transition in the Malangenfjord records seen in both the grain-size distribution (Figure 3.5) and the $CaCO_3$ content (Figure 3.6) at ~7.5 cal. kyr BP.

4.3 The Neoglacial 6 – 0 cal. kyr BP

The Malangenfjord record JM98-1 PC ends at 1.5 cal. kyr BP, with the core top missing from sampling with the piston corer (Hald et al. 2003). The high resolution $\delta^{18}O$ values from the Malangenfjord are gradually continuing getting more enriched from 2.3 ‰ to 3‰ in what could be interpreted as a long term cooling throughout this last part of the Holocene (Figure 4. 3). The calculated temperature is dropping from 8 to 6.4°C with a minimum temperature of 5.5°C at 1.6 cal. kyr BP, the latter being nearly 2°C colder than modern temperature in the fjord. The sedimentation rate in the Malangenfjord shows a large step around 2 cal. kyr BP and this is also picked up by the magnetic signal which clearly shows an increasing trend (Figure 3.6). The increasing clay content in this period indicates a changing bottom current regime (Figure 3.5). The Malangenfjord carbon isotopes gradually increases toward the core top (Figure 3.7). The minimum $\delta^{13}C$ value registered at ~2 cal. kyr BP coincides with the increased sedimentation rate and magnetic signal.

After what seemed to be the postglacial maximum in the Ingøydjupet core JM05-085 GC, the record is now culminating into another cold phase where the oxygen isotope signal is getting gradually heavier from 2.7‰ to 3.6‰ towards the core top (Figure 4. 2). Calculated bottom temperatures for the Ingøydjupet are dropping from 5 – 2.5°C. A microscopic hint if IRD appears around 2.5 cal. kyr BP and the fine sand fraction clearly increases between 3 and 2 cal. kyr BP, which could be interpreted as enhanced bottom current activity in the area (Figure 3.17). This grain-size signal is also picked up by the magnetic measurements, which shows a very small peak at this time. The total organic carbon is rather stable throughout this period, while the $CaCO_3$ content shows a clearly increasing trend and reaching its maximum level at 8% in the core top. The $\delta^{13}C$ values from JM05-085 GC, Ingøydjupet, increases gradually towards present day time just like the Malangenfjord record (Figure 4. 4).

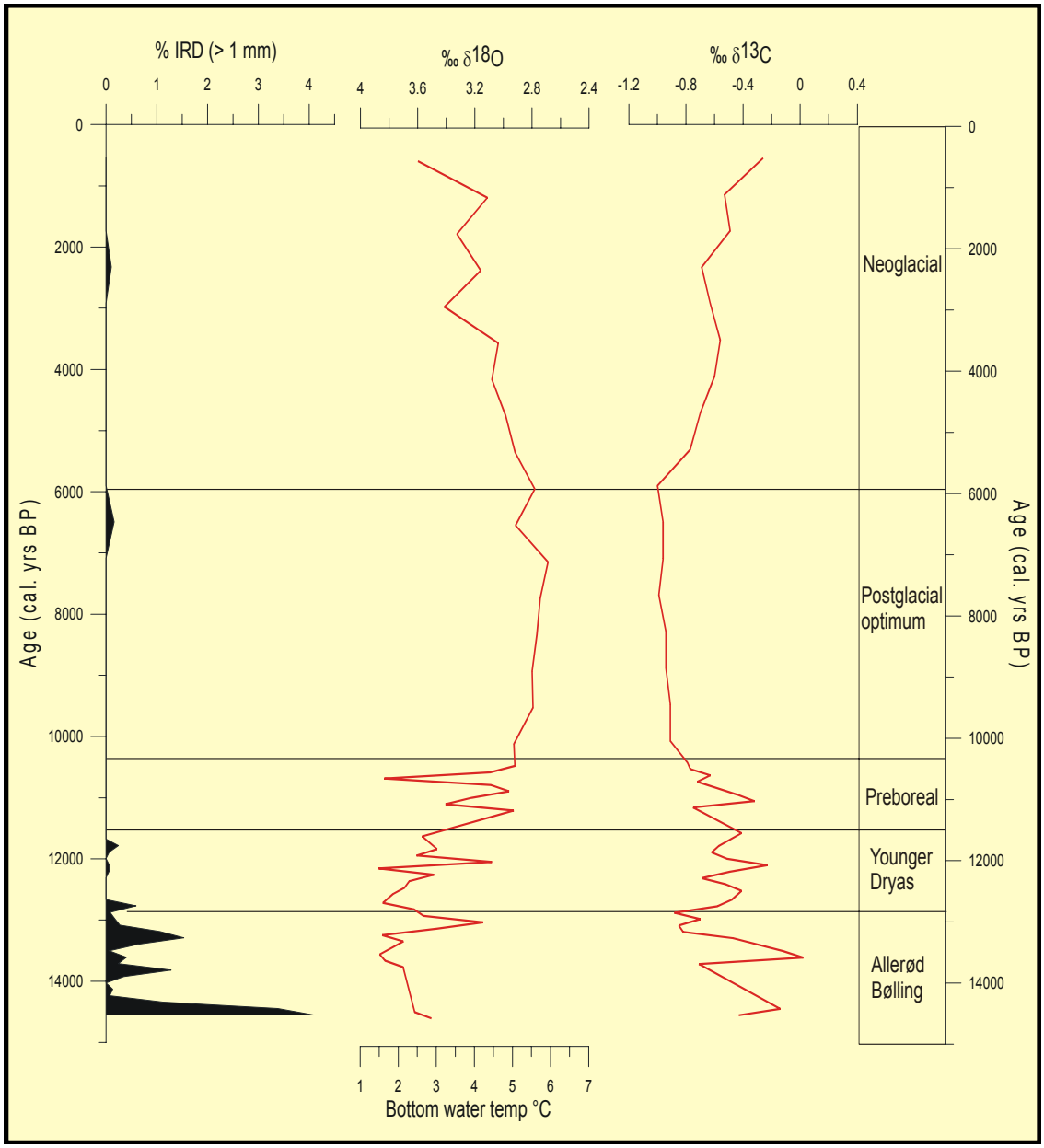

Figure 4. 2 Core JM05-085 GC from Ingøydjupet, southern Barents Sea, with a preliminary interpretation of the IRD, oxygen and carbon isotope signal. The tentative bottom water temperature is calculated from the equation of Shackleton (1974).

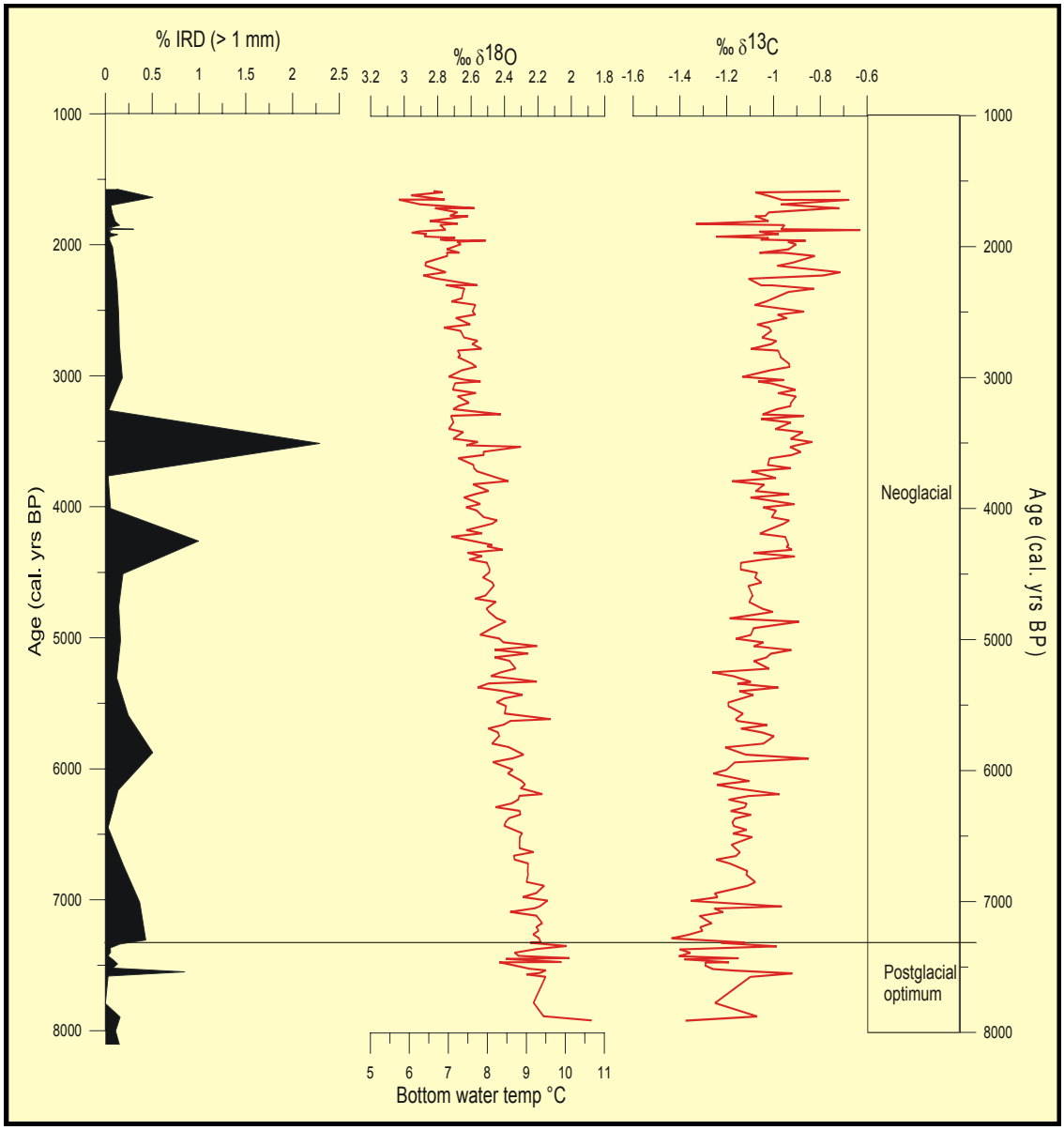

Figure 4. 3 Core JM98-1 PC from the Malangenfjord, with a interpretation of the IRD, oxygen and carbon isotope signal. The tentative bottom water temperature is calculated from the equation of Shackleton (1974).

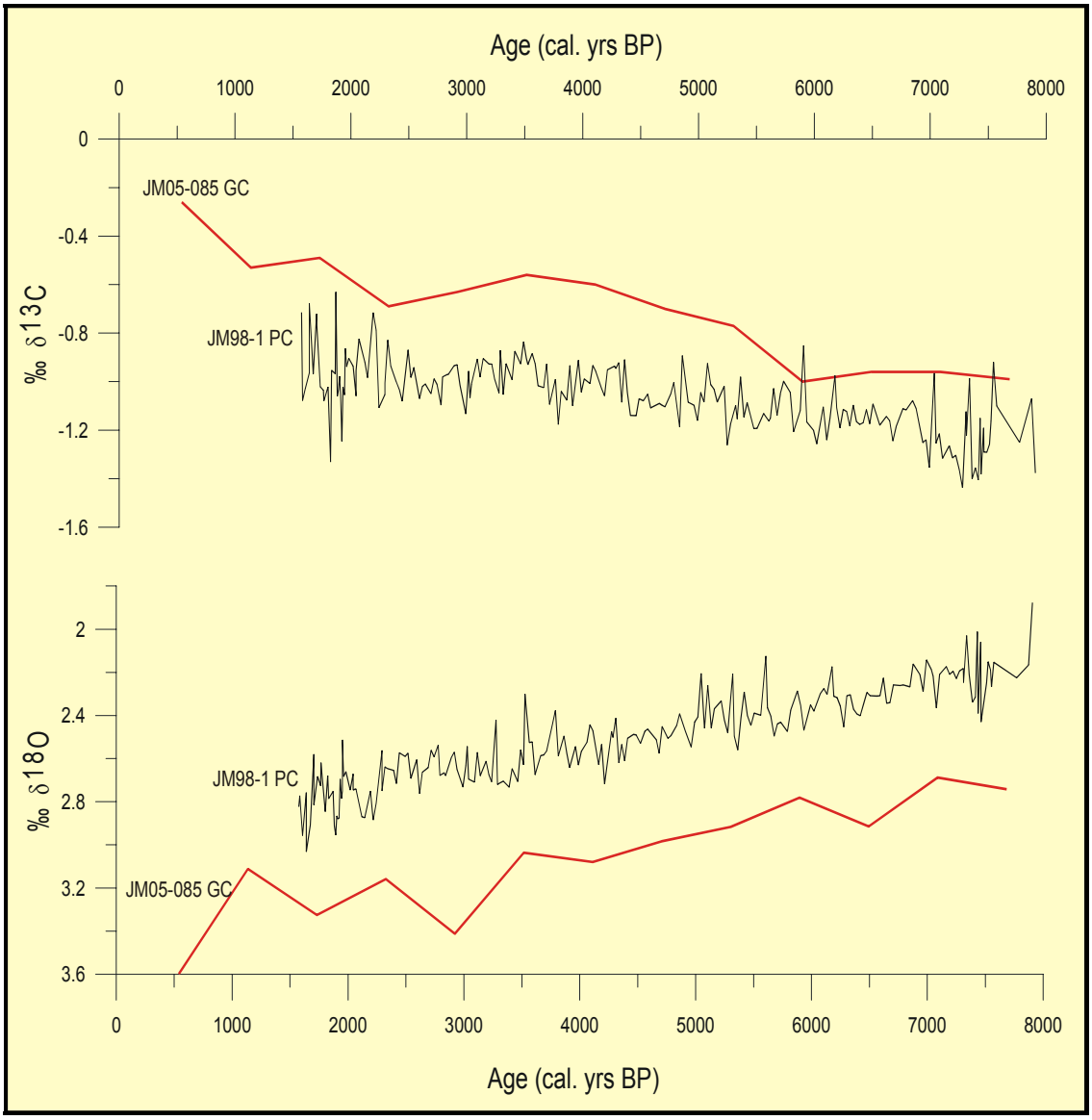

Figure 4. 4 Comparing stable isotopes over the last 8000 yrs BP from JM05-085 GC Ingøydjupet and JM98-1 PC Malangenfjord. Upper panel: Carbon isotopes. Lower panel: Oxygen isotopes.

4.4 Paleoceanographic reconstruction

4.4.1 The final phase of the deglaciation 15 – 10.5 cal. kyr BP

According to Bauch et al. (2001) modern-like circulation developed at 13.5 cal. kyr BP in the Nordic Seas, with a very unstable THC until approximately 10 cal. kyr BP when both IRD and freshwater supply halted. This is also recognized in the core JM05-085 GC from Ingøydjupet in the southern Barents Sea (Figure 4. 2). The Ingøydjupet record show large fluctuations in the bottom water temperature between 1°C – 5°C until the transition at 10.5 cal. kyr BP, and such variations suggest the existence of unstable conditions with regard to temperature (Figure 4. 2). Ebbesen and Hald (2004) suggested that the fluctuations seen in the final phase of the deglaciation reflected rapid shifts in the position of the Polar Front. With the intensity of the North Cape Current controlling the Arctic Front position and sea-ice limit in the SE Barents Sea (Duplessy et al. 2001) it is reasonable to link an unstable Atlantic inflow to the fluctuations seen in the final phase of the deglaciation in this area. Enormous amounts of meltwater from the decaying ice sheets was delivered to the area during the deglaciation, and freshwater will, with its less dense and less saline properties, reduce oceanic mixing (Hald et al. 1996) and hence change the THC and inflow of warm Atlantic Water. With similarity to the Ingøydjupet record (Figure 4. 2), the Bølling/Allerød warming is not evident in the bottom waters in the Norwegian Sea (Kristensen et al. 2001), and there the appearance of the benthic specie *Cassidulina laevigata* was used as an indicator of an unstable hydrographical regime. Low $\delta^{13}C$ values indicate warm, but poorly ventilated Atlantic Water (Sarnthein et al. 2003). This can be recognized from the Barents Sea record, JM05-085 GC, where the carbon isotopes are low during the deglacial warm phases and throughout the entire thermal optimum. The deglacial $\delta^{13}C$ depletions can however also be interpreted as meltwater pulses, with highly unstable ventilation and reduced convectional processes, as observed by Bauch et al. (2001) just prior to and after the Younger Dryas. When reading the carbon isotope signal, Berger and Vincent (1986) pointed out that long-period changes reflect external fractionation patterns, such as exchange of carbon from other reservoirs (terrestrial & atmosphere). The short-period signal reflects internal water-mass properties, such as productivity and ocean circulation.

4.4.2 The postglacial Optimum 10.5 – 6 cal. kyr BP

The enhanced inflow of Atlantic Water to the northern North Sea coincides with opening of both the English Channel and the Danish Strait (Kristensen et al. 2001). Thermal optimum in the Nordic Seas was identified by Bauch et al. (2001) between 10 – 6 cal. kyr BP, and this is in accordance with our findings in core JM05-085 GC from the southern Barents Sea. Duplessy et al. (2001) also found a warming trend in the northern Barents Sea, but this was short and ended abruptly around 6.9 cal. kyr BP with a 2°C cooling. The thermal optimum had maximum input of Atlantic water, and according to Duplessy et al. (2001), it occupied the entire water column in the northern Barents Sea allowing no cold bottom water to form. This could be read from his planktonic and benthic $\delta^{18}O$ records which had nearly the same values, leaving the water mass with no stratification and the dense bottom water formation was completely reduced during this period. This is in agreement with Sarnthein et al. (2003), who concluded that low planktic $\delta^{13}C$ values reflected warm, but poorly ventilated Atlantic surface water at this time. Both records from the Malangenfjord (Figure 4. 3) and Ingøydjupet (Figure 4. 2) show depleted benthic $\delta^{13}C$ values during the thermal optimum. As a consequence of the reduced overturning of the water masses during the thermal optimum, there was a reduced influx of Atlantic Water and subsequent cooling in the mid/late Holocene (Duplessy et al. 2001). From this point of view it seems like the stratification in the water masses is of crucial importance for the onset and attendance of the major heat conveyor.

4.4.3 The Neoglacial 6- 0 cal. kyr BP

Surface cooling in the Nordic Seas was explained with the establishment of the Arctic and Polar frontal systems (Bauch et al. 2001). Here the strong inflow of Atlantic Water and the subsequent outflow of cold polar water along the Greenland margin, the onset of the NADW formation itself, seem to have caused both the bottom and surface cooling after 6 cal. kyr BP. The late Holocene cooling in the Barents Sea is according to Duplessy et al. (2005) related to the reduced penetration of Atlantic Water. The later establishment of modern hydrological conditions from ~ 4.7 cal. kyr BP suggested that the area in this period once again experienced more stratified waters, where the bottom water cooled and

the surface water warmed (Duplessy et al. 2005). The enrichment in the carbon isotope records (Figure 4. 4) during Late Holocene could reflect increased productivity in the surface water which is later brought to deeper waters with the onset of convectional processes. This can also be seen in the increased $CaCO_3$ content from the Ingøydjupet record JM05-085GC (Figure 3.20), which is mainly controlled by dissolution, dilution and/or productivity changes (Stein et al. 1994). The Malangenfjord record, JM98-1 PC, with its long term-cooling trend and increasing $\delta^{13}C$ values (Figure 4. 4) could be affected by postglacial sea level changes due to isostatic movement. After the retreat of the ice sheet and with the existing glacial isostatic depression, the sea-level rise inundated the fjord system, creating deep basins and good hydrological connections across the sills which are in the fjord system. The isostatic adjustment during Holocene could have changed the hydrological connection with the Atlantic open ocean current system and hence the bottom water properties. Today the fjord system is influenced by Atlantic Water, but perhaps the fjord was occupied by another water source, such as the less saline coastal water. Drowned river valleys formed in response to the Early Holocene postglacial sea level rise are common estuaries. The large Målselv River at the fjord head contributes with freshwater to the fjord. Both sedimentation and hydrography are controlled by the bathymetry in the fjord, which consists of several submarine thresholds and basins.

4.5 Correlation to other proxy records

Core JM05-085 GC from Ingøydjupet, southern Barents Sea, was compared to the solar irradiance curve at 70°N from Berger and Loutre (1991), the ice core $\delta^{18}O$ record from NorthGRIP project on Greenland (Vinther et al., in press; Rasmussen et al., in press) and the SST at 75°N from Sarnthein et al. 2003 (Figure 4. 5). The record from Sarnthein et al. (2003) shows SST_{summer}[6] in the West Spitsbergen Current, which is a north westerly branch of the North Atlantic Current. Red lines drawn in figure 4.5 connect some of the peak-to-peak correlation with core JM05-085 GC; warming at ~11 cal. kyr BP, cooling at ~10.6 cal. kyr BP, warming at 5.9 cal. kyr BP and the M-shaped excursions at 2.2 and 1.8 - 1.6 cal. kyr BP. The record from Sarnthein et al. (2003) show undulating values during the

[6] SIMMAX transfer function (Pflaumann et al. 1996)

Preboreal Oscillations, and a shorter Holocene optimum, lasting from 10.7 to 7.6 cal. kyr BP, only interrupted by a 600 yrs cooling period at 8.8 cal. kyr BP. Our record from Ingøydjupet has not high enough resolution to recognize this cooling period. The Late Holocene cooling is interrupted by several short-lived warm periods, giving a drop in the $\delta^{13}C$ signal, which is characteristic for the warm, but poorly ventilated Atlantic surface waters. The solar insolation is decreasing throughout Holocene, and this could be connected to the cooling that we see in the records. The cooling trend after the Holocene Optimum is also recorded in the NorthGRIP data (Vinther et al., in press; Rasmussen et al., in press).

Core JM98-1 PC from the Malangenfjord was compared to the solar irradiance curve at 70°N (Berger and Loutre 1991) and the ice core $\delta^{18}O$ record from NorthGRIP (Vinther et al., in press; Rasmussen et al., in press) (Figure 4. 6). The ice core records have proven that climate changes on a decadal timescale has taken place over the North Atlantic region, but it is difficult to do a peak-to-peak comparison for the Malangenfjord record. However the general trend is definitely short-lived climate changes superimposed on a long-term cooling in both records.

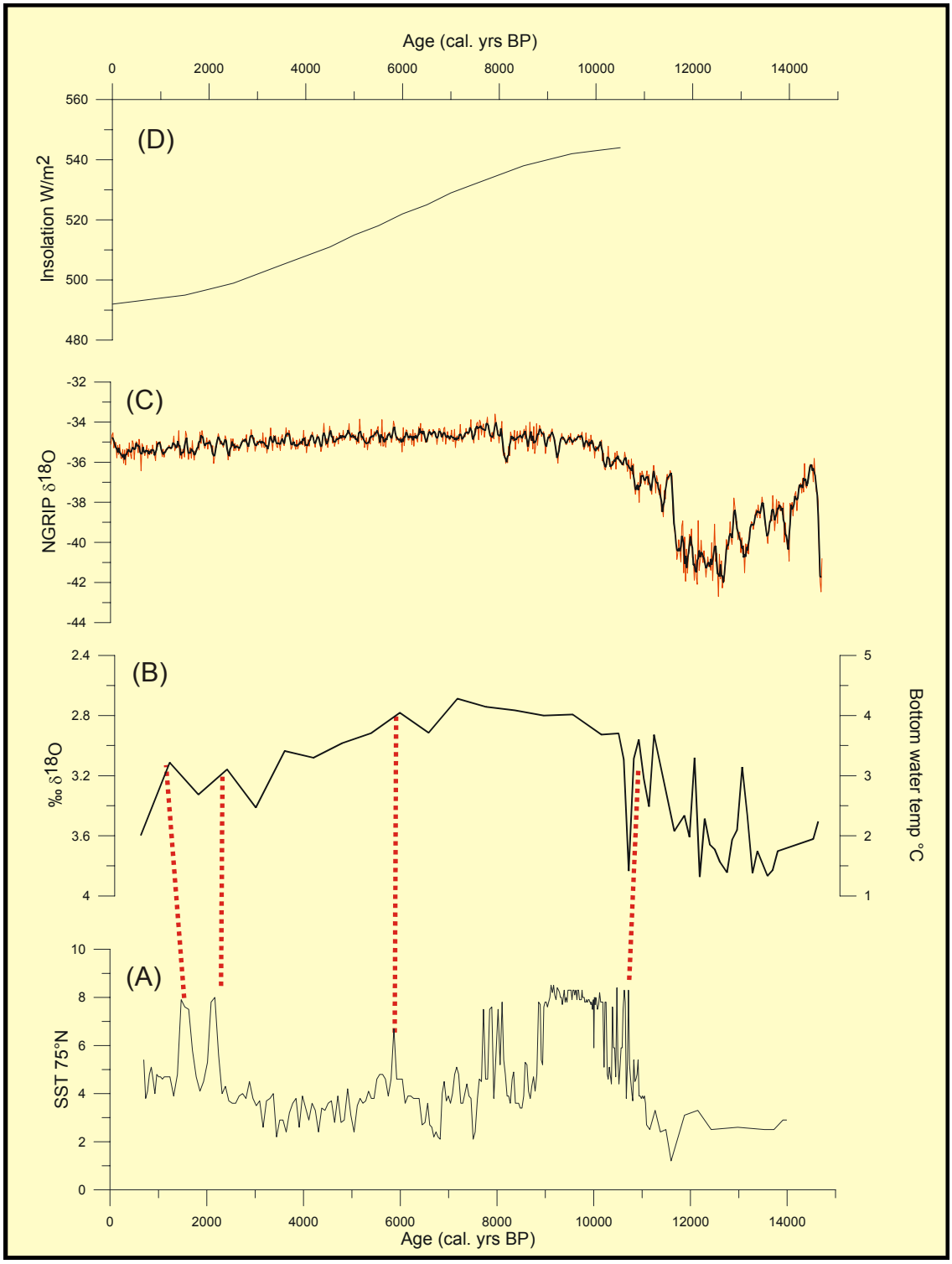

Figure 4. 5 The benthic record from JM05-085 GC Ingøydjupet (B) compared to (A) SST-summer from Sarnthein et al. 2003, (C) $\delta^{18}O$ data from NGRIP (Vinther et al. in press; Rasmussen et al. in press) and (D) June insolation at 70°N (Berger and Loutre 1991).

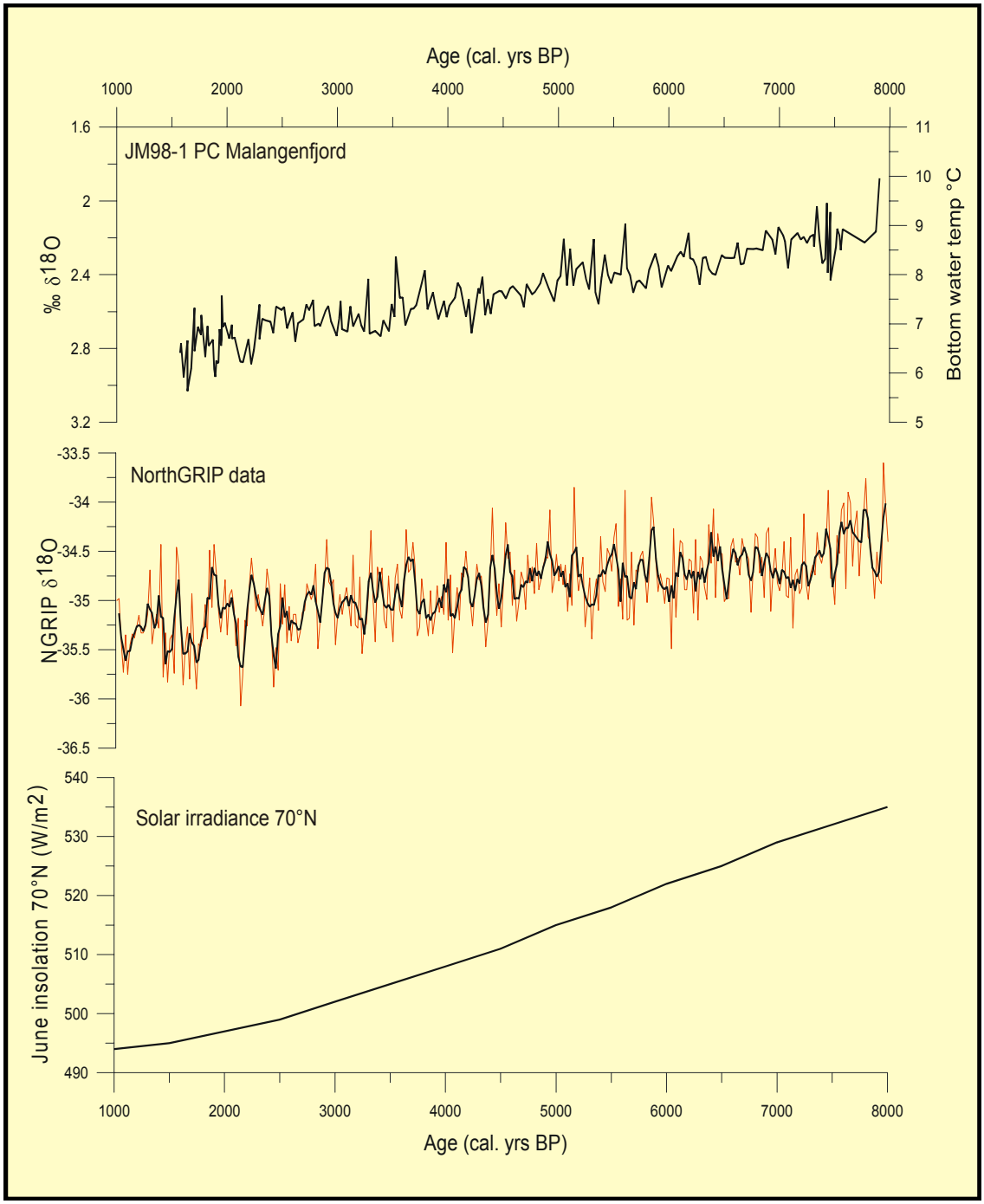

Figure 4. 6 The benthic record from core JM98-1 PC the Malangenfjord correlated with NGRIP data (Vinther et al. in press; Rasmussen et al. in press) smoothed with running average and June insolation at 70°N (Berger and Loutre 1991).

4.6 Climate forcing mechanisms

Millennial scale oscillations with rapid warming over few decades, followed by a gradual cooling over a long period of time, are often referred to as Dansgaard-Oeschger (D/O) cycles. The so called Heinrich-events with release of icebergs, IRD and meltwater across the North Atlantic are often connected with the cold periods of the D/O cycles, and are suggested to cause a disruption of the THC (Bond et al. 1999). Both records from the Malangenfjord and the southern Barents Sea show millennial scale changes, with the rapid warming and long term cooling trend throughout Holocene. No distinct IRD events are seen from the grain-size analysis in Holocene, but the final disintegration of the Laurentide Ice Sheet around ~ 6 cal. kyr BP must have contributed with large amounts of freshwater into the North Atlantic.

4.6.1 Orbital forcing

These forcing mechanisms are relatively speaking quite slow and cause changes on a long-term basis. At the last glacial maximum it is accepted that the ice sheets controlled the global climate, but orbital changes such as tilt of the axis and precessional movement favoured increasing and maximum summer insolation during the deglaciation (Ruddiman 2001, p.302). This orbital shift led to the onset of melting the glaciers and a concurrent increasing CO_2 level during the deglaciation. The CO_2 level measured from Greenland ice cores show that it was 90ppm lower than the preindustrial level of 280ppm during the glacial period (Ruddiman 2001, p.299).

4.6.2 North Atlantic Oscillation

The NAO displays a decadal to interdecadal variation (Luterbacher et al. 2002), and it could be possible to link our high resolution record from the Malangenfjord with atmospheric forcing from the variable NAO. The variations in surface water temperature have been related to the variations in the strength of the NAO (IPCC 2001). This is not in agreement with the findings of Ingvaldsen et al. (2005a), who could not see any linking between temperature and volume influx of Atlantic Water to the Barents Sea. The exchange

of heat from the North Atlantic Current is enhanced during years with a positive NAO-index, and is less during periods with a negative NAO-index, suggesting that the volume influx and strength of the inflowing Atlantic Water is connected to the atmospheric circulation (Ingvaldsen et al. 2005a). The other scenario with changing surface water temperature (and salinity) on the inflowing North Atlantic Current is connected to the Atlantic Subpolar Gyre (Hátún et al. 2005). Both positive and negative NAO phases will result in changing heat and moisture transport, in this case a positive NAO-index will give above-normal precipitation over Scandinavia. Nesje et al. (2000) related interannual changes in the Scandinavian winter weather to the NAO by looking at glaciers mass balance in terms of ablation and accumulation (Figure 4. 7). They found that years with high NAO-index gave high winter mass balance for the glaciers in terms of increased precipitation, and that cold/dry periods (negative NAO) correlates with marine record showing enhanced IRD (Figure 4. 7). Ottersen and Stenseth (2001) showed a significant relationship between variability in the Barents Sea climate and large-scale atmospheric forcing, the same system that drives the subtropical gyre feeding the North Atlantic Current.

There seems to be a concern regarding the more positive trend for the NAO over the past 30 years (Visbeck et al. 2001). From the 500yrs reconstruction for the NAO index done by Luterbacher et al. (2002), it was concluded that the high positive trend seen at the end of the twentieth century is not unusual. There are still uncertainties in knowing what controls the NAO, but it seems to be a consensus that it is a result of ocean-atmospheric interactions.

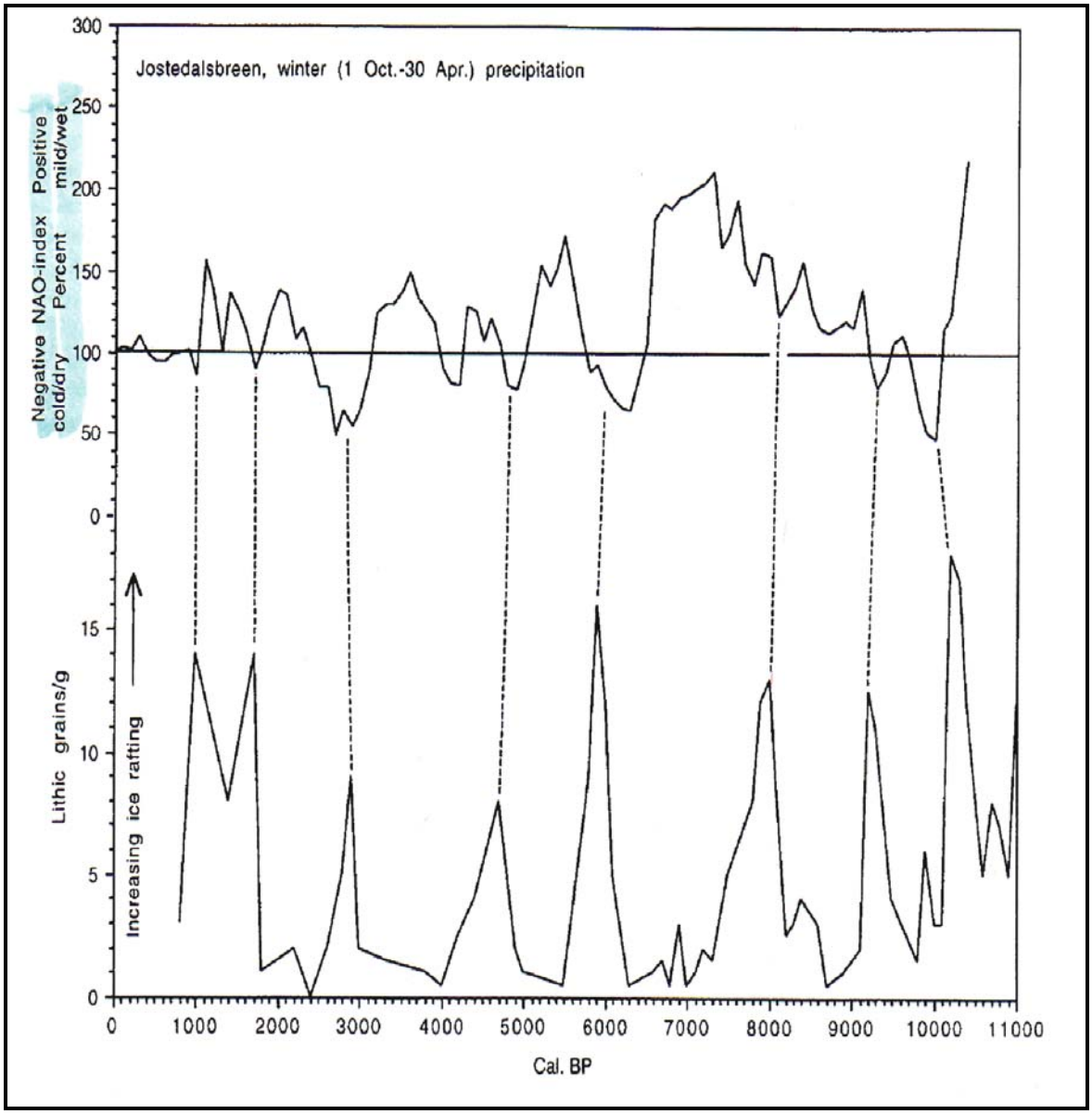

Figure 4. 7 Upper panel: Reconstruction of mean winter precipitation for Jostedalsbreen, western Norway. Periods of mild/wet and cold/dry conditions are indicated with positive and negative NAO-index respectively. Lower panel: Cold and dry periods from the precipitation reconstruction are correlated to the IRD signal in a marine record (Figure from Nesje et al. 2000).

4.6.3 Volcanism

The climatic influence from volcanic eruptions is limited to 3 – 5 years, but it is reasonable to believe that several succeeding large eruptions could have caused short climatic changes

in the past (Jørgensen et al. 1997). The large amounts of fine particles in the atmosphere after an eruption will shield solar insolation and thus prevent the effect from increasing content of CO_2 in the atmosphere. Another aspect related to volcanic eruptions, is the ash deposits which settles in the ocean water. The ash is quickly dissolved and nutrients are released to the water column which leads to increased productivity in the water. Studies have shown that volcanic eruptions with added nutrients and increased productivity will results in increased CO_2 storage in the ocean (Frogner et al. 2001). This can in addition to the previous mentioned shielding effect be regarded as a climatic feedback mechanism bringing the system back to balance, after the fact that volcanic eruptions have added high levels of CO_2 to the atmosphere.

4.6.4 Solar activity

Andersson et al. (2003) suggested that solar forcing alone does not seem to drive climate variability in the North Atlantic region, but it may be responsible for triggering feedback systems (Sea ice, albedo, sea level rise, calving of ice sheet faster, clouds). Is it possible to connect phases in the NADW production with variations in the solar origin? The report from IPCC (2001) concludes that changes in solar insolation and volcanic activity have caused global climate changes[7].

[7] IPCC report, page 709

5 Summary and conclusion

The results from core JM05-085 GC Ingøydjupet must be considered as preliminary only due to the low resolution and large uncertainties in the age model, but based on both records from the Malangenfjord and Ingøydjupet, these are the following conclusive marks;

- The final phase of the deglaciation was identified in the record from the southern Barents Sea between 15 – 11.5 cal. kyr BP. A period with highly unstable bottom water conditions is reflected in both the fluctuating $\delta^{18}O$ and $\delta^{13}C$ record.
- Meltwater pulses recognized during the final phase of the deglaciation.
- Onset of the Holocene interglacial with the Preboreal Oscillations at 11.5 – 10.5,
- Followed by a period with maximum inflow of Atlantic Water in the Barents Sea until 7 – 6 cal. kyr BP.
- Maximum inflow of Atlantic Water to the Malangenfjord seems of shorter duration, ending around 7 cal. kyr BP. The fjord system experienced isostatic adjustment during Holocene, which could have created different hydrological scenarios for the fjord.
- The Malangenfjord record has identified a long term cooling throughout the entire period from 8 – 1.5 cal. kyr BP, with small scale changes superimposed on the general trend.
- The Malangenfjord record correlates with the Ingøydjupet record.
- Variations in the surface water temperatures are controlled by the Atlantic Subpolar Gyre.
- Atmospheric circulation in terms of the North Atlantic Oscillation is controlling the volume influx and strength of the inflowing North Atlantic Water.

5.1 Future work

It could be of interest to perform time series analysis for the high resolution record JM98-1 PC from the Malangenfjord. This in order to recognize small scale cycles superimposed on the general trend.

6 References

Abbott, R. T. (1996). Skjell. LibriArte AS.

Andersson, C. et al. (2003). Late Holocene surface ocean conditions of the Norwegian Sea (Vøring Plateau). Paleoceanography **18**(2): 1044-1057.

Andresen, A. (1980). The age of the Precambrian basement in western Troms, Norway. Geologiska Föreningen i Stockholm Förhandlingar **101**(4): 291-298.

Bauch, H. A. et al. (2001). A multiproxy reconstruction of the evolution of deep and surface waters in the subarctic Nordic seas over the last 30,000 yr. Quaternary Science Reviews **20**(4): 659-678.

Berger, A. and Loutre, M. F. (1991). Insolation values for the climate of the last 10 million years. Quaternary Science Reviews **10**(4): 297-317.

Berger, W. H. and Vincent, E. (1986). Deep-sea carbonates; reading the carbon-isotope signal. Geologische Rundschau **75**(1): 249-269.

Bond, G. C. et al. 1999 The North Atlantic's 1-2 kyr climate rhythm; relation to Heinrich events, Dansgaard/ Oescher cycles and the Little Ice Age American Geophysical Union 35-58

Bondevik, S. et al. (2003). Record-breaking height for 8000-year-old tsunami in the North Atlantic. Eos, Transactions, American Geophysical Union **84**(31): 289, 293.

Bondevik, S. 2006, Personal communication

Bowman, S. (1990). Radiocarbon dating; Interpreting the past. British Museum Publications.

Broecker, W. S. (1997). Thermohaline circulation, the Achilles heel of our climate system: Will man-made CO2 upset the current balance? Science **278**: 1582-1588.

Coakley, J. P. and Syvitski, J. P. M. (1991). Sedigraph technique: in, Syvitski, J.P.M., ed., Principles, Methods, and Application of Particle Size Analysis. Cambridge University Press: 368 p.

Duplessy, J. C. et al. (1980). Deep water formation in the North Atlantic Ocean during the last ice age. Nature **286**: 47482.

Duplessy, J. C. et al. (2001). Holocene paleoceanography of the northern Barents Sea and variations of the northward heat transport by the Atlantic Ocean. Boreas **30**: 2-16.

Duplessy, J. C. et al. (2005). Paleoceanography of the Barents Sea during the Holocene. Paleoceanography **20**(PA4004): 13.

Ebbesen, H. and Hald, M. (2004). Unstable Younger Dryas climate in the northeast North Atlantic. Geology (Boulder) **32**(8): 673-676.

Ebbesen, H. et al. (2006). Late glacial and Early Holocene climatic oscillations in the western Svalbard margin, European Arctic. Submitted.

Fairbanks, R. G. (1989). A 17,000-year glacio-eustatic sea level record; influence of glacial melting rates on the Younger Dryas event and deep-ocean circulation. Nature (London) **342**(6250): 637-642.

Faleide, J. I. et al. (1993). Late Mesozoic-Cenozoic evolution of the south-western Barents Sea in a regional rift-shear tectonic setting. Marine and Petroleum Geology **10**(3): 186-214.

Forman, S. L. and Polyak, L. (1997). Radiocarbon content of prebomb marine mollusks and variations in the (super 14) C reservoir age for coastal areas of the Barents and Kara seas, Russia. Geophysical Research Letters **24**(8): 885-888.

Friis-Christensen, E. and Lassen, K. (1991). Length of the solar cycle; an indicator of solar activity closely associated with climate. Science **254**(5032): 698-700.

Grossman, E. L. (1987). Stable isotopes in modern benthic foraminifera; a study of vital effect. Journal of Foraminiferal Research **17**(1): 48-61.

Gunn, D. E. and Best, A. I. (1998). A new automatic nondestructive system for high resolution multi-sensor core logging of open sediment cores. Geo-Marine Letters **18**: 70-77.

Hald, M. et al. (1996). Paleoceanography on the European arctic margin during the last deglaciation. Late Quaternary Paleoceanography of the North Atlantic Margins, Geological Society Special Publication(111): 275 - 287.

Hald, M. et al. (2003). Holocene climate in the subarctic fjord Malangen, northern Norway: a multi-proxy study. Boreas **32**: 543-559.

Hansbo, S. (1957). A new approach to the determination of the shear strenght of clay by the fall-cone test. Royal Swedish Geotechnical Institute Proceedings **14**: 47p.

Hátún, H. et al. (2005). Influence of the Atlantic subpolar gyre on the thermohaline circulation. Science **309**(5742): 1841-1844.

Holtedahl, H. (1993). Marine Geology of the Norwegian continental margin, NGU Special Publication 6. Norges geologiske undersøkelse.

Hughen, K. A. et al. (2004). Marine04 marine radiocarbon age calibration, 0-26 cal kyr BP. Radiocarbon **46**(3): 1059-1086.

Hurrell, J. W. (1995). Decadal trends in the North Atlantic Oscillation: Regional temperatures and precipitation. Science **269**: 676-679.

Husum, K. and Hald, M. (2002). Early Holocene cooling events in Malangenfjord and the adjoining shelf, North-east Norwegian Sea. Proceedings of the Changes in climate and environment at high latitudes conference. Norsk Polarinstitutt, **21** (2): 267-274.

Husum, K. and Hald, M. (2004). A continuous marine record 8000-1600 cal. yr BP from the Malangenfjord, north Norway; foraminiferal and isotopic evidence. The Holocene **14**(6): 877-887.

Ingvaldsen, R. et al. (2005a). Modellering og observasjoner i det vestlige Barentshavet. Havforskningsnytt, www.imr.no **4**.

Ingvaldsen, R. et al. (2005b). Fisken og havet, særnummer 1. Havets ressurser og miljø - Havforskningsinstituttet.

IPCC (2001). The Scientific Basis. Working group 1, Third Assesment Report, Climate Change 2001. Cambridge University Press.

Jørgensen, P. et al. (1997). Kvartærgeologi. Landbruksforlaget.

Kearey, P. et al. (2002). An Introduction to Geophysical Exploration. Blackwell Science Ltd.

Kristensen, D. K. et al. (2001). The last 18kyr fluctuations in Norwegian Sea surface conditions and implications for the magnitude of climatic change: evidence from the North Sea. Paleoceanography **16**(5): 455-467.

Kristensen, D. K. et al. (2004). Eight-hundered-year temperature variability from the Norwegian continental margin and the North Atlantic thermohaline circulation. Paleoceanography **19**.

Larsen, K. B. 1986 Seismic stratigraphy and sedimentation in Malangen and Straumsfjord, Troms. Master thesis, University of Tromsø

Luterbacher, J. et al. (2002). Extending North Atlantic Oscillation reconstruction back to 1500. Atmospheric Science Letters.

Lyså, A. and Vorren, T. O. (1997). Seismic facies and architecture of ice-contact submarine fans in high-relief fjords, Troms, northern Norway. Boreas **26**: 309-328.

Midttun, L. (1985). Formation of dense bottom water in the Barents Sea. Deep Sea Research **32**: 1233-1241.

Mikalsen, G. et al. (2001a). Benthonic stable oxygen isotope records from the northern Norwegian fjords, showing temperature variations and regional climate changes. Abstract and Proceedings of the Norwegian Geological Society **2**: 72.

Munsell, R. (1973). Soil Color Charts. Macbeth division of Kollmorgen Corporation: 19 p.

Nesje, A. et al. (2000). Is the North Atlantic Oscillation reflected in Scandinavian glacier mass balance records? Journal of Quaternary Science **15**(6): 587 - 601.

O'Neil, J. R. and Adami, L. H. (1969). The oxygen isotope partition function ratio of water and the structure of liquid water. The Journal of Chemical Physics **73**: 1553-1558.

Ottersen, G. and Stenseth, N. C. (2001). Atlantic climate governs oceanographic and ecological variability in the Barents Sea. Limnology and Oceanography **46**(7): 1774 - 1780.

Poole, D. 1994 Neogene and Quaternary paleoenvironments in the Norwegian Sea shelf PhD-thesis Department of Geology University of Tromsø, Norway

Robinson, S. G. (1986). The late Pleistocene paleoclimatic record of North-Atlantic deep-sea sediments revealed by mineral-magnetic measurements. Physics of the Earth and Planetary Interiors **42**: 22-47.

Polyak, L. et al. (2002). Benthic foraminiferal assemblages from the southern Kara Sea, a river-influenced arctic marine environment. Journal of Foraminiferal Research **32**(3): 252-273.

Rasmussen, S. O., Andersen, K.K., Svensson, A.M., Steffensen,J.P., Vinther, B. M., H.B. Clausen, M.-L. Siggaard-Andersen, S.J. Johnsen, L.B. Larsen, D. Dahl-Jensen, M. Bigler, R. Röthlisberger, H. Fischer, K. Goto-Azuma, M.E. Hansson, and U. Ruth. A new Greenland ice core chronology for the last glacial termination. In press, Journ. Geophys. Res., vol. 111, doi:10.1029/2005JD006079

Reimer, P. J. and Reimer, R. W. (2001). A marine reservoir correction database and on-line interface. University of Arizona Department of Geosciences.

Reimer, P. J. et al. (2001). Marine radiocarbon reservoir corrections for the mid- to late Holocene in the eastern subpolar North Atlantic. The Holocene **12**(2): 129-135.

Reimer, P. J. et al. (2004). IntCal04 terrestrial radiocarbon age calibration, 0-26 cal kyr BP. Radiocarbon **46**(3): 1029-1058.

Risebrobakken, B. et al. (2003). A high-resolution study of Holocene paleoclimatic and paleoceanograpich changes in the Nordic Seas. Paleoceanography **18**(1): 1017.

Ruddiman, W. F. (2001). Earth's climate, past and future.

Sarnthein, M. et al. (2003). Centennial-to-millennial-scale periodicities of Holocene climate and sediment injections off the western Barents shelf, 75 degrees N. Boreas **32**(3): 447-461.

Shackleton, N. J. and Opdyke, N. D. (1973). Oxygen isotope and palaeomagnetic stratigraphy of Equatorial Pacific core V28-238: Oxygen isotope temperatures and ice volumes on a 105 year and 106 year scale. Quaternary Research **3**(1): 39-55.

Shackleton, N. J. (1974). Attainment of isotopic equilibrium between ocean water and the benthonic foraminifera genus Uvigerina; isotopic changes in the ocean during the last glacial. Colloques Internationaux du Centre National de la Recherche Scientifique **219**: 203-209.

Shackleton, N. J. (1974). Attainment of isotopic equilibrium between ocean water and the benthonic foraminifera genus Uvigerina; isotopic changes in the ocean during the last glacial. Colloques Internationaux du Centre National de la Recherche Scientifique **219**: 203-209.

Shackleton, N. J. et al. (1983). Oxygen and carbon isotope record of East Pacific Core V19-30; implications for the formation of deep water in the late Pleistocene North Atlantic. Earth and Planetary Science Letters **65**(2): 233-244.

Solheim, A. et al. 1996 Impact of glaciations on basin evolution; data and models from the Norwegian margin and adjacent areas; introduction and summary Elsevier 1-9

Stein, R. et al. (1994). Organic carbon, carbonate, and clay mineral distributions in eastern central Arctic Ocean surface sediments. Elsevier.

Syvitski, J. P. M. et al. (1987). Fjords: Processes and products. Springer-Verlag.

Tebble, N. (1966). British Bivalve Seashells - A handbook for identification. Her Majesty Stationary Office, Edinburgh.

Thomsen, E. (2006), Personal communication

Vinther, B.M., H.B. Clausen, S.J. Johnsen, S.O. Rasmussen, K.K. Andersen, S.L. Buchardt, D. Dahl-Jensen, I.K. Seierstad, M.-L. Siggaard-Andersen, J.P. Steffensen, A.M. Svensson, J. Olsen, and J. Heinemeier A synchronized dating of three Greenland ice cores throughout the Holocene. In press, Journ. Geophys. Res., doi:10.1029/2005JD006921

Visbeck, M. H. et al. (2001). The North Atlantic Oscillation: Past, present and future. Proceedings of the National Academy of Sciences of the United States of America **98**(23): 12876-12877.

Urey, H. (1947). The thermodynamic properties of isotopic substances. Journal of Chemistry Society **pt. 1**: 562-581.

Weber, M. E. et al. (1997). Calibration and application of marine sedimentary physical properties using a multi-sensor core logger. Marine Geology **136**: 151-172.

Zwaan, K. B. (1995). Geology of the West Troms basement complex, Northern Norway, with emphasis on the Senja shear belt; a preliminary account. Bulletin 427 Norges Geologiske Undersokelse.

7 Appendix

Please find the appendix on the enclosed CD. All files are in Microsoft Word or Excel-format.

7.1 Sediment core JM98-1 PC

7.1.1 Age model

7.1.2 Calibration of ^{14}C ages

7.1.3 Stable isotopes

7.1.4 Grain-size distribution

7.1.5 Total carbon / total organic carbon

7.1.6 Magnetic susceptibility

7.1.7 Undrained shear strength

7.1.8 Water content

7.2 Sediment core JM05-085 GC

7.2.1 Age model

7.2.2 Calibration of ^{14}C ages

7.2.3 Stable isotopes

7.2.4 Grain-size distribution

7.2.5 MSCL results

7.2.6 CTD-data

7.2.7 Undrained shear strength